PERFORMANCE EVALUATION OF PIEZOELECTRIC SENSOR/ACTUATOR ON INVESTIGATION OF VIBRATION CHARACTERISTICS AND ACTIVE VIBRATION CONTROL OF A SMART BEAM

A THESIS SUBMITTED TO
THE GRADUATE SCHOOL OF NATURAL AND APPLIED SCIENCES
OF
MIDDLE EAST TECHNICAL UNIVERSITY

BY

MUSTAFA UĞUR ARIDOĞAN

IN PARTIAL FULFILLMENT OF THE REQUIREMENTS
FOR
THE DEGREE OF MASTER OF SCIENCE
IN
AEROSPACE ENGINEERING

JUNE 2010

Approval of the thesis:

PERFORMANCE EVALUATION OF PIEZOELECTRIC SENSOR/ACTUATOR ON INVESTIGATION OF VIBRATION CHARACTERISTICS AND ACTIVE VIBRATION CONTROL OF A SMART BEAM

submitted by **MUSTAFA UĞUR ARIDOĞAN** in partial fulfillment of the requirements for the degree of **Master of Science in Aerospace Engineering Department, Middle East Technical University** by,

Prof. Dr. Canan Özgen
Dean, Graduate School of **Natural and Applied Sciences** _____

Prof. Dr. Ozan Tekinalp
Head of Department, **Aerospace Engineering** _____

Asst. Prof. Dr. Melin Şahin
Supervisor, **Aerospace Engineering Dept., METU** _____

Dr. Volkan Nalbantoğlu
Co-supervisor, **Aselsan** _____

Examining Committee Members:

Prof. Dr. Yavuz Yaman
Aerospace Engineering Dept., METU _____

Asst. Prof. Dr. Melin Şahin
Aerospace Engineering Dept., METU _____

Asst. Prof. Dr. Gökhan O. Özgen
Mechanical Engineering Dept., METU _____

Assoc. Prof. Dr. Metin U. Salamcı
Mechanical Engineering Dept., Gazi University _____

Dr. Volkan Nalbantoğlu
Microelectronics, Guidance and Electro-Optics Division, Aselsan _____

Date: _____

I hereby declare that all information in this document has been obtained and presented in accordance with academic rules and ethical conduct. I also declare that, as required by these rules and conduct, I have fully cited and referenced all material and results that are not original to this work.

Name, Last Name: MUSTAFA UĞUR ARIDOĞAN

Signature :

ABSTRACT

PERFORMANCE EVALUATION OF PIEZOELECTRIC SENSOR/ACTUATOR ON INVESTIGATION OF VIBRATION CHARACTERISTICS AND ACTIVE VIBRATION CONTROL OF A SMART BEAM

Arıdoğan, Mustafa Uğur

M.S., Department of Aerospace Engineering

Supervisor : Asst. Prof. Dr. Melin Şahin

Co-Supervisor : Dr. Volkan Nalbantoğlu

June 2010, 101 pages

In this thesis, the performance of piezoelectric patches on investigation of vibration characteristics and active vibration control of a smart beam is presented. The smart beam is composed of eight surface-bonded piezoelectric patches symmetrically located on each side of a cantilever aluminium beam.

At first, vibration characteristics of the smart beam is investigated by employment of piezoelectric patches as sensors and actuators. Smart beam is excited by either impact hammer or piezoelectric patch and the response of the smart beam particular to these excitations is measured by piezoelectric patches used as sensors. In order to investigate the performance of piezoelectric patches in sensing, the measurements are also conducted by commercially available sensing devices.

Secondly, active vibration suppression of the smart beam via piezoelectric sensor/actuator pair is considered. For this purpose, system identification of the smart beam is conducted by using four piezoelectric patches as actuators and another piezoelectric patch as a sensor. The designed robust controller is experimentally implemented and active vibration suppression of

the free and first resonance forced vibration is presented.

Thirdly, active vibration control of the smart beam is studied by employment of piezoelectric patches as self-sensing actuators. Following the same approach used in the piezoelectric sensor/actuator pair case, system identification is conducted via self-sensing piezoelectric actuators and robust controller is designed for active vibration suppression of the smart beam. Finally, active vibration suppression via self-sensing piezoelectric actuators is experimentally presented.

Keywords: Vibration Suppression, System Identification, Robust Control, Piezoelectric Sensor and Actuator, Self-Sensing Piezoelectric Actuator

ÖZ

PİEZOELEKTRİK YAMALARIN AKILLI BİR KİRİŞİN TİTREŞİM ÖZELLİKLERİNİN BULUNMASINDA VE TİTREŞİM KONTROLÜNDEKİ ETKİNLİĞİNİN DEĞERLENDİRİLMESİ

Arıdoğan, Mustafa Uğur
Yüksek Lisans, Havacılık ve Uzay Mühendisliği Bölümü
Tez Yöneticisi : Y. Doç. Dr. Melin Şahin
Ortak Tez Yöneticisi : Dr. Volkan Nalbantoğlu
Haziran 2010, 101 sayfa

Bu çalışmada, akıllı bir kirişin titreşim özelliklerinin bulunmasında ve titreşim kontrolünde piezoelektrik yamaların etkinliği sunulmuştur. Akıllı kiriş olarak tanımlanmış yapı, piezoelektrik yamaların tek ucu tutturulmuş ve diğer ucu serbest olan alüminyum kirişin her iki yüzeyine simetrik olarak yapıştırılmasıyla oluşturulmuştur.

Çalışmanın ilk bölümünde, akıllı kirişin titreşim özellikleri piezoelektrik yamaların algılayıcı ve uyarıcı olarak kullanılmasıyla deneysel olarak araştırılmıştır. Akıllı kiriş darbe çekici ve piezoelektrik yama ile uyarılmış ve akıllı kirişin uyarıya cevabı piezoelektrik yamanın algılayıcı olarak kullanılmasıyla ölçülmüştür. Piezoelektrik yamanın etkinliğini karşılaştırmak amacıyla, akıllı kirişin uyarıya karşı cevabı, yaygın olarak kullanılan diğer tipte algılayıcılarla da ölçülmüştür.

Çalışmanın ikinci bölümünde, akıllı kirişin titreşim kontrolünde piezoelektrik yamaların algılayıcı ve uyarıcı olarak kullanılması çalışılmıştır. Bu amaçla, dört adet piezoelektrik yama uyarıcı olarak ve bir adet piezoelektrik yama da algılayıcı olarak seçilmiş, sistemin analitik modeli bulunmuştur. Tasarlanan gürbüz kontrolcü deneysel olarak uygulanmış ve titreşim

kontroloündeki performansı kirişin serbest ve ilk rezonans frekansındaki zorlanmış titreşim sonuçları ile gösterilmiştir.

Çalışmanın üçüncü bölümünde ise, akıllı kirişin titreşim kontrolünün kendiliğinden algılayıcı olan piezoelektrik uyarıcı yama ile sağlanması üzerine çalışılmıştır. Bir önceki çalışma ile benzer yol izlenerek, öncelikle kendiliğinden algılayıcı olan piezoelektrik uyarıcı yamalar ile analitik sistem modeli oluşturulmuş ve sonrasında aktif titreşim sönümlemesi için gürbüz kontrolcü tasarlanmıştır. Son olarak da, kendiliğinden algılayıcı olan piezoelektrik uyarıcı yamaların kullanılmasıyla elde edilen deneysel titreşim kontrolü sonuçları sunulmuştur.

Anahtar Kelimeler: Titreşim Sönümlemesi, Sistem Modellenmesi, Gürbüz Kontrol, Piezoelektrik Algılayıcı ve Uyarıcı, Kendiliğinden Algılayıcı Piezoelektrik Uyarıcı

Dedicated to my parents Tülay and İsmet.

ACKNOWLEDGMENTS

I gratefully thank my supervisor Asst. Prof. Dr. Melin Şahin and my co-supervisor Dr. Volkan Nalbantoğlu for their continuous support and wisdom. Throughout this study, Dr.Şahin and Dr.Nalbantoğlu helped and guided me for the first class of research work.

Asst. Prof. Dr. Melin Şahin opened my mind for experimental modal analysis and structural dynamics. Dr. Şahin's supervision, guidance and inspiration encouraged me to work on this thesis. I would like to thank for his guidance and friendship.

Dr. Volkan Nalbantoğlu supported me during my all graduate studies. Dr. Nalbantoğlu taught and guided me for robust control design and implementation. I would like to express my deepest appreciation to Dr. Nalbantoğlu for his encouragements and friendship.

I would like to thank Prof. Dr. Yavuz Yaman. During my undergraduate and graduate studies, Dr. Yaman enlightened me with his guidance and encouragements.

I would like to thank my company Havelsan and my colleagues for their understandings and support. I gratefully thank Turkish Aerospace Industries for valuable industrial experience during my first year of graduate study.

I want to acknowledge Dr. Kam Leang for his supervision, Yingfeng Shan for his friendship during my graduate studies at Virginia Commonwealth University. Dr. Leang taught me how to deal with electronics and work courageously and patiently. Dr. Leang gave me the opportunity to design and implement feedback and feedforward controllers for nano-positioning systems.

Finally, I would like to thank all of my friends and my family members, especially to my father İsmet and my mother Tülay. Throughout my life, they guided me for the truth way of living, learning and discovering.

TABLE OF CONTENTS

LIST OF TABLES

TABLES

LIST OF FIGURES

FIGURES

CHAPTER 1

INTRODUCTION

The common sources of mechanical stresses on aerospace structures are dynamic loads and in fact, dynamical load cycles can damage or cause a reduction in the service life of aerospace structures. Therefore, the investigation of vibration characteristics is an important design phase of aerospace structures which are frequently experiencing dynamic loading conditions. In essence, there are tremendous amounts of numerical and experimental studies focused on investigation of the vibration characteristics and attenuation of vibration levels of aerospace structures. When the frequency of the dynamic loading matches with the natural frequency of the structure, the resonance occurs, and it may cause severe structural vibrations. In this situation, severe vibrations may damage components of aerospace vehicles, as aerospace structures are mostly lightweight and have low-stiffness characteristics.

The undesirable effects of induced-vibration in aerospace vehicles can be exemplified by research studies for a fighter-jet, a helicopter and a satellite. Over the past decade, research studies showed that severe vibrations in the form of buffet can damage the components of a fighter-jet [1, 2]. Since flight envelope of fighter-jets includes many highly acrobatic maneuvers and certain speeds higher than the speed of sound, severe vibrations occur and may damage their components. The cracks in the components of fighter-jets may cost millions to be replaced and maintained. On the other hand, helicopters are the aerial vehicles whose structures are under dynamic loading in all flight envelopes because of their rotary elements such as main rotor, tail rotor and transmission units. Their cabin crew are exposed to the high levels of vibration in all flight zones and therefore, there are researches focusing on the investigation of vibration characteristics of a helicopter seat and effects on cabin crew health [3, 4, 5]. Among these studies, Chen et al. [5] mentioned that vibration at the helicopter seat causes excitation at the natural frequency of the spine and abdominal of the cabin crew

and exposition to these types of vibrations for long time causes variety of health problems on cabin crew. Satellites are other type of aerospace vehicles which are under dynamic loading during launch and in-orbit operations. The induced-vibrations may cause both reduction of the precision of pointing accuracy and cracks on the components of small satellites [6, 7].

Meanwhile, the effort on miniaturization of aerospace vehicles continues and the deployment of micro-vehicles depends on actuation mechanisms and controlling the vibration levels at minimal components of these type vehicles [8]. There are recent studies focused on undesirable effects of vibration and new design patterns of these micro-air vehicles [9, 10].

As a summary, the outcomes of vibration attenuation of aerospace vehicles can be listed as follows:

- Increasing the service life of aerospace structures,
- Decreasing ambient noise caused by vibratory-behavior structures of aerospace vehicles,
- Reducing pollution by increasing the efficiency of propulsion system of aerospace vehicle,
- Increasing the fuel efficiency of aerospace vehicle by reducing the drag caused by vibratory-behavior of structures,
- Increasing the precision pointing accuracy of aerospace vehicles such as satellites,
- Protection of the cabin crew and the avionics from the hazards of long-hour exposition to vibration environment.

It is obvious that vibration suppression of structures is very crucial for better, safer and easier life. Therefore, engineers are attempting to suppress such vibrations of structures by using passive and active methodologies. However, passive vibration suppression techniques are generally not suitable for low frequency applications [11]. Recently, active and adaptive vibration control are receiving considerable attention as alternative solutions to those passive methods. The technological advances in piezoelectric materials also motivate scientists and engineers to use these materials for the active vibration control as well. The atomic lattice structure of piezoelectric materials provides the transformation of mechanical deformation

into electric signal and vice versa [12]. This property of piezoelectric materials enables them to be used as an actuator and as a sensor. Besides, piezoelectric materials have various additional advantages of being lightweight, easy to implement, exhibiting good strain sensitivity and having high bandwidths [13]. Hence, they are offering effective solutions when used as patches in the active vibration suppression problems of flexible structures due to their direct (i.e. sensing) and converse (i.e. actuation) piezoelectric effects.

1.1 Background of the Study

This section presents literature review for this thesis. In the first section, piezoelectric materials for active systems are explained with historical perspectives. Research works focused on employment of piezoelectric materials as sensors, actuators and self-sensing actuators are exemplified with their successes and challenges in the different areas of technology and industry. In the second section, control methodologies for active vibration control are described. Finally, the research studies on smart structure applications conducted in the Department of Aerospace Engineering at Middle East Technical University are presented.

1.1.1 Piezoelectric Materials for Active Systems

Sensor and actuators based on piezoelectric materials have been widely used in different areas of technology and industry [8]. Today, piezoelectric materials are used for auto-focusing of camera lenses [14], reducing the vibration of a kitchen hood [15], increasing precision of nano-positioners [16, 17], active vibration control of aerospace structures [18]. Especially in active vibration control of structures, the piezoelectric ceramics are built as thin plates to be bonded on or embedded into structures to have smart and intelligent structures [19, 20]. The piezoelectricity which is used to make our lives easier, better and safer is discovered by Curie brothers in the last quarter of the 19^{th} century [21, 22]. Curie brothers correlated the direction of applied pressure and development of polar electricity in hemihedral crystals and this phenomenon is named as ”piezoelectricity” by Hankel [22]. Then, Lippmann who is awarded Nobel Prize in Physics found that imposition of electric charges causes mechanical deformation [22]. Eventually, Curies’ and Lippmann’s discoveries enabled piezoelectric materials to be employed as sensors and actuators. In the following sections, employment of piezoelectric material as actuators, sensors and self-sensing piezoelectric actuator are explained.

1.1.1.1 Piezoelectric Actuators

The transformation of electrical signal to mechanical deformation enables piezoelectric materials to be used as actuators. Since piezoelectric materials are very effective with their small elongation and large force capabilities, they are used as actuators in different industrial applications such as active vibration control [18], forming process [23], nano and micro robotics [24] and nano-positioning [16].

The aim of this research study is to use each piezoelectric patch bonded on the smart beam for excitation, disturbance, and disturbance rejection of the smart beam independently. The piezoelectric materials' actuation and sensing capabilities depend on the location where they are bonded to the host structure. Therefore, in order to effectively use piezoelectric materials' actuator capability for active vibration suppression, optimization studies were conducted for placements of piezoelectric actuators on different structures such as beams, plates etc. [25, 26, 27, 28, 29]. Bruant et al. [28] considered the minimization of mechanical energy for actuators and maximization of the state output of sensor. They found out that the optimal locations for piezoelectric actuator and sensor patches for a cantilever beam are fixed-end and very close to fixed-end. By choosing these locations, the effectiveness of piezoelectric sensor and actuator pair can be maximized for vibration suppression. Barboni et al. [25] also used an analytical approach in order to optimize the geometry and location of the piezoelectric patch on the cantilever-beam. Their research study focused on the structure's bending moment induced by the piezoelectric material. For this purpose, they modelled interaction of the beam and piezoelectric material by using pin-force model. Their results revealed that optimal locations of piezoelectric materials exist to maximize the authority over a certain mode of the structure. Meanwhile, Main et al. [27] explained that the stiffness of piezoelectric patch affects stiffness of the host structure. Authors also pointed out that in order to use piezoelectric patches effectively, the thickness of piezoelectric patch should also be considered. Halim et al. [26] conducted an analysis to find an optimal position for collocated sensors and actuators on a thin plate. Their research work focused on controllability of the structure by collocated sensors and actuators. Their maximum modal controllability approach claims that the optimal location for collocated piezoelectric actuator and sensor is the middle of the simply supported plate, however their spatial controllability approach's solution for optimal placement is near to the corner of the plate. The conclusion of this study is that the optimization study should

be conducted for the selected modes of the complex structures by using different modelling techniques.

As a conclusion for the review of the optimization studies for placement of piezoelectric materials, the common optimal solution for the location of the piezoelectric actuator and sensor is the near fixed-end due to the strain characteristics at the free and the first resonance frequency forced vibrations of the cantilever beam-like structures . The other remark is that the stiffness of the structure can be kept unaffected via keeping the thickness of the piezoelectric material less than the thickness of the structure.

1.1.1.2 Piezoelectric Sensors

In this study, piezoelectric material bonded on the smart beam is employed as a vibration sensor and its sensing capability is also verified by commercially available sensing devices. Besides, several researches have been conducted on structural health monitoring and damage identification by employing piezoelectric materials as sensors since the mechanical deformation of the piezoelectric material can be detected by its electrical response. Giurgiutiu et al. [30] identified seeded cracks and corrosion on aging-aircraft panels by employing piezoelectric materials as sensors. The piezoelectric wafer sensors were installed to the realistic panels and by using elastic wave propagation and electro-mechanical approaches, the damages were detected satisfactorily. Liberatore et al. [31] used piezoelectric material as a sensor and developed a new detection method for structural health monitoring of a simply supported beam. In this research work, structural faults were investigated by using piezoelectric sensor. It is concluded that the structural damage with its location can be detected by piezoelectric sensors. The results of these research studies also show that the sensing capability of piezoelectric materials enables them to be used as sensors for investigation of characteristics of the host structures. However, it is obvious that the verification of the sensing capability of the piezoelectric material should be studied before implementing them to real structures which is mentioned by Glaser et al. [32]. In their report, the smart materials and active sensing technology are reviewed and it is concluded that sensor confidence and failure shall be identified prior to employment in the structural health monitoring.

As the importance of piezoelectric material in structural health monitoring and intelligent systems increased, the electrical model of piezoelectric material has also been studied. For

instance, Guan and Liao [33] studied the specifications of piezoelectric materials for stand-alone and bonded to the structure cases. They constructed circuitry models of the piezoelectric materials and experimentally verified their models. It is found that the impedance of piezoelectric materials are very high at low frequencies and the behavior of the impendence with frequency reveals that piezoelectric materials behave like a capacitor. This behavior of the piezoelectric material enables them to be modelled as a voltage source and capacitor in self-sensing actuation configurations.

1.1.1.3 Self-Sensing Piezoelectric Actuators

The understanding of the behavior of piezoelectric materials bonded on structure leaded the usage of piezoelectric material as a sensor and an actuator simultaneously. The self-sensing actuation of piezoelectric materials provides the advantageous of usage of one piezoelectric material as a sensor and actuator at the same time. However, it has many drawbacks that are studied and solved by several researches. In fact, the key element of the self-sensing actuation is to build a special bridge circuit to decompose actuation and sensing signals of piezoelectric material.

In this thesis, piezoelectric material bonded on the smart beam is used as a self-sensing actuator in order to suppress vibration of the smart beam. The bridge circuit used in the microdispensing system by Putra et al. [34] is selected to be used in the self-sensing piezoelectric configuration for the active vibration suppression. Putra et al. satisfactorily used self-sensing piezoelectric actuator for trajectory tracking of an injector of the microdispensing system. In their research study, classical proportional-integral-derivative (PID) and adaptive feedforward controllers were designed and implemented for self sensing piezoelectric actuator for trajectory tracking and it is mentioned that the adaptive controller for self sensing piezoelectric actuator is needed to have better controller performance due to the uncertainties in the system.

Simmers et al. [35] studied uncertainties due to the variation of capacitance of piezoelectric material employed as a self-sensing actuator. The capacitance variation of the piezoelectric materials with environmental conditions is the primary cause of disruption of the balance of the bridge circuit. It is analytically and experimentally shown that the mismatches in the electrical model of the piezoelectric material causes unstabilities with negative feedback

controllers. In addition to these, it is stated that the order of resonances and anti-resonances in frequency response obtained via self-sensing actuator reveals the evidence of stability of the system. They experimentally showed that if the matched capacitance in the bridge circuit is selected greater than the capacitance of the piezoelectric material, the anti-resonance occurs before the resonance in the frequency response and it results in unstability of the self-sensing actuator with negative feedback controller.

1.1.2 Active Vibration Control via Piezoelectric Materials

The analytical model for the piezoelectric actuator is developed and verified experimentally for active vibration control by Crawley and Luis [36] in 1983. Their study showed that piezoelectric materials can be used effectively for vibration suppression and initiated the era of active vibration control via piezoelectric material. In the following sections, control design methodologies for different piezoelectric actuator and sensor configurations and literature review of robust control are presented.

1.1.2.1 Control Design Methodologies for Piezoelectric Sensors and Actuators

The attenuation of vibration levels of structures has many outcomes in different areas of our lives. Alkhatib and Golnaraghi [37] reviewed active vibration control strategies for civil and mechanical engineering applications. In their review paper, research studies conducted on active vibration control are classified according to their controller types as feedback and feedforward. It is mentioned that the accuracy of the model restricts the performance of the feedback controller, in contrast to this disadvantage, feedback controllers guarantee stability when the actuator and sensor are collocated. For feedforward controller, it is stated that controllers in this type can successfully suppress the vibration for a local region in frequency domain, yet they need high amount of real-time computations. The conclusion drawn from this review paper is that the design of active vibration control system should be specific for the type of vibration problem and tradeoff studies should be conducted for controller designs.

Flexible continuous systems have infinite-number of modes and if the controller is designed for finite-number of modes, it can cause unstabilities at high frequency modes when it is implemented to real structures and this effect is called as ”spillover effect” [38]. In order to

avoid this spillover effect, researchers proposed positive position feedback (PPF) controller for active vibration control since PPF controller rolls off at high frequencies [39] and does not cause spillover effects [40].

The other challenging issues of active vibration control via piezoelectric materials are the collocated sensor and actuators and also self-sensing actuators. Interlacing of poles and zeros occurs when the frequency response of the structure is obtained via collocated sensor and actuators. Integral resonant control is applied to a cantilever-beam like structure which has collocated piezoelectric sensor and actuators on it by Aphale et al. [41]. In order to solve the interlacing issue of the poles and zeros of the system, the addition of a feed-through term is proposed and changes in the system due to this addition is solved by negative feedback controller.

As also mentioned earlier, the challenges of active vibration control via self-sensing piezoelectric actuator have been studied and self-sensing piezoelectric actuator is used effectively in vibration suppression [35]. For example, Yang and Jeng [12] studied active vibration suppression via self-sensing piezoelectric actuator by the feedback controller. At first, the optimal location of self-sensing piezoelectric actuator was investigated by considering the maximum stiffness effect of actuator on structure and it is found that the best location is the near to the fixed-end of a cantilever beam. Then, they presented their strain rate circuit for using piezoelectric material as a sensor and an actuator simultaneously. After this, using a classical feedback controller, the effectiveness of self-sensing actuator for vibration suppression is presented. The unstable response of the controller is shown because of unbalanced bridge circuit, but these drawbacks are not considered in their controller design. Meanwhile, Zhang et al. [42] also built a circuit to sense the rate of strain and decompose the sensing and actuation signals. They investigated the issues with self-sensing piezoelectric actuator for active vibration suppression for a clamped plate. By considering the parametric uncertainty in the compensator circuit, they designed a robust controller via μ synthesis. It is presented that the μ synthesis can be used to design a robust controller via self-sensing piezoelectric actuator, however the stability of the controller is not well guaranteed.

1.1.2.2 Robust Control Design

Zhou et al. [43] named robust control as the best blend of classical control and modern control theories since robust control design methodology offers many advantageous compared to other feedback control techniques for robust stability and performance. Historical aspects of robust controller design methodologies with its role in active vibration control are reviewed in this section.

Almost three decades ago, Zames [44] described the plant uncertainty and sensitivity reduction as an optimization problem and presented a systematic solution to feedback controller design problems by introducing weighted seminorms and approximate inverses. This research of Zames is the first spark of studies regarding to the design of feedback controller by minimizing the H_∞ norm of a closed loop transfer function. Francis [45], Glover [46] and Doyle [47] presented results for state-space formulations for H_∞ controller problems and it is showed that the solution of algebraic Riccati Equation leads to the solution of state-feedback H_∞ problem [43]. After the μ analysis is introduced by Doyle, the performance of H_∞ controller is assessed and μ analysis with H_∞ controller became a popular and reliable technique to design and assess the controller.

H_∞ controller has been used for active vibration control of flexible structures [37]. The vibration suppression of the high speed flexible linkage system was conducted with piezoelectric sensor and actuator via H_∞ controller by Zhang et al. [48]. In their study, high frequency dynamics of the flexible linkage system is considered as an uncertainty in the system and the effectiveness of the robust H_∞ controller is numerically shown.

Active vibration control of a plate is achieved via H_∞ controller by Seto and Kar [49]. In their study, analytical model of the plate is estimated as lumped mass with a three degree of freedom. They implemented the designed H_∞ controller and demonstrated active vibration suppression of the plate experimentally.

Regarding the research studies on smart structure applications in the Department of Aerospace Engineering at Middle East Technical University, H_∞ and μ controllers are designed and μ analysis are used to suppress the vibration of the smart structures [18, 50]. The details of these research studies are presented in the next section.

1.1.3 Research Studies on Smart Structure Applications in the Department of Aerospace Engineering at Middle East Technical University

Sahin et al. [18] presented theoretical and experimental studies on investigation of vibration characteristics and active vibration control in Aerospace Engineering Department of Middle East Technical University. The structures used in these studies are cantilever-beam like and plate-like structures called as smart beam and smart fin respectively. The theoretical studies are conducted in order to optimize the location of piezoelectric materials, to determine maximum admissible actuation value for piezoelectric material and to find out the effect of bonding piezoelectric materials to host cantilever-beam like and plate-like structures. Furthermore, the experimental studies are carried out to demonstrate effectiveness of active vibration suppression via designed controllers [18]. For experimental studies, piezoelectric materials were used as actuator while laser displacement sensor and strain gages were employed as sensors.

Caliskan [20] presented finite element approach for investigation of static and dynamic behaviors of the smart structures. He underlined that finite element approach is a very effective analysis tool for bonded piezoelectric materials when thermo-mechanical-electrical specifications of piezoelectric material are included. For a cantilever-beam, Yaman et al. [51] pointed out that the piezoelectric materials have more actuation ability as they are placed closer to clamped-end and selected bigger in size.

Ulker [52] designed H_∞ and μ controllers for active vibration suppression of smart beam and smart fin for free and forced vibration. In the framework of Ulker [52] studies, experimental demonstration of active vibration control were conducted by building experimental setups and implementing controllers. Ulker [52] showed that H_∞ and μ controllers can satisfactorily suppress free and forced vibrations of smart beam and smart fin while piezoelectric materials are used as actuators, laser displacement sensor and strain gages are employed as vibration sensors.

Kircali [53] worked on a spatial H_∞ controller for active vibration suppression of a smart beam. The aim of spatial H_∞ controller is to suppress the vibration over the entire structure in a spatial sense. In his research work, Kircali [53] used piezoelectric material as actuator and laser displacement sensor as the sensor and also used assumed-modes technique in order to acquire spatial model of the smart beam. He designed and implemented spatial H_∞ controller

and also designed pointwise H_∞ controller to compare the effectiveness of the controllers. Kircali et al. [50] pointed out that designed spatial H_∞ controller can effectively suppress the first two flexural modes of the smart beam.

Karadal [54] studied active flutter suppression of the smart fin by considering unsteady aerodynamic loads on the structure. He obtained numerical model of piezoelectric patches bonded on smart fin and a state-space representation of the aeroelastic model of smart fin. Using the state-space model, he designed H_∞ controller by using parametric uncertainty and concluded that H_∞ controller via piezoelectric actuator can be used in order to suppress flutter of a smart fin.

1.2 Motivation of the Study

In the former research studies [18] piezoelectric materials are employed for active vibration suppression of cantilever-beam like and plate-like structures. In these studies, piezoelectric materials are used as actuators; and strain gauges and laser displacement sensor are chosen as sensing devices. In this particular study, piezoelectric materials are used as sensors [55, 56], actuators [55, 56] and self-sensing actuators [57] for the investigation of vibration characteristics and active vibration suppression of a smart beam by also evaluating the performances of each piezoelectric sensor/actuator configurations.

1.3 Objectives of the Study

The objectives of this thesis are stated as follows:

- employment of piezoelectric patches on smart beam as a sensor,
- investigation of vibration characteristics of smart beam by piezoelectric patches,
- verification of vibration characteristics of smart beam obtained from piezoelectric patches by comparing them with commercially available off-the-shelf sensors,
- obtaining the analytical model of smart beam by piezoelectric sensor/actuator pair,
- design a robust controller by using piezoelectric sensor/actuator pair via experimentally obtained uncertainties,

- performance demonstration of the designed controller on free and forced vibration,
- employment of piezoelectric patches on smart beam as a self-sensing piezoelectric actuator,
- obtaining the analytical model of smart beam by self-sensing piezoelectric actuator,
- design a robust controller by using self-sensing piezoelectric actuator pair via experimentally obtained uncertainties,
- performance demonstration of the designed controller on free and forced vibration,
- evaluation and comparison of each piezoelectric sensor/actuator configuration from the active vibration control point of view.

1.4 Outline of the Study

The organization of this thesis is as follows:

In Chapter 2, vibration characteristics of a smart beam are obtained by employing piezoelectric patches as sensors and actuators. Excitation of smart beam is conducted by either impact hammer or piezoelectric patch and the response of the smart beam under these excitations is measured by piezoelectric patches used as sensors. Frequency responses of the system are then obtained for each configuration. In addition to these, modal analysis results of each configuration are compared to that of obtained from single axis accelerometer and laser displacement sensor.

In Chapter 3, active vibration suppression of the smart beam via piezoelectric sensor/actuator pair is considered. The experimental model of the smart beam is obtained by using piezoelectric patches as sensors and actuators and through this experimental model, a robust controller is designed for the active vibration control of the smart beam. After implementing the designed robust controller, the performance of this controller via piezoelectric sensor/actuator pair is experimentally demonstrated for free and the first resonance forced vibrations of the smart beam.

In Chapter 4, piezoelectric patches are employed as self-sensing actuators in the active vibration control of the smart beam. In this configuration, piezoelectric material is used as an

actuator and a sensor simultaneously. A bridge circuit comprising the electrical model of the piezoelectric material is designed in order to decompose the sensing and actuation signals. An experimental model of the smart beam is also obtained by using the aforementioned self-sensing actuator configuration and following the same approach used in piezoelectric sensor/actuator pair configuration, a robust controller is designed for the active vibration suppression of the smart beam via self-sensing piezoelectric actuators. Afterwards, the designed controller for self-sensing piezoelectric configuration is experimentally implemented. Finally, the performance of controller via self-sensing piezoelectric actuator is presented in a way to compare with the one designed by using piezoelectric sensor/actuator pair.

In Chapter 5, the outcomes of this thesis are discussed and research problems are proposed for future work.

Finally in Chapter 6, the concluding remarks are presented.

CHAPTER 2

INVESTIGATION OF VIBRATION CHARACTERISTICS OF A SMART BEAM VIA PIEZOELECTRIC PATCH

2.1 Introduction

In this chapter, vibration characteristics of the smart beam is investigated by employment of piezoelectric patches (SensorTech BM500 [58]) as sensors and actuators. At first, the excitation of smart beam is performed by an impact hammer and the response of smart beam to this excitation is measured by using two piezoelectric patches located at different positions on smart beam. Having the purpose of evaluating the performance of piezoelectric patch in sensing by comparing with commercially available sensing devices (single axis accelerometer and laser displacement sensor), the response of smart beam to the impact hammer excitation is also monitored by these sensing devices. In further experimental studies, the piezoelectric patch is employed as an actuator to excite the smart beam. Similar to the previous configuration, the response of the smart beam is again measured by two piezoelectric patches located at different positions and also commercially available sensing devices. The time records of excitation and response signals are gathered by data acquisition device (Brüel and Kjær PULSE 3560C [59]) and the vibration characteristics of smart beam is obtained. For each measurement, sample time record and frequency response function are presented. By comparing the first three modes of the smart beam, the performance of piezoelectric patch in the investigation of vibration characteristics is studied with the effect of locations of piezoelectric patches for actuation and sensing. Finally, the effect of bimorph configuration of piezoelectric patches is presented.

2.2 Smart Beam

The smart beam in Figure 2.1 is a cantilever aluminium beam (490 x 51 x 2 mm) with eight surface bonded SensorTech - BM500 [58] piezoelectric (PZT, Lead - Zirconate -Titanate) patches (25 x 20 x 0.5 mm) which is shown in Figure 2.2. A thin isolation layer is placed between the aluminium beam and piezoelectric patches so that each piezoelectric patch may be employed as a sensor and an actuator independently.

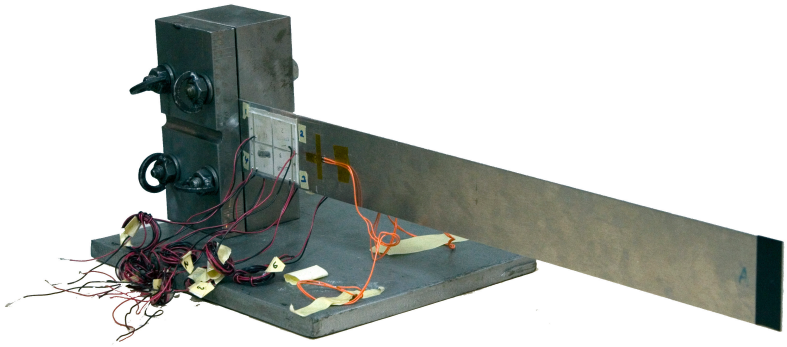

Figure 2.1: Smart Beam

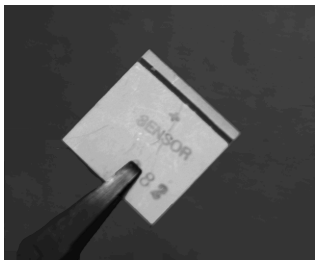

Figure 2.2: Piezoelectric Patch (SensorTech - BM500 PZT Patch)

In this thesis, piezoelectric patches are labeled according to their positions on each surface of the aluminium beam (Figure 2.3). On surface A, piezoelectric patches are labeled from 1 to 4 in clockwise direction and on surface B, it is labeled from 1 to 4 in counter-clockwise direction. Piezoelectric patches are identified by numbers and associated surface codes, such as piezoelectric patch 1A.

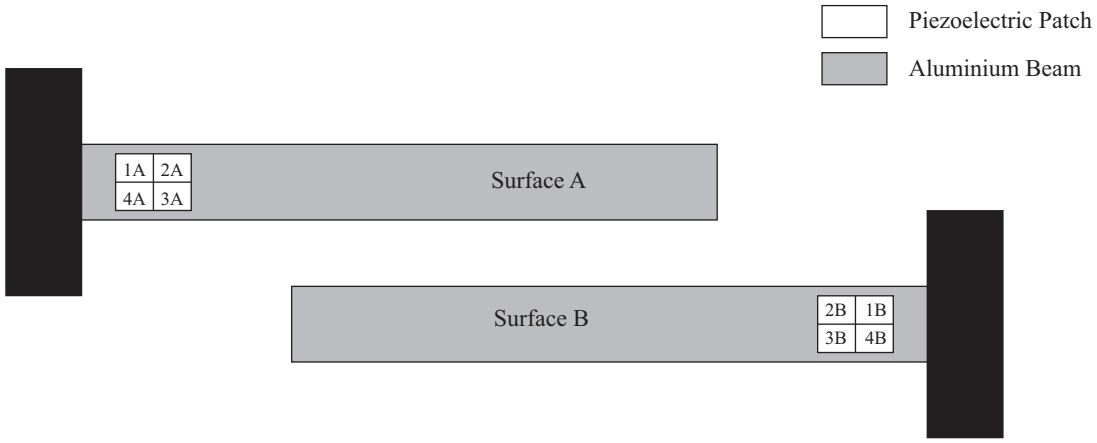

Figure 2.3: Piezoelectric Patches on Smart Beam

2.3 Excitation of Smart Beam via Impact Hammer

In this section, investigation of vibration characteristics of the smart beam is performed by using impact hammer for the excitation and measuring the response of the smart beam by single-axis accelerometer, laser displacement sensor and piezoelectric patches (1B and 4A) separately. The Brüel and Kjær Impact Hammer 8206 [60] is used to excite and measure impact forces on the smart beam. The impact location is at the center of the beam along the cantilever-to-free end shown in Figure 2.4.

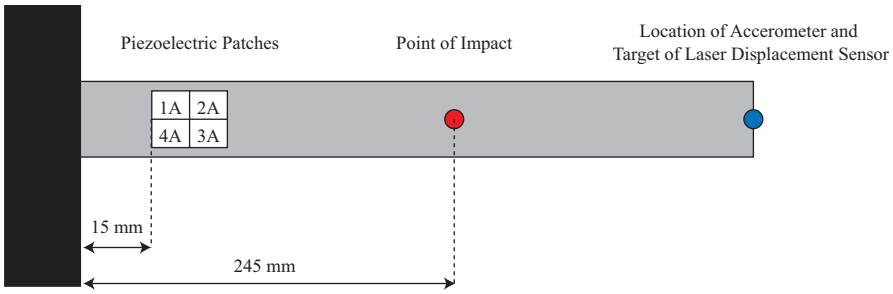

Figure 2.4: Location of Impact Hammer and Sensing Devices on Smart Beam

Experimental setup for impact hammer excitation is presented in Figure 2.5. In this figure, the excitation and sensing devices are shown with their corresponding measurement locations on the smart beam. Each sensing device is used individually in four different modal tests to measure the response of the smart beam to impact hammer excitation. Brüel and Kjær Pulse Data Acquisition System 3560C is used to record impact forces and corresponding response signals.

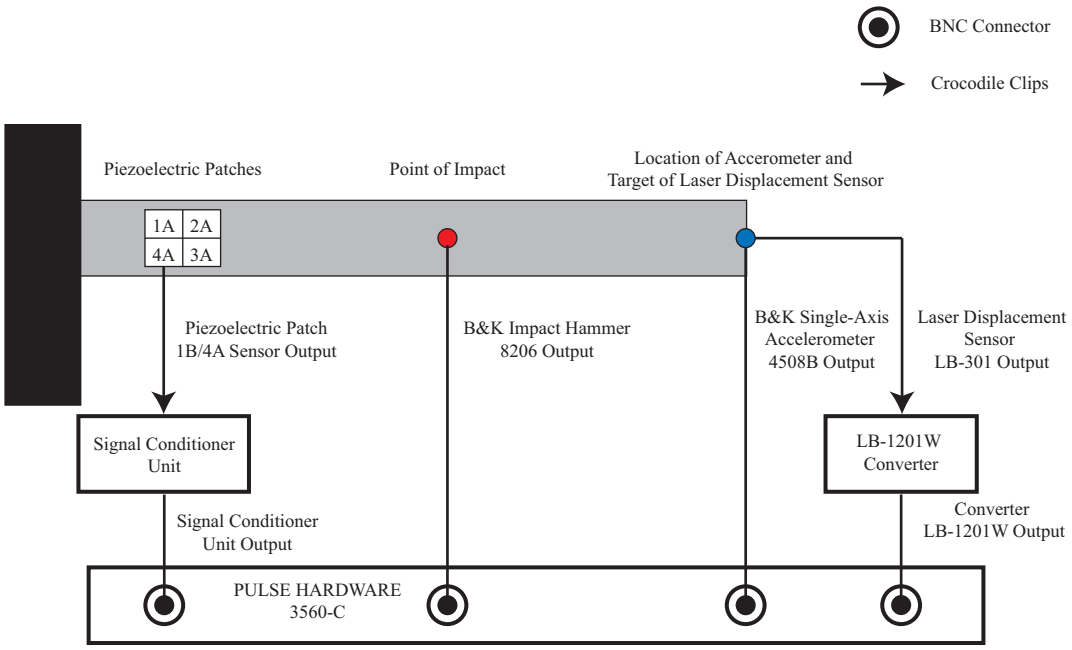

Figure 2.5: Experimental Setup for Impact Hammer Excitation

The impact hammer is supplied with aluminium tip. For high bandwidth of the excitation and small duration of impact, aluminium tip is selected and used with the impact hammer. Throughout the analysis, PULSE Modal Test Consultant (MTC) software [61] is used with a frequency span of 0 - 200 Hz with 0.125 Hz resolution. For each measurement device, the excitation by the impact hammer is conducted five times and then the resulting frequency response is obtained via mentioned software by linear averaging five frequency response estimates. The objective of averaging is to have an accurate and reliable final frequency response [62]. Analysis properties for modal analysis software are listed in Table 2.1.

Table 2.1: Analysis Setup Configuration for Impact Hammer

Analyzer Property	**Value/Type**
Frequency Span	0 Hz - 200 Hz
Number of Lines	1600 lines
Number of Averages	5 Averages
Averaging Mode	Linear
Analysis Mode	Baseband

2.3.1 Single-Axis Accelerometer

The response of smart beam to impact force is monitored by single-axis accelerometer. Brüel and Kjær 4508B accelerometer [63] with its mounting clip is attached to the structure with a thin layer of wax. The attachment location of the accelerometer is at the free end along the center line of the smart beam and is also shown in Figure 2.4.

Impact force is applied to the smart beam by the impact hammer and the response of the smart beam to this particular excitation is measured. The excitation and response signals are then recorded by Brüel and Kjær PULSE 3560C platform and the frequency response function is derived using these recorded signals. Figure 2.6 shows a sample of recorded signals and Figure 2.7 shows the frequency response for excitation performed by impact hammer and response measured by accelerometer.

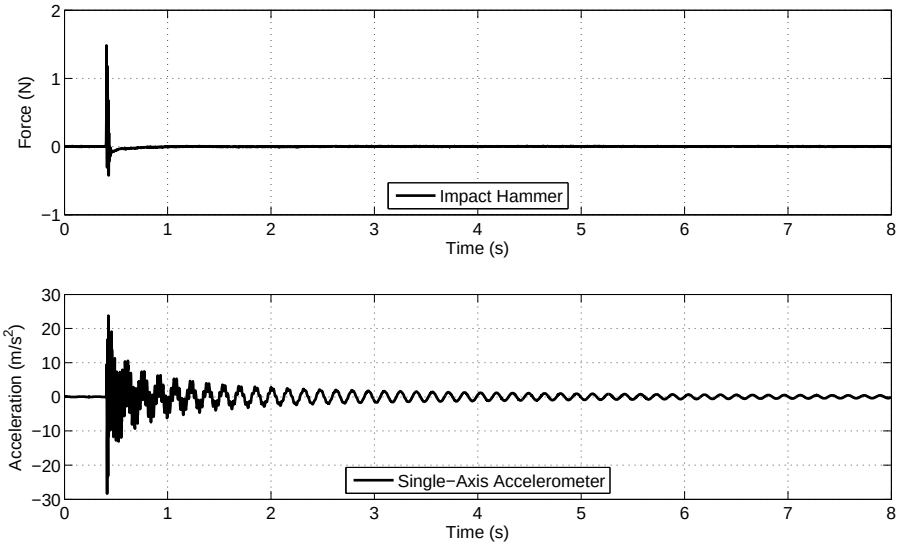

Figure 2.6: Sample Time Records of Impact Force and Acceleration

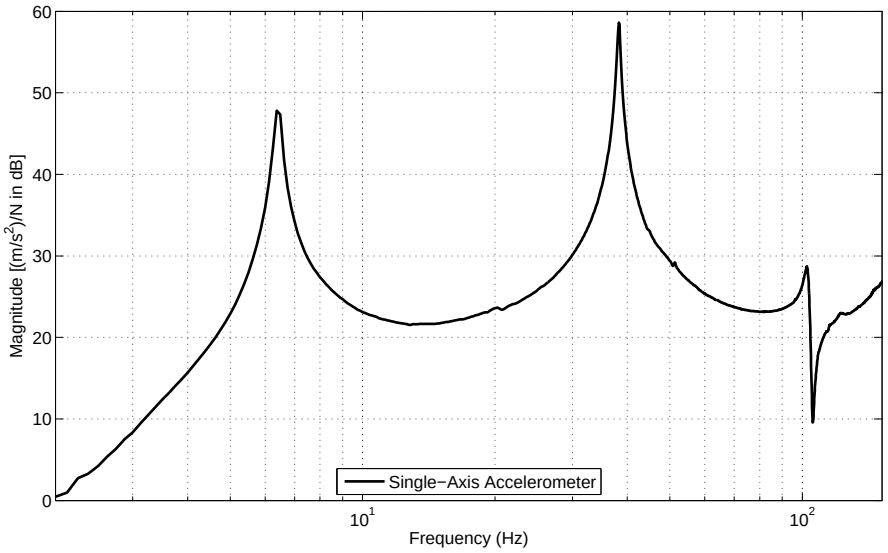

Figure 2.7: Frequency Response Obtained by Impact Hammer and Accelerometer

2.3.2 Laser Displacement Sensor

The response of smart beam to impact force is monitored by Keyence LB-1201(W) LB-301 Laser Displacement Sensor [64]. The target of laser displacement sensor is the free end along the center line of smart beam as shown in Figure 2.4. The tip displacement of smart beam is measured by LB-301 laser displacement sensing device and the output signal of sensing device is converted to a calibrated voltage value by LB-1201(W) converter. The experimental setup for displacement measurement of the tip of the smart beam is presented in Figure 2.5. The excitation and response signals are recorded Brüel and Kjær PULSE 3560C platform and the frequency response function is derived using the recorded signals in a same way in aforementioned single-axis accelerometer case. Figure 2.8 shows a sample of recorded signals and Figure 2.9 shows the resulting frequency response of the smart beam obtained by impact hammer and laser displacement sensor.

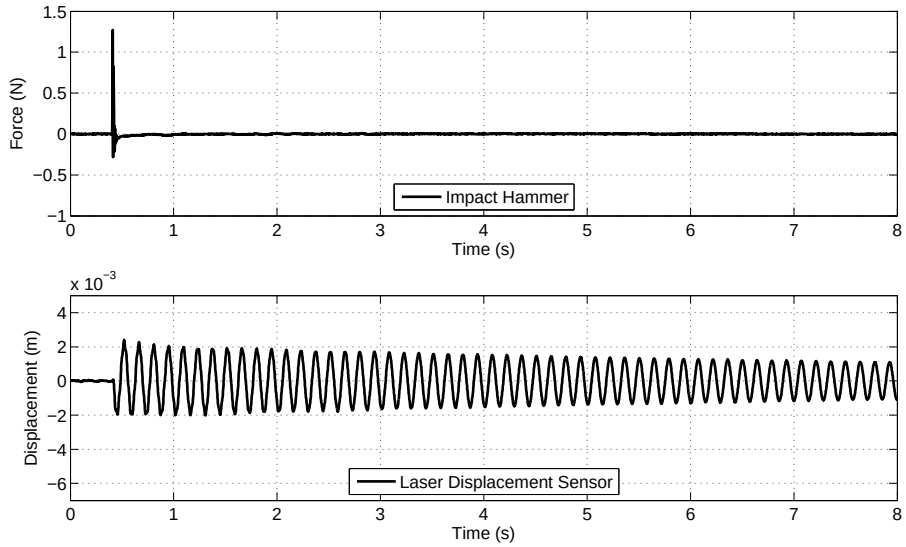

Figure 2.8: Sample Time Records of Impact Force and Tip Displacement

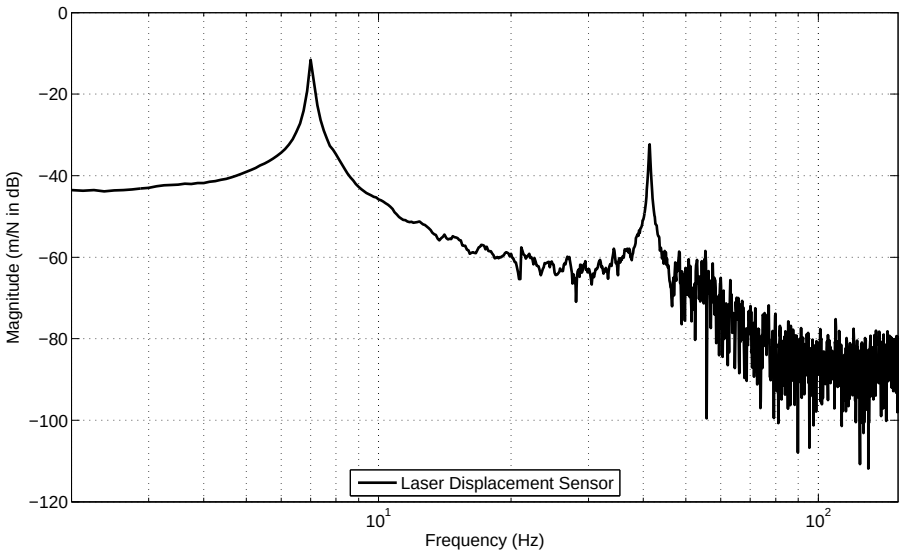

Figure 2.9: Frequency Response Obtained by Impact Hammer and Laser Disp. Sensor

2.3.3 Piezoelectric Patch as Sensor

The excitation of smart beam is performed by an impact hammer and the response of smart beam to this excitation is measured by using two piezoelectric patches at different locations on the smart beam. Piezoelectric materials have high impedance values at low frequencies. When this high impedance value is higher than the input of data acquisition system, the voltage of piezoelectric patch is not monitored successfully. In order to avoid this circumstance, a signal conditioner circuit should be used. For this purpose, an inverting voltage amplifier circuit is designed and used, the details can be found in Appendix A.

2.3.3.1 Piezoelectric Patch 1B

The response of smart beam to impact force is measured by piezoelectric patch 1B. The output of piezoelectric patch 1B is connected oppositely to the inverting voltage amplifier circuit and the output of voltage amplifier circuit is transferred to Brüel and Kjær PULSE 3560C platform. The excitation and response signals are also recorded and the frequency response function is derived by using the recorded signals as formerly presented in acceleration and displacement measurements. The sample of recorded excitation and response signals are presented in Figure 2.10 and the frequency response obtained by conducting impact hammer tests and measuring the response by piezoelectric patch 1B is given in Figure 2.11.

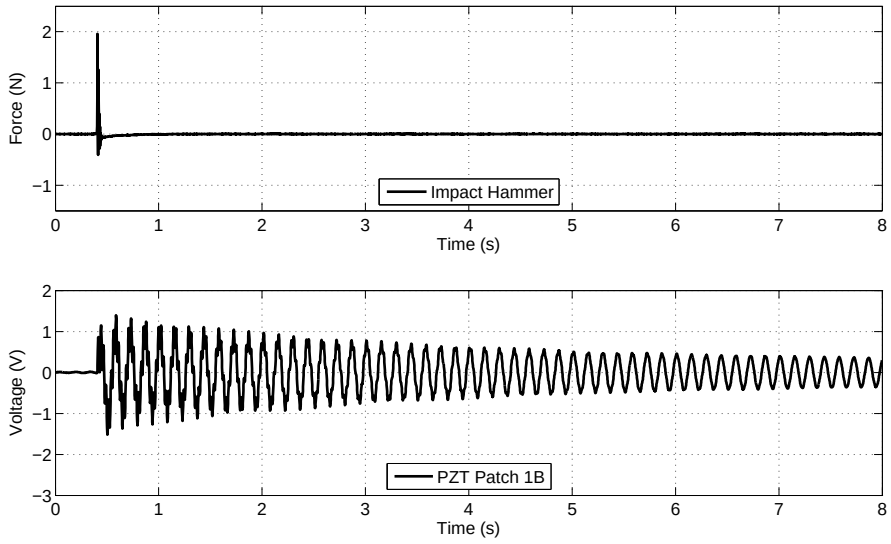

Figure 2.10: Sample Time Records of Impact Force and Piezoelectric Patch 1B

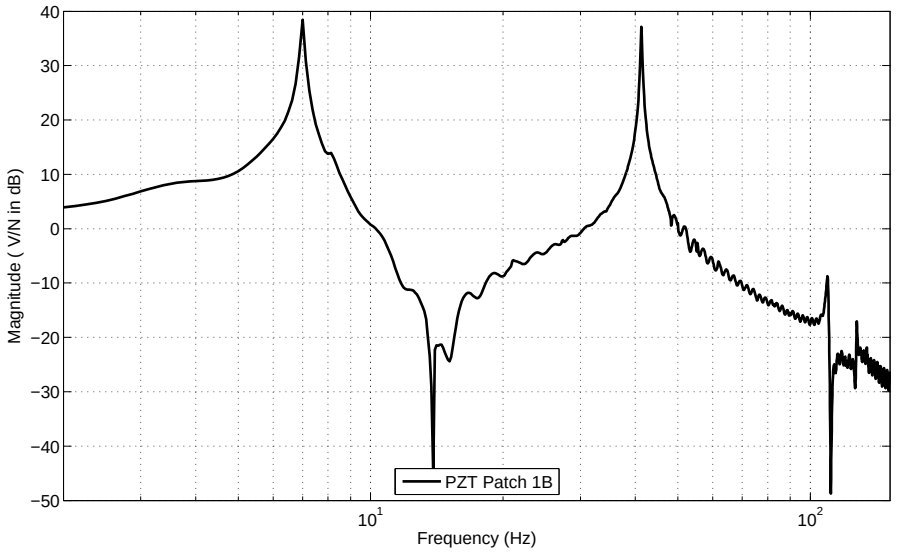

Figure 2.11: Frequency Response Obtained by Impact Hammer and Piezoelectric Patch 1B

2.3.3.2 Piezoelectric Patch 4A

The impact force is applied to the smart beam and the response of smart beam to this associated excitation is measured by piezoelectric patch 4A. The prementioned configuration in piezoelectric patch 1B is also used for piezoelectric patch 4A. The output of piezoelectric patch 4A is connected to the voltage amplifier circuit and the output of voltage amplifier circuit is transferred to Brüel and Kjær PULSE 3560C platform. Figure 2.12 shows a sample of recorded signals and Figure 2.13 presents the resulting frequency response gathered by impact hammer and piezoelectric patch 4A.

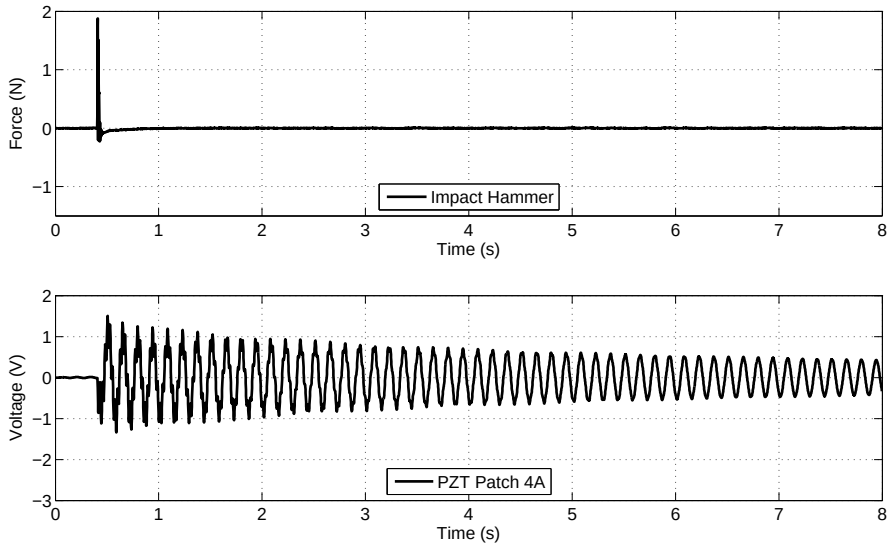

Figure 2.12: Sample Time Records of Impact Force and Piezoelectric Patch 4A

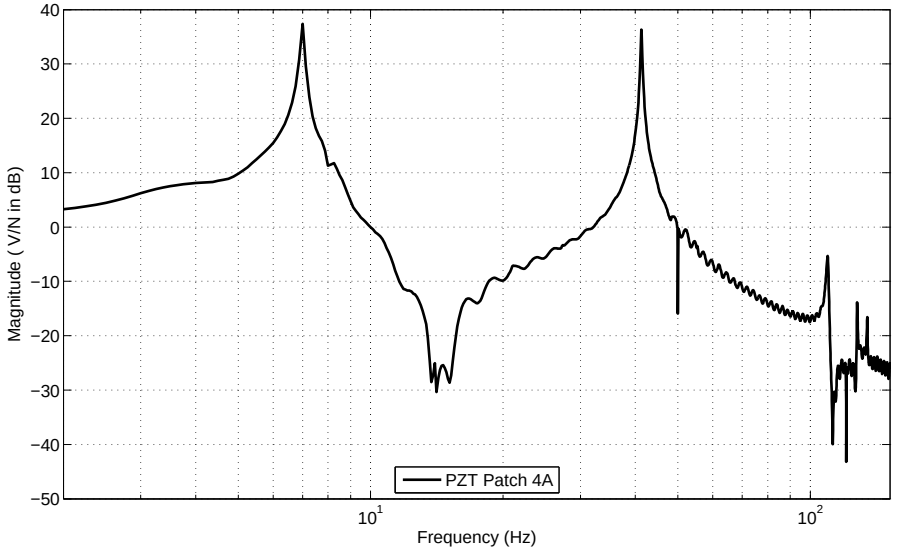

Figure 2.13: Frequency Response Obtained by Impact Hammer and Piezoelectric Patch 4A

2.3.4 Results of Excitation of Smart Beam via Impact Hammer

The experimentally obtained first three resonance frequencies are listed in Table 2.2. As mentioned earlier, each sensing device is used separately to measure the response of the smart beam. The first three resonance frequencies acquired by using single-axis accelerometer is lower than the results of non-contact laser displacement sensor. These differences in resonance frequencies point that the additional mass of accelerometer adversely affects the investigation of vibration characteristics of smart beam as a reduction in resonance frequencies. However, there is a disadvantage of using laser displacement sensor which has high frequency noise. Due to the noise at high frequencies in frequency response (Figure 2.9), the third resonance frequency is not acquired. On the other hand, the first and second resonance frequencies acquired by piezoelectric patches are identical with the results of laser displacement sensor. Moreover to this, the third resonance frequency is also acquired by piezoelectric patches. These results show that vibration characteristics of smart beam are satisfactorily investigated via piezoelectric sensor under impact hammer excitation.

Table 2.2: Resonance Frequencies of Smart Beam Obtained via Impact Hammer Excitation

	Resonance Frequencies [Hz]			
Mode No	Accelerometer	Laser Displacement Sensor	Piezoelectric Patch 1B	Piezoelectric Patch 4A
1st Bending	6.375	7.000	7.000	7.000
2nd Bending	38.250	41.250	41.250	41.250
3rd Bending	102.375	Not observed	109.375	109.500

2.4 Excitation of Smart Beam via Piezoelectric Patch

In this section, vibration characteristics of smart beam is investigated by using piezoelectric patches as actuator for the excitation and the response of smart beam is measured by single-axis accelerometer, laser displacement sensor and piezoelectric patches (1B and 4A). Piezoelectric patch 1A is excited with 150 V peak-to-peak sinusoidal signal within the bandwidth of 2 Hz and 152 Hz. This swept-sine signal is generated by signal generator HP33120A [65] and amplified 30 times by SA10 high voltage amplifier [66]. SA21 high voltage power supply is used to supply power for SA10 high voltage amplifier. The experimental setup for this configuration is shown in Figure 2.14.

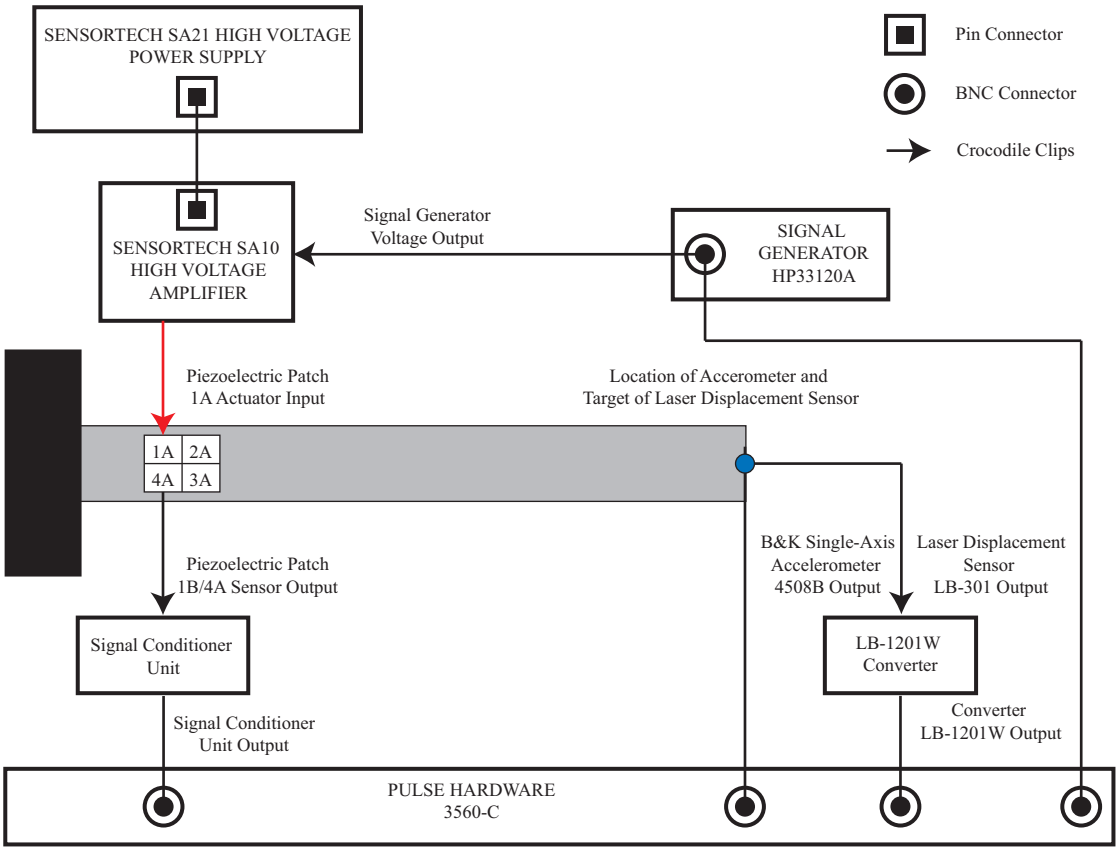

Figure 2.14: Excitation Configuration for Piezoelectric Patch

Output signal of the signal generator and output responses of the sensing devices are connected to PULSE 3560C data acquisition system and frequency response functions are derived [61]. This analysis properties are listed in Table 2.3.

Table 2.3: Analysis Setup Configuration for Piezoelectric Patch

Analyzer Property	**Value/Type**
Frequency Span	0 Hz - 200 Hz
Number of Lines	1600 lines
Number of Averages	125 Averages
Duration of Analysis	325.3 seconds
Averaging Mode	Linear
Analysis Mode	Baseband
Overlap Ratio	%66.67

2.4.1 Single-Axis Accelerometer

The response of the smart beam under excitation of piezoelectric patch is monitored by single-axis accelerometer. As in Section 2.3.1, Brüel and Kjær 4508B accelerometer with its mounting clip is attached to the structure with a thin layer of wax to the free end along the center line of smart beam which is shown in Figure 2.4.

Using the data acquisition platform, the excitation and response signals are recorded simultaneously and the frequency response is derived from the recorded data. Figure 2.15 shows a sample of recorded signals for analysis time period (8 seconds) and Figure 2.16 shows the averaged frequency response for excitation by piezoelectric patch 1A and response measurement by accelerometer.

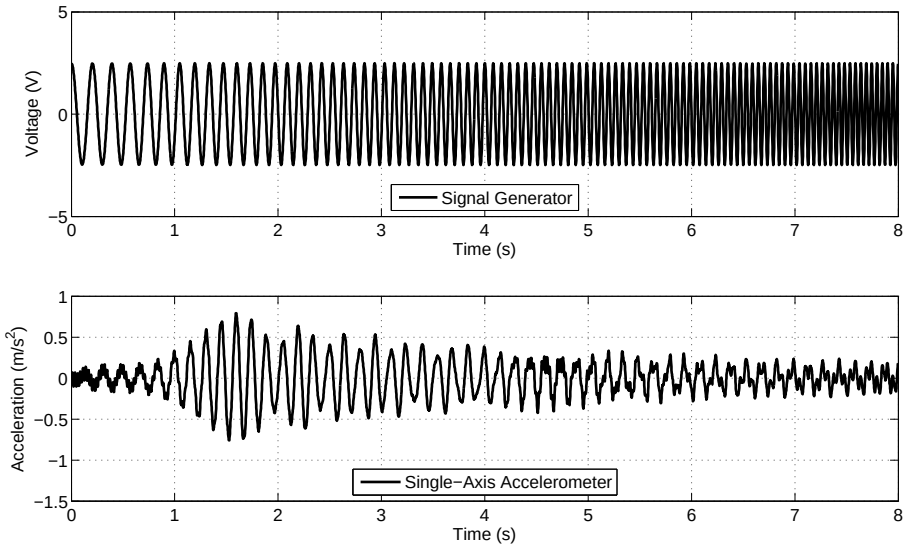

Figure 2.15: Sample Time Records of Signal Generator and Accelerometer

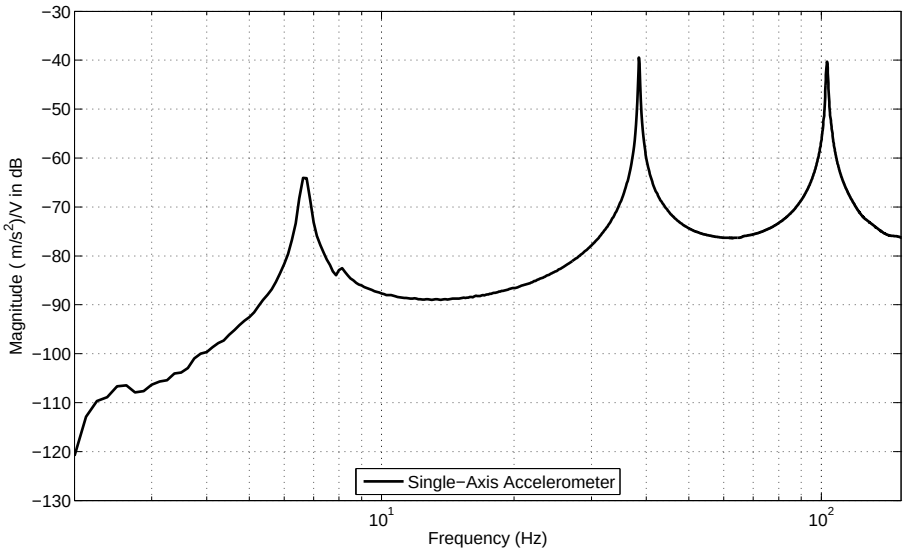

Figure 2.16: Frequency Response Obtained by Piezoelectric Patch 1A and Accelerometer

2.4.2 Laser Displacement Sensor

The response of smart beam to excitation with piezoelectric patch 1A is measured by Keyence LB-1201(W) LB-301 Laser Displacement Sensor. As in Section 2.3.2, the target of laser displacement sensor is the free end along the center line of smart beam shown in Figure 2.4. The excitation and response signals are recorded by Brüel and Kjær PULSE 3560C platform and the frequency response function is derived using the recorded signals as in prementioned experiments. Figure 2.17 shows a sample of recorded signals and Figure 2.18 shows the frequency response obtained from the excitation by piezoelectric patch 1A and the response measurement by laser displacement sensor.

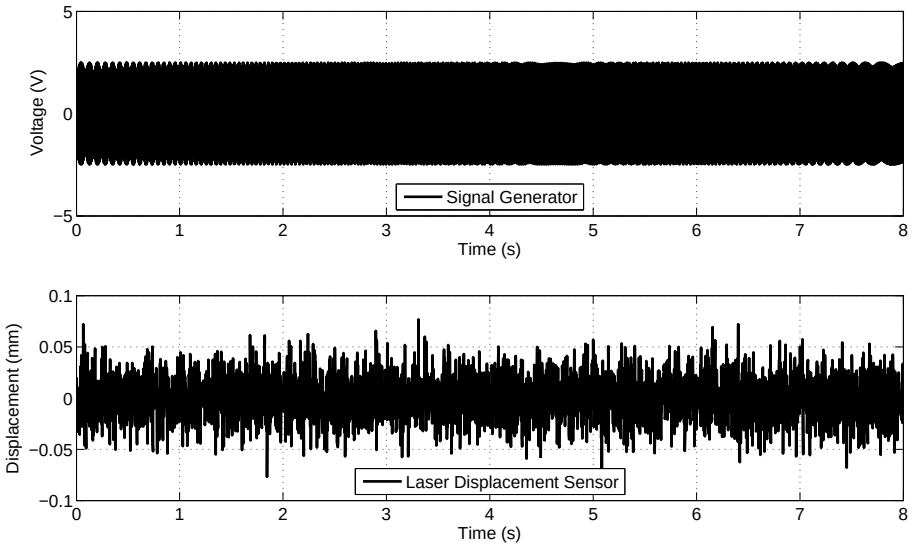

Figure 2.17: Sample Time Records of Signal Generator and Laser Displacement Sensor

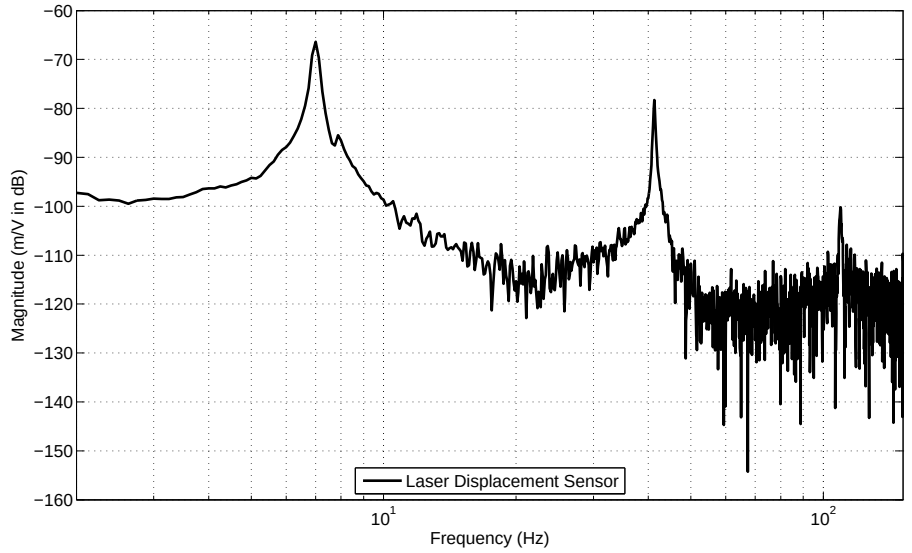

Figure 2.18: Frequency Response Obtained by Piezoelectric Patch 1A and Laser Displacement Sensor

2.4.3 Piezoelectric Patch as Sensor

The response of smart beam to excitation with piezoelectric actuator is measured by using two piezoelectric patches (1B and 4A) located at different positions on smart beam. Signal conditioner circuit in Figure A.1 is used to transfer output of piezoelectric patch 1B and 4A to data acquisition platform.

2.4.3.1 Piezoelectric Patch 1B

The voltage of piezoelectric patch 1B is recorded simultaneously with signal generator output by data acquisition platform. Using the recorded signals, the frequency response between piezoelectric patch 1B and piezoelectric patch 1A is acquired. A sample recorded signal for 8 seconds is shown in Figure 2.19 and Figure 2.20 shows the averaged frequency response obtained from the excitation signal for piezoelectric patch 1A and response measurement by piezoelectric patch 1B.

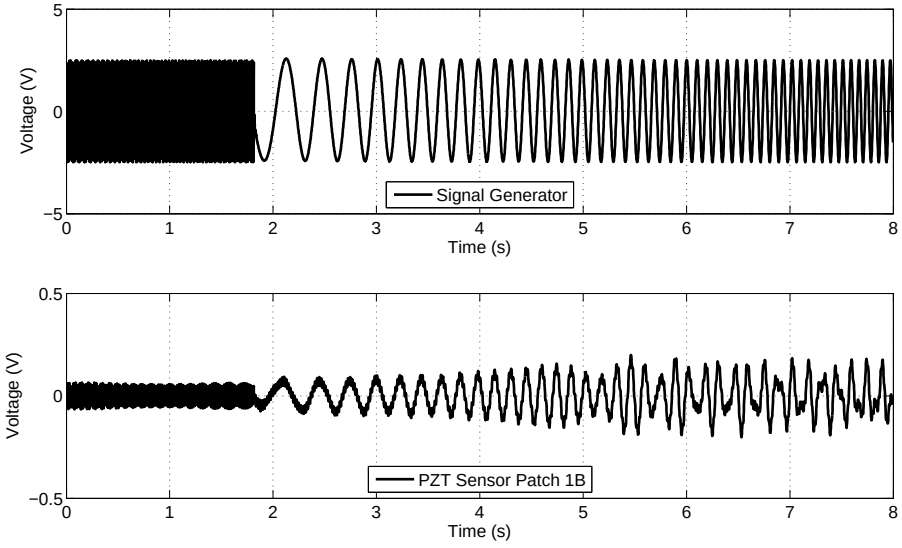

Figure 2.19: Sample Time Records of Signal Generator and Piezoelectric Patch 1B

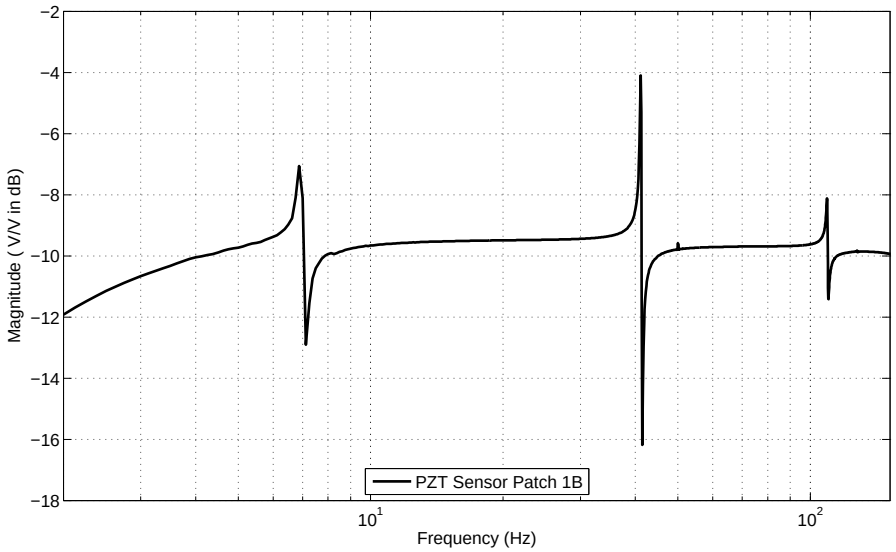

Figure 2.20: Frequency Response Obtained by Piezoelectric Actuator Patch 1A and Piezoelectric Sensor Patch 1B

2.4.3.2 Piezoelectric Patch 4A

As in piezoelectric patch 1B, the voltage of piezoelectric patch 4A is recorded simultaneously with signal generator output by data acquisition platform by using signal conditioner circuit. Then, the frequency response between piezoelectric patch 4A and piezoelectric patch 1A is acquired. Figure 2.21 presents again a sample time recorded of signals and Figure 2.22 shows the frequency response gathered from the excitation signal of piezoelectric patch 1A and response measurement from piezoelectric patch 4A.

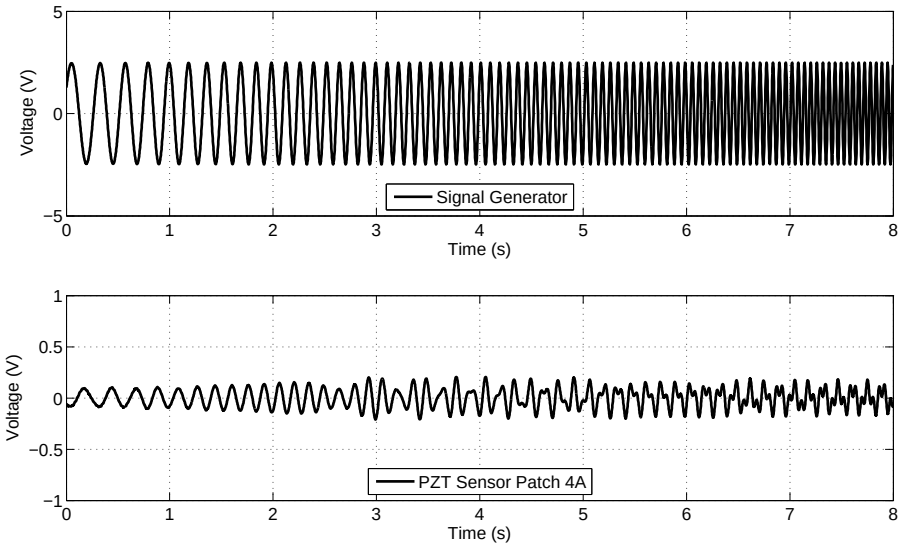

Figure 2.21: Sample Time Records of Signal Generator and Piezoelectric Sensor Patch 4A

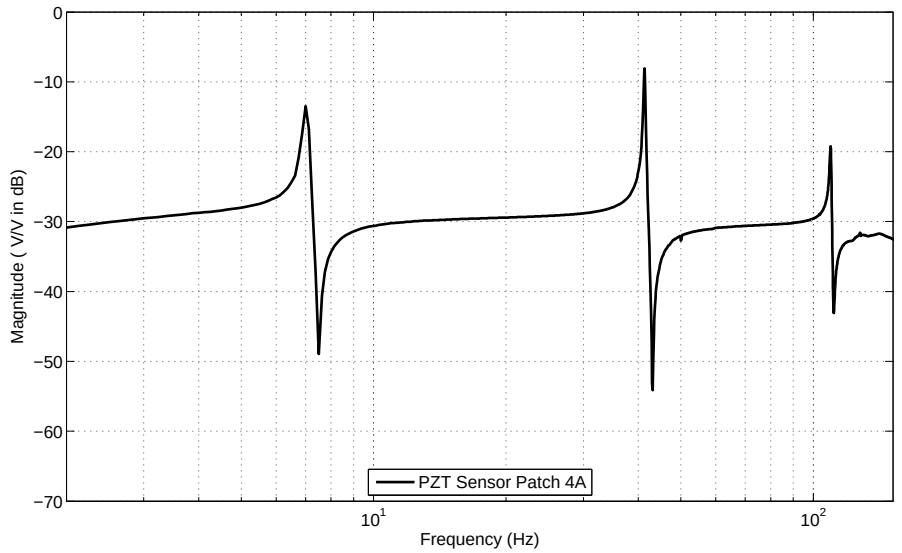

Figure 2.22: Frequency Response Obtained by Piezoelectric Actuator Patch 1A and Piezoelectric Sensor Patch 4A

2.4.4 Results of Excitation of Smart Beam via Piezoelectric Actuator

The experimentally obtained first three resonance frequencies are listed in Table 2.4. The first three resonance frequencies acquired by using single-axis accelerometer is lower than the results of non-contact laser displacement sensor as mentioned in results of excitation of smart beam via impact hammer. On the other hand, the first three resonance frequencies acquired by piezoelectric patches are identical with the results of laser displacement sensor. These results show that vibration characteristics of smart beam is satisfactorily investigated via piezoelectric sensor with piezoelectric actuator.

Table 2.4: Resonance Frequencies of Smart Beam via Piezoelectric Patch Excitation

	Resonance Frequencies [Hz]			
Mode No	Accelerometer	Laser Displacement Sensor	Piezoelectric Patch 1B	Piezoelectric Patch 4A
1st Bending	6.625	7.000	7.000	7.000
2nd Bending	38.500	41.250	41.125	41.250
3rd Bending	103.125	109.500	109.125	109.375

Figure 2.23 shows the effect of the location of the piezoelectric sensor on obtaining frequency response of the system. In this Figure 2.23, it is obvious that the level of resonance-peaks are very low for the frequency response between piezoelectric sensor patch 1B and piezoelectric actuator patch 1A. As shown in Figure 2.3, piezoelectric patches 1A and 1B are co-located. This collocation of sensor and actuator patches causes interlacing of system poles and zeros. Recent studies [41, 67] are being conducted on properties of collocated sensor/actuator pairs of smart materials.

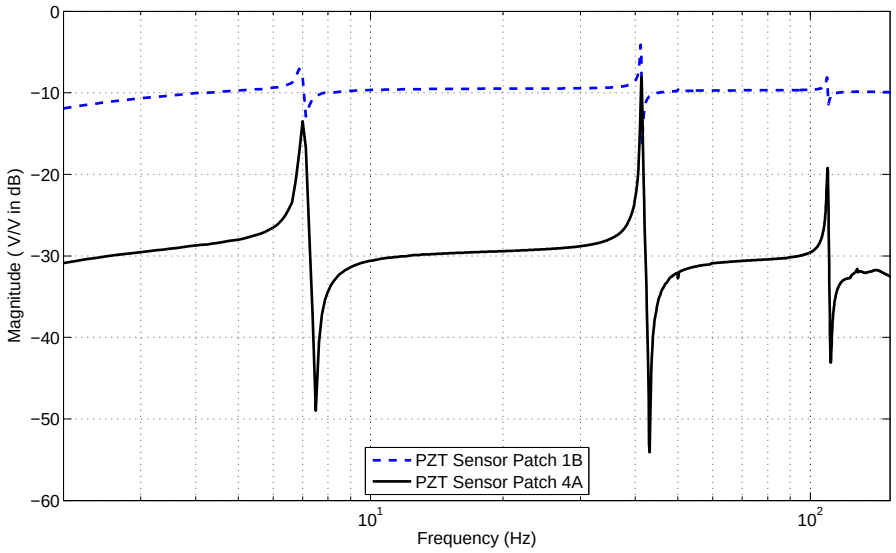

Figure 2.23: Frequency Responses Obtained by Piezoelectric Sensor Patch 1B and Piezoelectric Sensor Patch 4A

2.5 Piezoelectric Patches in Bimorph Configuration

The authority of piezoelectric actuator patches increases in bimorph configuration. The increase in authority is achieved by connecting opposite actuation signal to piezoelectric patches. In this configuration, when one of the patch extends, the other one contracts. This bimorph configuration effect on actuation is examined by exciting the smart beam with piezoelectric actuator patches (1A-1B) in bimorph configuration and measuring the response of the smart beam by piezoelectric sensor patch 4A. Figure 2.24 shows a sample of recorded signals and Figure 2.25 shows the frequency response obtained by the excitation via bimorph configured piezoelectric actuator patches (1A-1B) and the response measurement by piezoelectric sensor patch 4A.

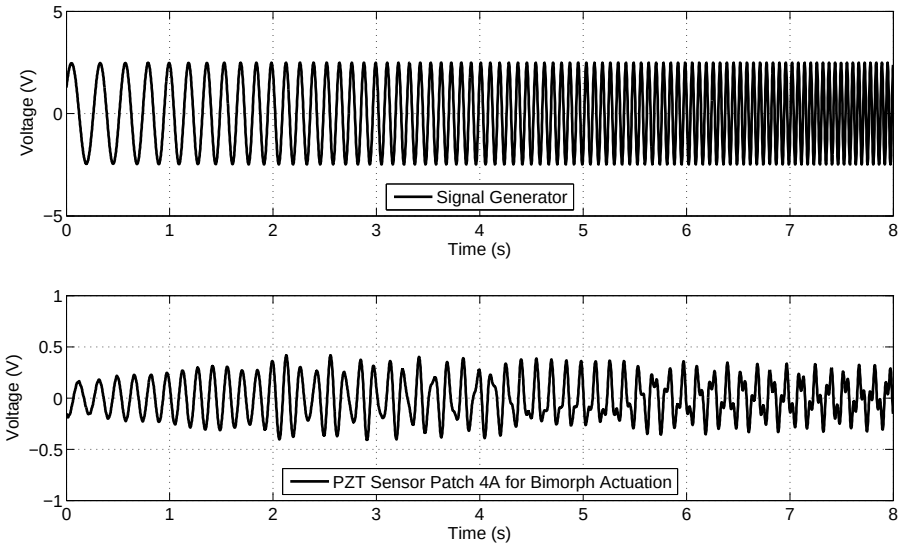

Figure 2.24: Sample Time Records of Signal Generator and Piezoelectric Sensor Patch 4A for Bimorph Configuration of Piezoelectric Actuator Patches (1A-1B)

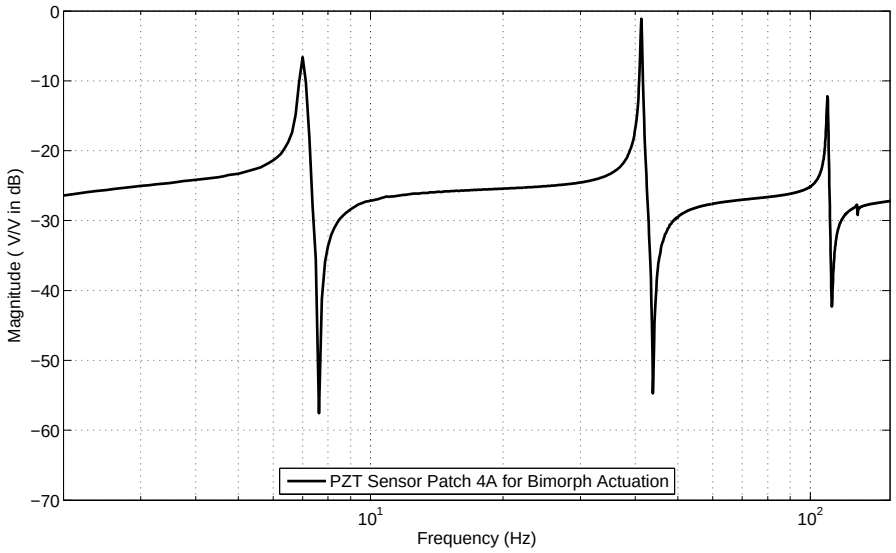

Figure 2.25: Frequency Response Obtained by Piezoelectric Actuator Patches (1A-1B) and Piezoelectric Sensor Patch 4A

The difference between monomorph and bimorph configuration in frequency response is shown with Figure 2.26. There is approximately 6 dB difference in the magnitude at the first resonance frequency of the smart beam between these two configurations. The 6 dB level corresponds to the double in magnitude.

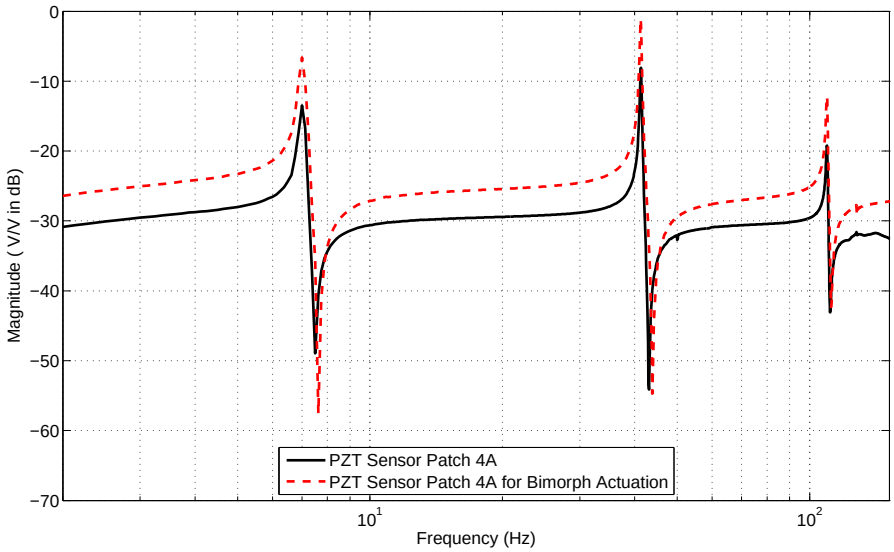

Figure 2.26: Comparison of Frequency Responses of Monomorph and Bimorph Patch Excitations

2.6 Conclusion

In this chapter, the investigation of the vibration characteristics of smart beam by employment of piezoelectric patches as sensors and actuators is presented. The excitation of smart beam is conducted by an impact hammer and the response of smart beam to this excitation is measured by using two piezoelectric patches, single axis accelerometer and laser displacement sensor. In further sections, the piezoelectric patch is employed as an actuator to excite smart beam. Similar to the previous configuration, the response of smart beam is again measured by two piezoelectric patches bonded at different locations and by commercially available sensing devices. The time records of excitation and response signals are gathered by data acquisition device and the vibration characteristics of smart beam is obtained. For each measurement, sample time record and frequency response function are presented. By comparing the first three modes of smart beam, the performance of piezoelectric patch in the investigation of vibration characteristics is studied with the effect of location of piezoelectric patch for actuation and sensing and also the effect of bimorph configuration of piezoelectric patches.

As a conclusion for this chapter, vibration characteristics of smart beam are satisfactorily investigated via piezoelectric sensors and piezoelectric actuators. Additionally, it is observed that the bimorph configuration doubles the actuation authority of piezoelectric patches.

CHAPTER 3

ACTIVE VIBRATION CONTROL OF A SMART BEAM VIA PIEZOELECTRIC SENSOR/ACTUATOR PAIR

3.1 Introduction

In this chapter, active vibration suppression of a smart beam is considered by applying robust controller via piezoelectric sensor/actuator pair. Piezoelectric patches (1A-1B and 4A-4B) are used as actuators in bimorph configuration and piezoelectric patch (2A) is employed as a sensor. At first, frequency response of the system is obtained by using prementioned piezoelectric sensor and actuator patches. Then, analytical system model is acquired from the measured frequency response. Following this, robust controller is designed for the active vibration control of the smart beam. The objective of the robust controller design is to achieve active vibration suppression by considering the system uncertainties and noises with incoming disturbances to the system. For this purpose, system uncertainties and noise in measurement are experimentally obtained. In order to qualify the effectiveness of the designed robust controller, μ analysis is performed. Finally, the robust controller is applied by using a programmable controller and the time responses of free and forced vibration at the first resonance frequency of the smart beam are acquired for open-loop and closed-loop cases. In addition to time domain, the effectiveness of the controller is also presented by open-loop and closed-loop frequency responses.

3.2 System Identification of the Smart Beam via Piezoelectric Sensor/Actuator Pair

In this section, the aim is to build mathematical model of the smart beam based on experimental frequency response. Piezoelectric patches are used as actuators and sensors to obtain necessary experimental frequency response for system identification. For this purpose, the smart beam is excited with piezoelectric actuator patches (1A-1B and 4A-4B) and the response of the smart beam is measured by piezoelectric sensor patch (2A). In Chapter 2, vibration characteristics of the smart beam is investigated by employment of piezoelectric patches as sensors and actuators. Using this knowledge gained on the vibration characteristics of the smart beam, it is excited within the bandwidth which covers the first three resonance modes. Then, mathematical model of the smart beam is estimated using this experimentally obtained frequency response.

3.2.1 Experimental Frequency Response

The experimental frequency response is obtained by simultaneous measurement of excitation and response signals. Smart beam is excited by four piezoelectric patches which are configured as bimorph to have more actuation ability. These bimorph configured piezoelectric actuator patches are 1A-1B and 4A-4B. During the excitation, the response of the smart beam is monitored by piezoelectric patch 2A. The signal conditioner unit presented in Appendix A is also used here to have correct measurement of output signal of piezoelectric sensor patch.

3.2.1.1 Experimental Setup

Figure 3.1 shows frequency response measurement system for piezoelectric sensor/actuator pair. The excitation signal is a swept sine signal from 2 Hz to 152 Hz with 5 V peak-to-peak generated by HP33120A signal generator. Before transferring this excitation signal to piezoelectric patches from the signal generator, the signal is amplified 30 times by SensorTech SA10 High Voltage Amplifier which uses SensorTech SA21 High Voltage Power Supply. The amplified excitation signal is transferred to piezoelectric actuator patches. The response to this particular excitation is monitored by piezoelectric sensor patch by using signal conditioning circuit presented in Figure 3.1 and described in Appendix A.

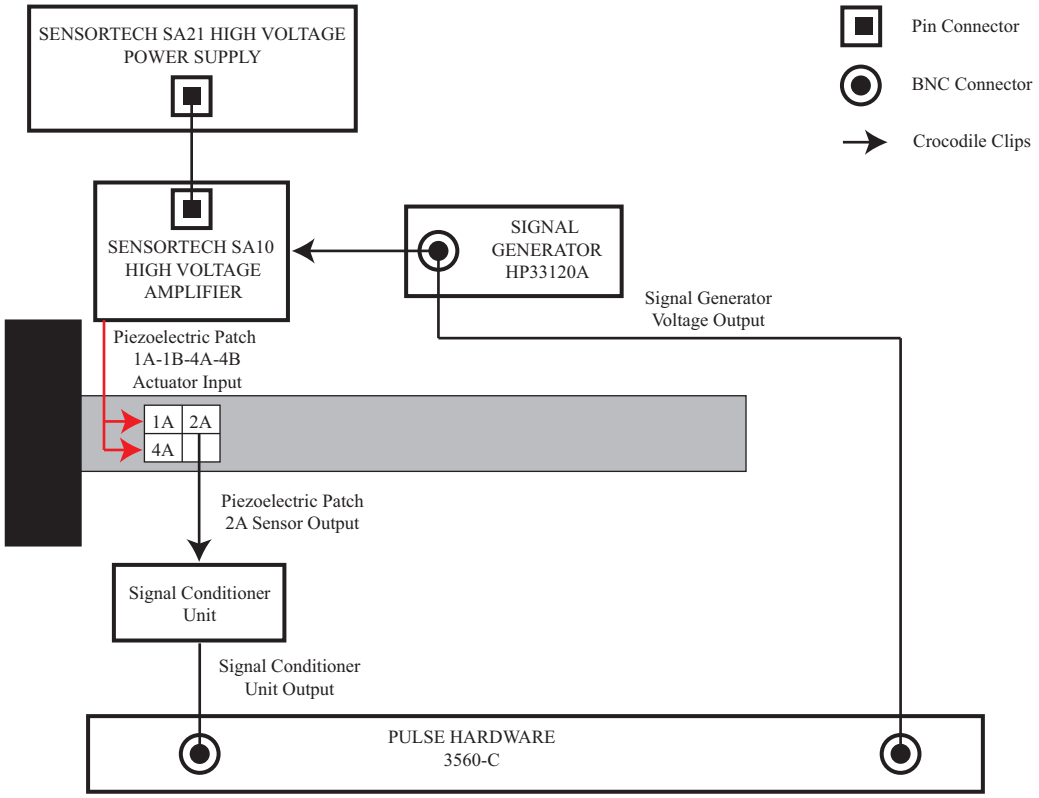

Figure 3.1: Experimental Setup for Modelling

Brüel and Kjær PULSE 3560C platform is used as the signal analyzer to record the output signal of signal generator with response of the smart beam and derive the frequency response. For the frequency domain analysis, analyzer properties are listed in Table 3.1.

Table 3.1: Analysis Setup Configuration for System Identification by Piezoelectric Sensor/Actuator Pair

Analyzer Property	**Value/Type**
Frequency Span	0 Hz - 200 Hz
Number of Lines	1600 lines
Number of Averages	125 Averages
Duration of Analysis	325.3 seconds
Averaging Mode	Linear
Analysis Mode	Baseband
Overlap Ratio	%66.67

3.2.1.2 Frequency Response

The measured frequency response in Figure 3.2 shows the relation between the output signal of the signal generator (in Volts) which is amplified and applied to piezoelectric actuator patches (1A-1B and 4A-4B) and the response signal measured by piezoelectric sensor patch 2A (in Volts). This frequency response of the smart beam acquired via the piezoelectric sensor/actuator pair configuration shows a stiffness-like characteristics at low frequencies. This results from high impedance values of piezoelectric material at low frequencies. The other feature of frequency response of the smart beam via piezoelectric sensor/actuator pair is the coincidence of resonance and antiresonance characteristics, in other words, resonance and anti-resonance frequencies are not well separated from each other. The frequency resolution of the measurement is selected in such a way that this behavior of frequency response of the smart beam could be avoided.

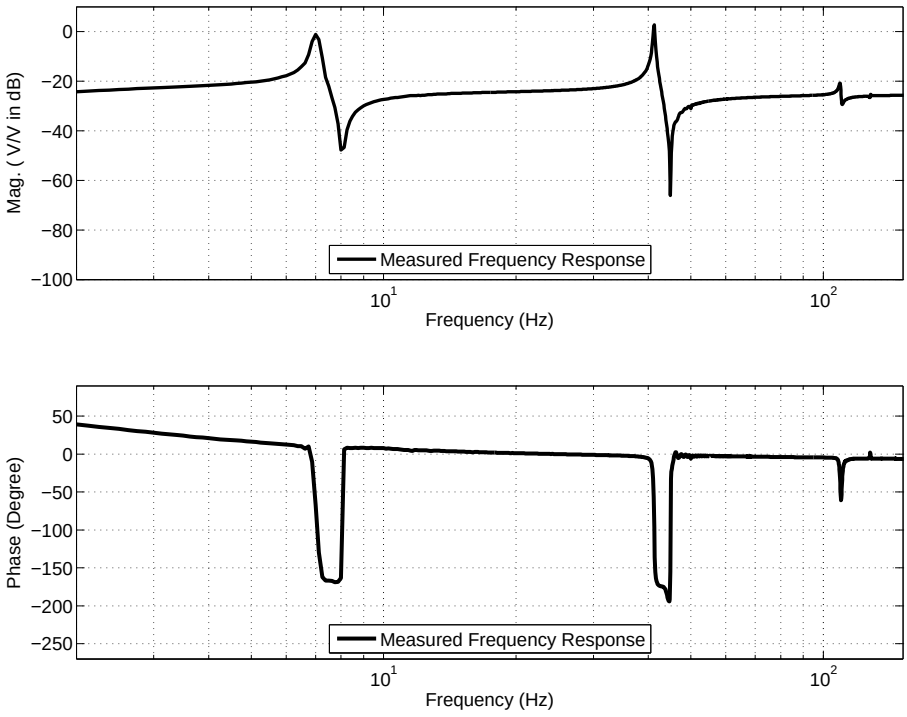

Figure 3.2: Measured Frequency Response for Piezoelectric Sensor/Actuator Pair

3.2.2 Analytical Model of the Smart Beam

In this section, mathematical model of the smart beam is derived by processing the measured frequency response in Figure 3.2. The transfer function of the smart beam is estimated between the excitation signal generated by the signal generator and the response signal measured by the piezoelectric sensor patch (2A) by using MATLAB's "fitsys" command located in μ Analysis and Synthesis Toolbox [68]. This "fitsys" command builds a state-space model based on estimated transfer function. This command is constructed by least square method. In order to use this command, measured frequency response data and additional arguments such as desired order of model, weighting matrix and optional restrictions for stable transfer functions are needed.

Transfer function of the smart beam is estimated within the frequency range between 2 Hz and 152 Hz. This frequency range includes first three bending modes of the smart beam. In order to find the accurate and the necessary model for controller application, transfer function of the smart beam is obtained for different orders. Figure 3.3 shows frequency responses of 4^{th} , 8^{th} and 16^{th} order estimated transfer function of the smart beam.

The 4^{th} order estimated transfer does not include information concerning third bending resonance mode of the smart beam. 16^{th} order estimated transfer perfectly fits the measured frequency response and includes this aforementioned third resonance mode as well. However, 16^{th} order transfer function seems not to be feasible for controller applications because it is computationally expensive. For less computational effort [69] and more accurate mathematical model, 8^{th} order model is selected and used in the controller applications.

The 8^{th} order transfer function of the smart beam is also presented in Equation 3.1.

$$G(s) = \frac{0.05s^8 + 0.68s^7 + 2.88 \times 10^4 s^6 + 1.73 \times 10^5 s^5 + 2.09 \times 10^9 s^4 + \dots}{s^8 + 11.81 \times s^7 + 5.43 \times 10^5 s^6 + 2.82 \times 10^6 s^5 + 3.38 \times 10^{10} s^4 + \dots} \frac{9.54 \times 10^9 s^3 + 8.72 \times 10^{12} s^2 + 2.12 \times 10^{13} s + 9.25 \times 10^{15}}{9.22 \times 10^{10} s^3 + 1.25 \times 10^{14} s^2 + 1.69 \times 10^{14} s + 1.2 \times 10^{17}} \quad (3.1)$$

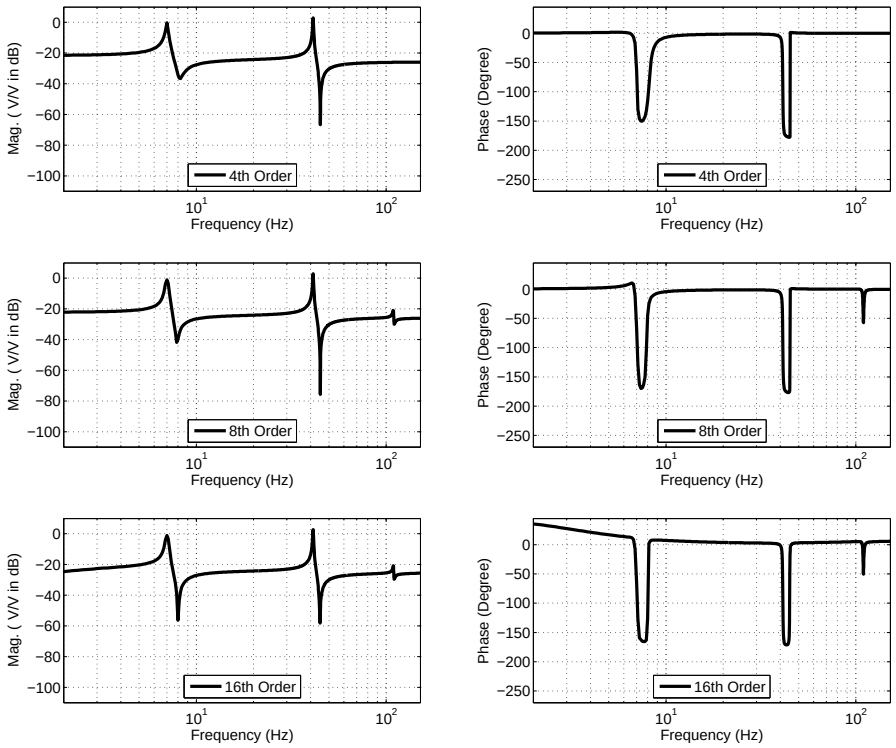

Figure 3.3: Frequency Responses of Estimated Transfer Function of Smart Beam via Piezoelectric Sensor/Actuator Pair

3.3 Robust Controller Design

In this section, the design of robust controller for suppression of free and the first resonance frequency forced vibration is presented. First, the theory of the robust controller design tools (H_∞ controller and μ analysis) are explained. Then, system uncertainties and performance expectations for controller design are introduced. Next, the generalized plant for system inputs and outputs is constructed for H_∞ controller design with H_∞ synthesis. After the design of H_∞ controller, the robustness and performance specifications are further studied by using μ analysis.

3.3.1 H_∞ Control Theory

The aim is to minimize the effect of general disturbances on general errors. The constraint on minimization is to provide internal stability of the closed loop system. In the following, a general H_∞ controller problem is stated and its solution is presented.

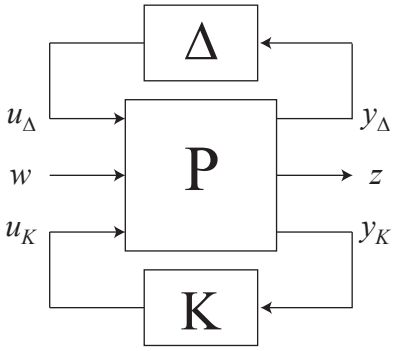

Figure 3.4: General Interconnection Structure

Figure 3.4 shows a general interconnection structure which includes plant P, uncertainty block Δ and controller K in linear fractional transformation form with the input and output signals. The input signals to the plant P are general disturbances w, controller and uncertainty output signals u_K and u_Δ. On the other hand, the output signals of the plant P are general error signal z, measurements for controller and uncertainty block y_K and y_Δ.

For the H_∞ controller problem, the uncertainty block Δ is assumed to be bounded within the magnitude 1. By taking out uncertainty block Δ from general interconnection structure, the lower fractional transformation between plant P and controller K in Figure 3.5 is obtained. Then, Equation 3.2 shows a generic cost function $F(P, K)$ between general disturbances and general errors for a plant and a controller in linear fractional transformation form.

$$F(P,K) = P_{11} + P_{12}K(I - P_{22})^{-1}P_{21} \qquad where \qquad P = \begin{bmatrix} P_{12} & P_{21} \\ P_{21} & P_{22} \end{bmatrix} \tag{3.2}$$

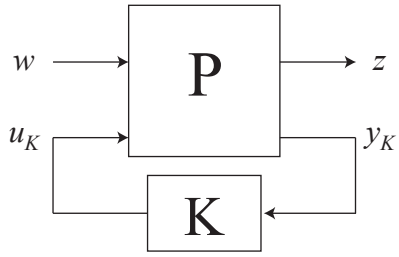

Figure 3.5: Lower Fractional Transformation Block Diagram of Plant P and Controller K

Minimizing the effect of general disturbances on general errors by satisfying internal stability is an optimization problem. Zames [44] introduced H_∞ operator norm for the feedback optimization problems and showed that H_∞ norm of a frequency response function $E(jw)$ can be written as follows,

$$\|E\|_\infty = \sup_\omega (\overline{\sigma} E(j\omega)) \tag{3.3}$$

where $\overline{\sigma}(\cdot)$ denotes the maximum singular value in overall frequencies and $sup(\cdot)$ denotes the least upper bound. In other words, this maximum singular value corresponds to the distance in the complex plane from the origin to the farthest point on the Nyquist plot of $E(jw)$ and peak value on the Bode plot of $E(jw)$.

Glover [46] and Doyle [47] followed the light of Zames's research and presented the state space formula for all stabilizing H_∞ controllers. In these researches, H_∞ norm of a generic cost function $F(P, K)$ is bounded as follows :

$$\|F(P, K)\|_\infty < \gamma \tag{3.4}$$

for $\gamma \in \mathbf{R}$ and the existence of controller K which satisfies the condition presented in Equation 3.4 is determined by following an iteration procedure. This technique to design H_∞ output feedback controller is implemented in MATLAB and "hinfsyn" function is constructed and published in μ Analysis and Synthesis Toolbox. The aim of the function is to normalize $\|F(P, K)\|_\infty$ to 1 for the selected weighting functions. By doing this, the objective of robust controller is achieved by minimizing H_∞ norm of transfer function between the general disturbances and general errors of the system. In this thesis, this "hinfsyn" function is used to design robust controller for an active vibration suppression of a smart beam via piezoelectric sensor/actuator pair.

3.3.2 μ Analysis Theory

The primary consideration of H_∞ control design is to maintain internal stability of the closed-loop system. However, in order to ensure the stability, the controller may be designed too conservatively. The structured singular value μ analysis provides an environment for analysis of the robustness and performance of the controller by considering assumed uncertainties and selected weights. In general, uncertainty block Δ is eliminated in H_∞ controller design problems, hence in μ analysis this uncertainty block is used to analyze the robustness and performance specifications of the design problem. For this purpose, upper linear fractional transformation between the closed-loop system M and uncertainty block Δ is considered and presented in Figure 3.6.

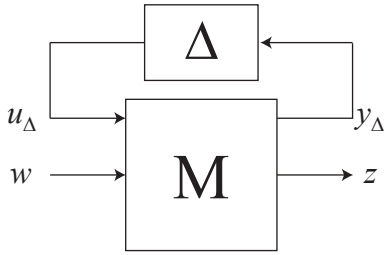

Figure 3.6: Upper Fractional Transformation Block Diagram of Closed-Loop System M and Uncertainty Block Δ

Equation 3.5 shows a generic cost function which includes relation between the closed-loop system M and the uncertainty block Δ.

$$F(M,\Delta) = M_{22} + M_{21}\Delta(I - M_{11})^{-1}M_{12} \qquad where \qquad M = \begin{bmatrix} M_{12} & M_{21} \\ M_{21} & M_{22} \end{bmatrix} \tag{3.5}$$

In the μ analysis, the aim is to find out how the output of $F(M,\Delta)$ changes with Δ values in permissable region. So that, the performance specifications of the H_∞ controller is assessed. This μ analysis of H_∞ controller is implemented in MATLAB and "*mu*" function is constructed and published in μ Analysis and Synthesis Toolbox [68]. The aim of the "*mu*" function is to calculate structured singular values μ of the interconnected structures closed loop system M and uncertainty block Δ over all frequencies in the determined bandwidth. Then, the peak-value of the structure singular value gives information about the robust per-

formance of the closed-loop system. The robust performance is guaranteed if and only if maximum structured singular value μ is less than 1.

The definition of the structured singular value μ_Δ of closed-loop system M is given in the following:

$$\mu_\Delta(M) = \frac{1}{min\{\overline{\sigma}(\Delta) : \Delta \in \mathbf{\Delta}, det(I - M\Delta) = 0\}} \tag{3.6}$$

where $\overline{\sigma}(\Delta)$ is the largest singular value of perturbation matrix Δ and $\mathbf{\Delta}$ denotes norm-bounded subsets [43].

3.3.3 System Control Objectives and Uncertainty Models

System uncertainties and desired performance criterions are included in design phase of robust controller to have effective, robust and stable controller. The block diagram used for robust controller design is given in Figure 3.7. In this diagram, the mathematical model of the smart beam and forthcoming controller are shown in blocks labeled as G and K respectively. The block diagram also contains design parameters. These design parameters are composed of characteristics of desired performance (W_p), disturbance (W_d), noise (W_n), actuation limitations (W_a) and uncertainty in mathematical model of the smart beam (W_m and Δ). In following, these design parameters are explained in detail.

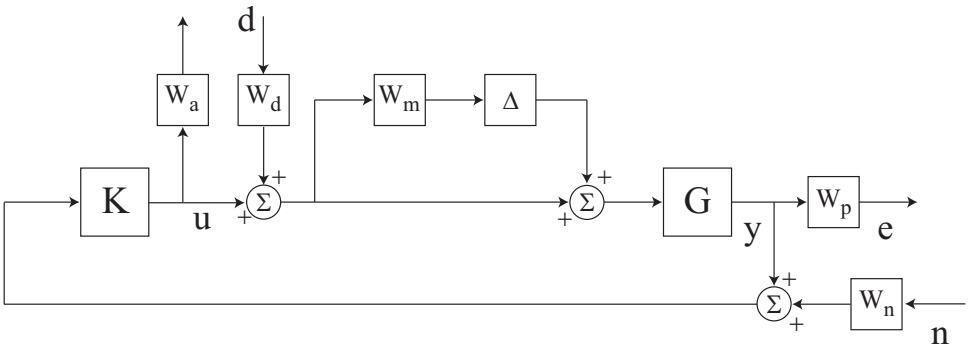

Figure 3.7: Block Diagram for Robust Controller Design via Piezoelectric Sensor/Actuator Pair

3.3.3.1 Desired Performance Weight (W_p)

The input of desired performance weight is the output of the smart beam model (y) which corresponds to the vibration of the smart beam. As previously explained, a piezoelectric sensor patch is used to monitor the vibration characteristics of the smart beam to particular excitation. Herein, the aim is to suppress free and first resonance frequency forced vibration of the smart beam. For this purpose, desired performance (W_p) is constructed as a low pass filter in the form of second order transfer function shown in Equation 3.7.

$$W_p = \frac{354000}{s^2 + 700s + 122500} \tag{3.7}$$

The frequency response of desired performance W_p block is shown in Figure 3.8. The characteristics of desired performance at low frequencies is constant smooth-line up to first resonance frequency (7 Hz). Whereas the magnitude of desired performance decreases after the first resonance frequency of the smart beam since high frequency performance is not expected. The second-order transfer function form of the low pass filter provides rapid attenuation at the frequencies higher than the first resonance frequency compared to its first-order form.

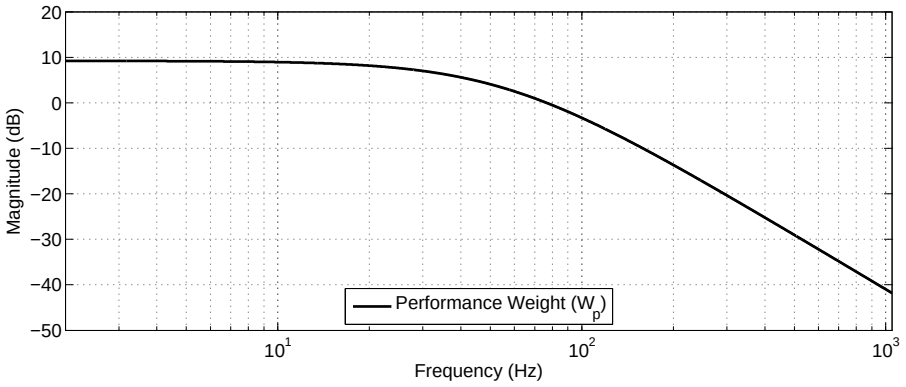

Figure 3.8: Frequency Response of Desired Performance Weight (W_p)

3.3.3.2 Disturbance Weight (W_d)

In general, the disturbance inputs (d) are input forces which generate undesirable behavior in the system. In our case, the undesirable behavior of the system points out the vibration of smart beam. The undesired vibration of the smart beam may be originated by external dis-

turbances at low frequencies. The effect of these disturbance inputs regarding to the free and the first resonance forced vibration is integrated in controller design by considering disturbance weight (W_d). Since the expected disturbance input includes frequencies up to the first resonance mode, the disturbance weight is also selected as a low pass filter form. Compared to desired performance weight W_p, a low decay rate at the frequencies higher than the first resonance mode is selected and therefore the disturbance weight (W_d) is designed as a first order transfer function. This transfer function of the disturbance weight is given in Equation 3.8 and its frequency response is presented in Figure 3.9.

$$W_d = 0.22 \times \frac{300}{s + 300} \tag{3.8}$$

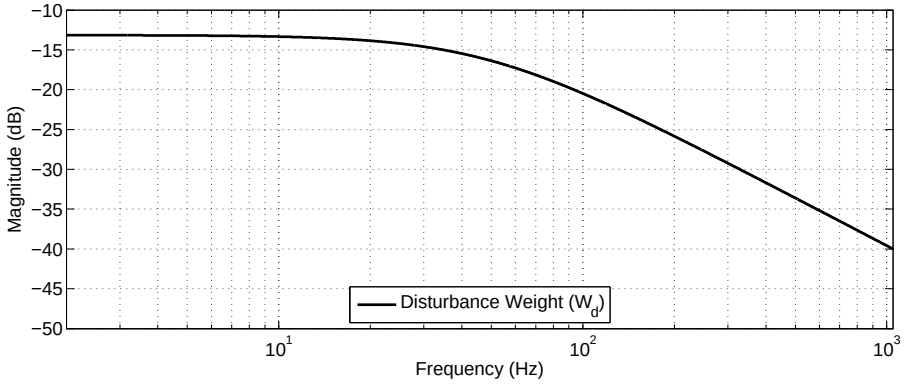

Figure 3.9: Frequency Response of Disturbance Input Weight (W_d)

3.3.3.3 Noise Weight (W_n)

The noise weight (W_n) is included to consider the quality of vibration measurement of the smart beam. Vibration of the smart beam is monitored by measuring the output of signal of piezoelectric sensor patch in volts. Signal conditioner unit is used to minimize the measurement problems due to the characteristics of piezoelectric material. Herein, the aim of noise identification is to tolerate signal-to-noise ratio in vibration measurement of the smart beam. To do this, input noise of the programmable controller is measured and presented in Figure 3.10. Then, power spectral density of the recorded noise signal is obtained and shown in Figure 3.11. As can be seen from the power spectral density, signal-to-noise ratio is constant over the frequency range. So that noise weight is selected as 0.01 to represent the average signal-to-noise ratio in vibration measurement.

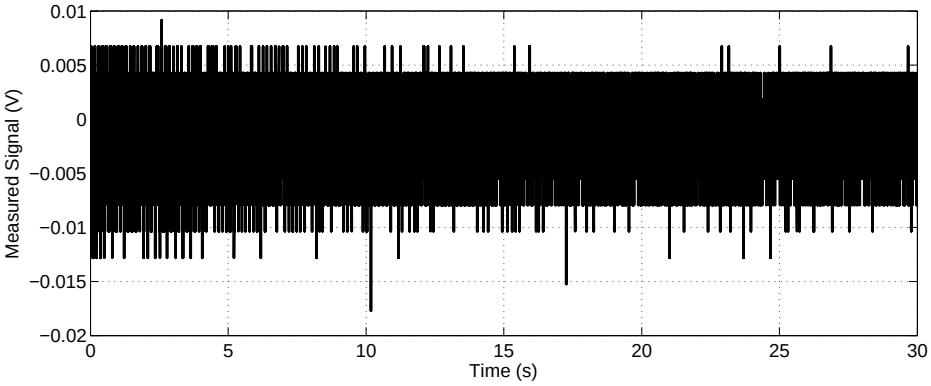

Figure 3.10: Recorded Noise Signal

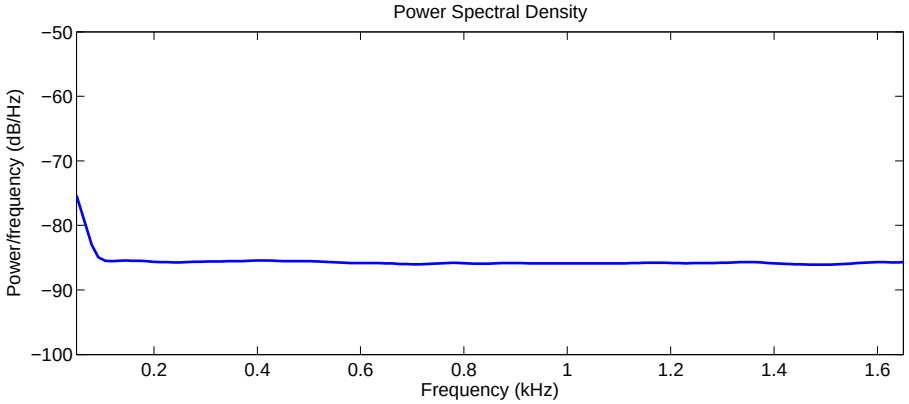

Figure 3.11: Power Spectral Density of the Noise Signal

3.3.3.4 Actuator Limitation Weight (W_a)

The main concern for the actuator limitation weight (W_a) in controller design is to limit controller output voltage since this voltage is amplified and applied to the piezoelectric actuator patches. The maximum allowable voltage for the piezoelectric actuator is $150V$. In order to prevent possible damage of the piezoelectric patches, this actuation voltage should not be exceeded. The output of the programmable controller is amplified 30 times. Because of this, the output limit of the controller is determined as $5V$. This actuation signal limitation is considered with actuator limitation weight (W_a). The actuator limitation weight is assumed to be constant over the frequency range and its magnitude is calculated as 0.2 by normalizing the unity voltage by the output limit of the controller which is $5V$.

3.3.3.5 Multiplicative Input Uncertainty (W_m and Δ)

In robust controller design, the modelling uncertainty is included to prevent undesirable behaviors of the controller because of modelling errors. The spillover is such a problem when the controller excites the unmodelled modes [38, 70]. The block diagram for multiplicative input uncertainty is shown in Figure 3.12. The block diagram includes nominal plant G with multiplicative uncertainty weight W_m and structured uncertainty Δ and the perturbed plant shown with dashed line.

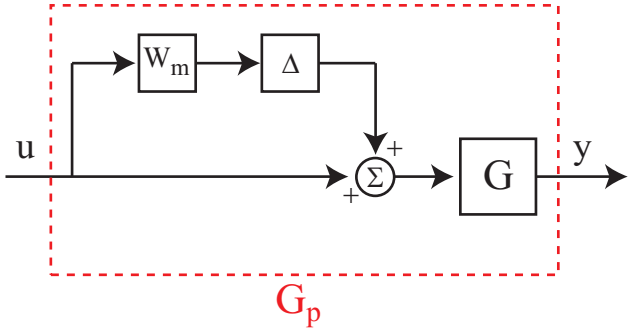

Figure 3.12: Block Diagram for Multiplicative Input Uncertainty

From the relationships between the output signal y and the input signal u, the relation for the perturbed plant can be found as,

$$G_p = (1 + \Delta W_m)G. \tag{3.9}$$

When the structured uncertainty block is eliminated, the multiplicative uncertainty can be expressed as follows,

$$W_m = \frac{G_p - G}{G}. \tag{3.10}$$

This multiplicative input uncertainty weight W_m can be estimated experimentally by acquiring frequency responses of the nominal and perturbed plants. For the modelling, the frequency response of the smart beam is obtained in the frequency range between 2 Hz and 152 Hz and afterwards the mathematical model of the smart beam is constructed for the first three bending modes of the smart beam. This mathematical model is chosen as the nominal plant for the controller design. Meanwhile, smart beam has infinitely many modes and degrees of freedom and the nominal plant includes first three modes of the smart beam only. In order to consider input and output errors between the model and physical system, the perturbed plant

shall include the high frequency dynamics. Therefore, the frequency response of the smart beam is obtained between 2 Hz and 1000 Hz and this frequency response is assumed as the frequency response of the perturbed plant. Figure 3.13 shows frequency responses of nominal and perturbed plants.

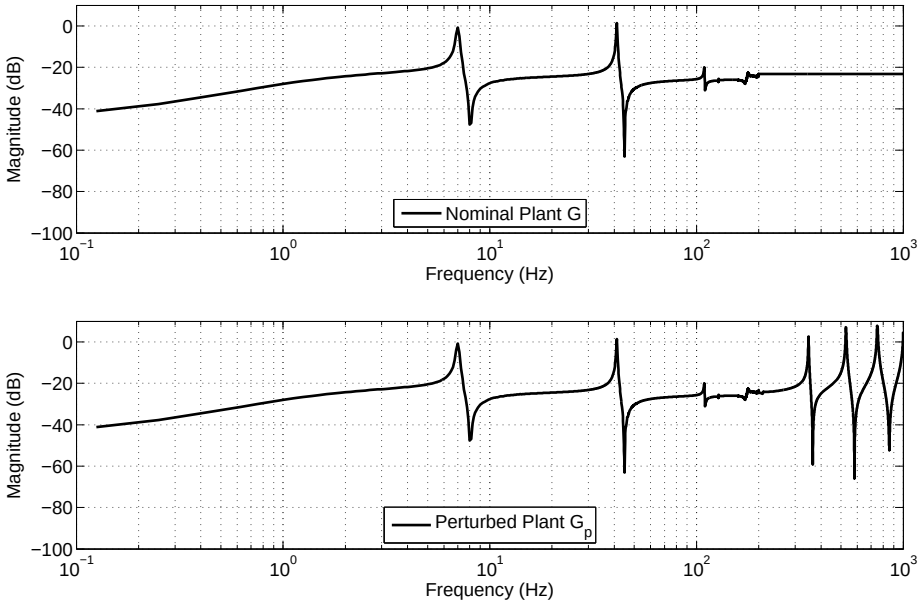

Figure 3.13: Frequency Response of Nominal and Perturbed Plants

Using the equation 3.10, the frequency response of the multiplicative input uncertainty is calculated and shown in Figure 3.14. In order to have simple model for the uncertainty, this calculated frequency response is covered by an estimated transfer function which is given in Equation 3.11 and presented with dashed line in the Figure 3.14.

$$W_m = \frac{51.92s^4 + 3.477 \times 10^4 s^3 + 7.412 \times 10^6 s^2 + 7.577 \times 10^8 s + 1.395 \times 10^4}{s^4 + 2841s^3 + 4.041 \times 10^6 s^2 + 7.609 \times 10^8 s + 1.4 \times 10^5} \tag{3.11}$$

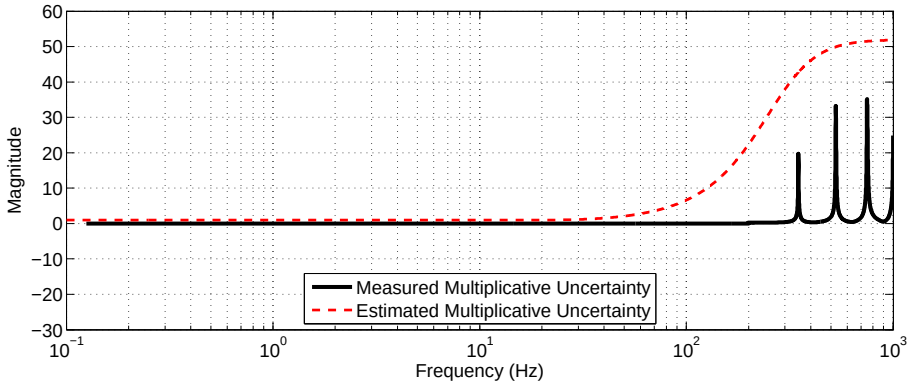

Figure 3.14: Frequency Response of Multiplicative Modelling Uncertainty (W_m)

3.3.4 H_∞ Synthesis

In Section 3.3.1, the solution of H_∞ controller problem is explained for a plant and a controller in linear fractional transformation form. The main concern in this section is to obtain a lower fractional transformation form of the plant and the controller by considering system uncertainties and performance specifications. For this purpose, at first each output signal is defined in terms of input signals. Figure 3.15 shows the input and output signals considered in the synthesis of system inputs and outputs.

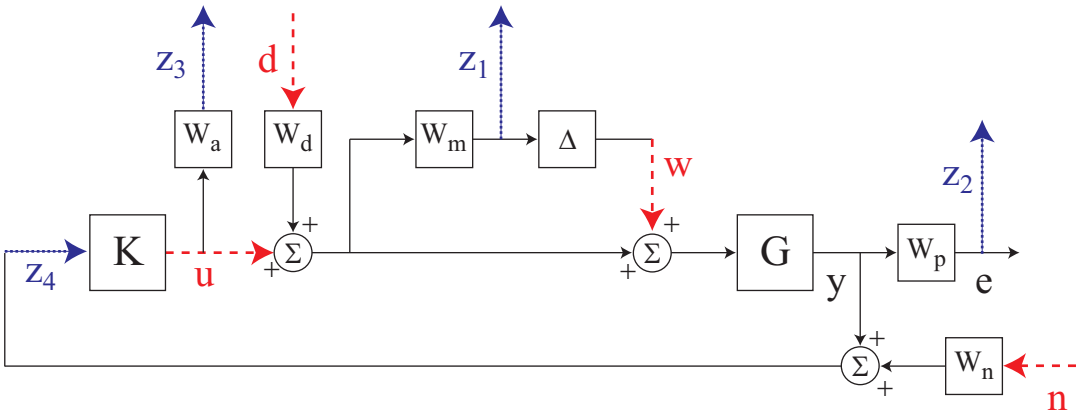

Figure 3.15: Block Diagram for Robust Controller Design

The output signal z_1 is the output signal of multiplicative input uncertainty, z_2 is the output signal of performance weight, z_3 is the output signal of actuator limitation weight, and z_4 is the feedback signal to the controller K. The input signals are the output signal of uncertainty w, noise signal n, disturbance d and controller u.

Following Equations 3.12 - 3.15 show the relations between the system inputs and outputs.

$$z_1 = W_m(W_d d + u) \tag{3.12}$$

$$z_2 = W_p G(w + W_d d + u) \tag{3.13}$$

$$z_3 = W_a u \tag{3.14}$$

$$z_4 = G(w + W_d d + u) + W_n n \tag{3.15}$$

The system inputs and outputs are shown in the matrix form in Equation 3.16.

$$\begin{bmatrix} z_1 \\ z_2 \\ z_3 \\ z_4 \end{bmatrix} = \underbrace{\begin{bmatrix} 0 & 0 & W_m W_d & W_m \\ W_p G & 0 & W_p W_d G & W_p G \\ 0 & 0 & 0 & W_a \\ G & W_n & G W_d & G \end{bmatrix}}_{\mathrm{P}} \times \begin{bmatrix} w \\ n \\ d \\ u \end{bmatrix} \tag{3.16}$$

Figure 3.16 shows corresponding generalized plant P, uncertainty block Δ and controller K with system inputs and outputs.

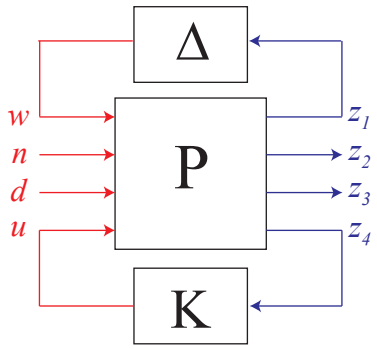

Figure 3.16: Generalized Plant with Inputs and Outputs

In order to acquire lower linear fractional transformation, the input and output signals are grouped as follows.

$$r = \begin{bmatrix} w \\ n \\ d \end{bmatrix} \qquad z = \begin{bmatrix} z_1 \\ z_2 \\ z_3 \end{bmatrix} \qquad v = z_4 \tag{3.17}$$

The matrix form of generalized plant equation is in Equation 3.18.

$$\begin{bmatrix} z \\ v \end{bmatrix} = \begin{bmatrix} P_{11} & P_{12} \\ P_{21} & P_{22} \end{bmatrix} \times \begin{bmatrix} r \\ u \end{bmatrix} \tag{3.18}$$

And, the output of controller signal u can be expressed with the signal addition of system output and noise signal (formerly z_4, now it is named as v).

$$u = Kv \tag{3.19}$$

Then the equation for each output signal group can be written as follows,

$$z = P_{11}r + P_{12}Kv, \tag{3.20}$$

$$v = P_{21}r + P_{22}Kv, \tag{3.21}$$

where the partitions of the generalized plant P are

$$P_{11} = \begin{bmatrix} 0 & 0 & W_m W_d \\ W_p G & 0 & W_p W_d G \\ 0 & 0 & 0 \end{bmatrix} \qquad P_{12} = \begin{bmatrix} W_m \\ W_p G \\ W_a \end{bmatrix}, \tag{3.22}$$

$$P_{21} = \begin{bmatrix} G & W_n & W_d G \end{bmatrix} \qquad P_{22} = \begin{bmatrix} G \end{bmatrix}. \tag{3.23}$$

And when we solve Equation 3.21 for v and we obtain that,

$$v = (I - P_{22}K)^{-1} P_{21} r, \tag{3.24}$$

and we substitute v in Equation 3.20, we obtain a relation between output signal z and input signal r which is shown in Equation 3.25.

$$\begin{aligned} z &= \left[P_{11} + (I - P_{22}K)^{-1} P_{21}\right] r, \\ &= F(P, K) r. \end{aligned} \tag{3.25}$$

In Equation 3.25, the weighted output signals are expressed as a function of disturbance and noise. As explained earlier, the objective of H_∞ controller is to minimize the $\|F(P, K)\|_\infty$ by finding a stabilizing controller K.

3.3.5 μ Analysis of H_∞ Controller

In this section, μ analysis of H_∞ Controller is explained. The aim of the robust controller is the minimization of the effects of the input signals on output signals. In the aforementioned sections, the input and output signals are defined in order to be used in design of H_∞ controller. In this section, the input and output signals is going to be used in the design and analysis of the controller.

In order to clarify the robust controller design process, Figure 3.17 shows interconnections of output and input signals in each step of the controller design. In Figure 3.17 (a), the generalized interconnection diagram includes input and output signals. Then in Figure 3.17 (b), the Δ block is eliminated and it is used for H_∞ synthesis and finally Figure 3.17 (c) shows the interconnection structure used in μ analysis.

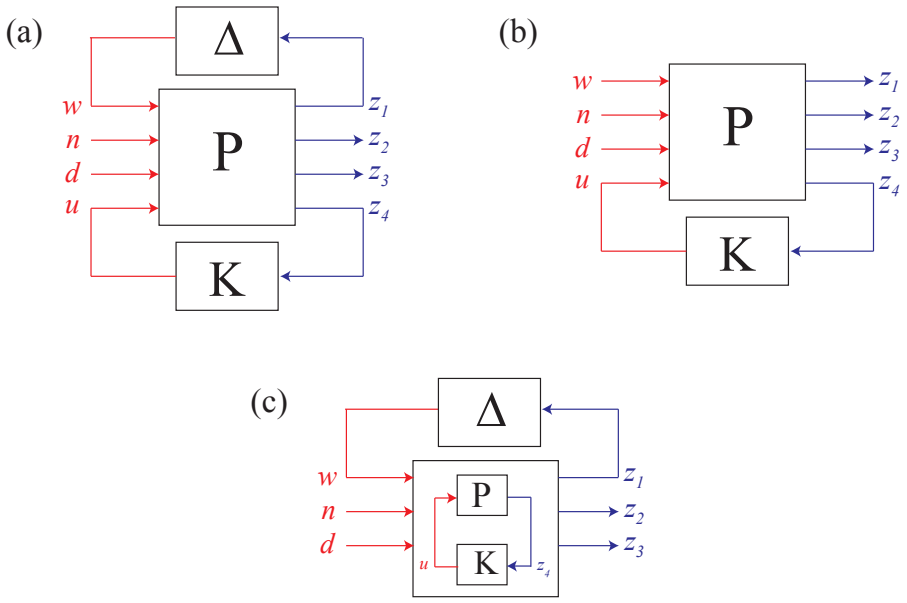

Figure 3.17: Steps in Robust Controller Design **(a)** System Input and Outputs **(b)** H_∞ Controller Design **(c)** μ Analysis of H_∞ Controller

In Figure 3.18, the closed-loop system (M) with structured uncertainty and performance blocks (Δ and Δ_{per}) are shown in detail. The structured uncertainty block is composed of uncertainty block (Δ) and performance block (Δ_{per}). The input of the uncertainty block (Δ) is the multiplicative uncertainty output z_1, while input signals of the performance block (Δ_{per}) are weighted performance output z_2 and actuator limitation weight output z_3. These signals are shown in Figure 3.15.

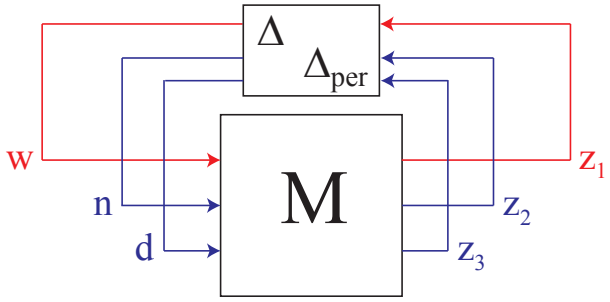

Figure 3.18: μ Analysis for Designed H_∞ Controller

3.3.6 H_∞ Controller Design and Performance Specifications

By considering the system uncertainties and performance criteria, H_∞ controller is designed. MATLAB "hinfsyn" function is used to calculate the stabilizing controller K by minimizing prementioned cost function $\|F(P,K)\|_\infty$. The size of obtained controller K equals to the plant order of 8. This high-order controller increases the complexity of computation by hardware [71]. In order to prevent hardware problems which may cause performance reduction or unstability in the closed-loop system, the order of controller K is reduced by model reduction [71]. The order of reduced-order approximation of the controller K is 6. The frequency responses of open and closed loops are shown Figure 3.19. Applying designed robust controller, a considerable reduction ($10dB$) in the first mode is achieved for the piezoelectric sensor/actuator pair.

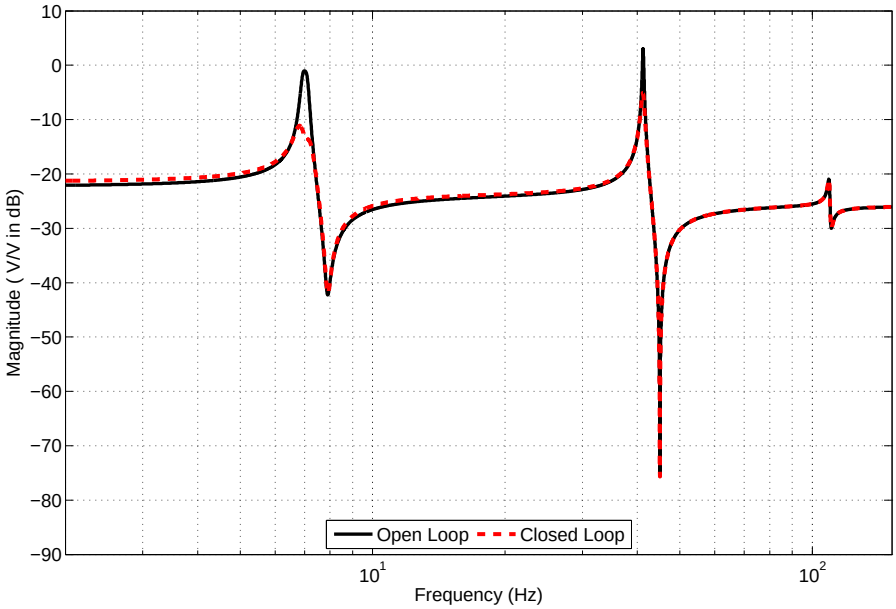

Figure 3.19: Open Loop and Closed Loop Frequency Responses

3.3.7 μ Analysis for Designed H_∞ Controller

The μ-analysis is conducted to assess the performance of the designed H_∞ controller. MATLAB "mu" function is used to calculate the bounds of the singular values of the closed-loop system and Figure 3.20 shows these calculated singular values over the frequency range. From the graph, it can be seen that the maximum singular value is 0.99 at the 2^{nd} Bending Mode. Since the maximum singular value is smaller than 1, robust performance is guaranteed for the designed H_∞ controller.

3.4 Active Vibration Control Experiments

In this section, active vibration suppression of the free and first resonance forced vibration is presented for piezoelectric sensor/actuator pair by using the designed robust controller. First, experimental setup for controller application is presented on the vibration measurement of the smart beam. Then, experimental results are presented for suppression of the free and the first resonance frequency vibration of the smart beam.

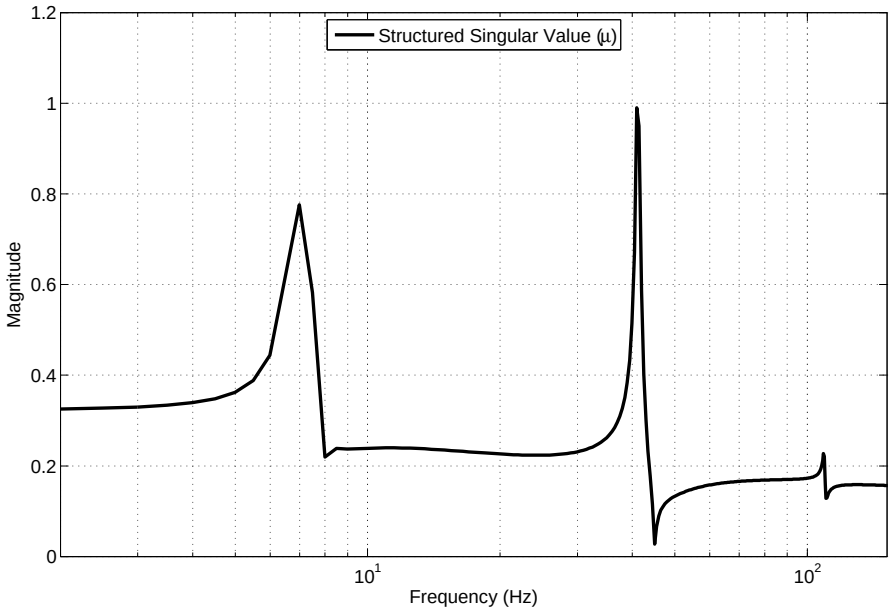

Figure 3.20: Singular Values of the Closed-Loop System

3.4.1 Experimental Setup

Robust controller is applied to suppress vibration of the smart beam with the experimental setup presented in Figure 3.21. The difference of this experimental setup from the aforementioned experimental setups used in the determination of the characteristics of vibration and modelling experiments is that the four-channel programmable controller SensorTech SS10 is included with actuator and sensor signals. The output of the programmable controller (actuator output signal) is amplified 30 times with the SensorTech SA10 high voltage power amplifier. As explained in Section 3.2, piezoelectric patches (1A-1B and 4A-4B) are used as actuator and meanwhile the vibration of the smart beam is monitored by a single piezoelectric patch (2A) . The output voltage of piezoelectric patch is passed through the signal conditioner unit and is supplied to the SS10 programmable controller and PULSE data acquisition platform.

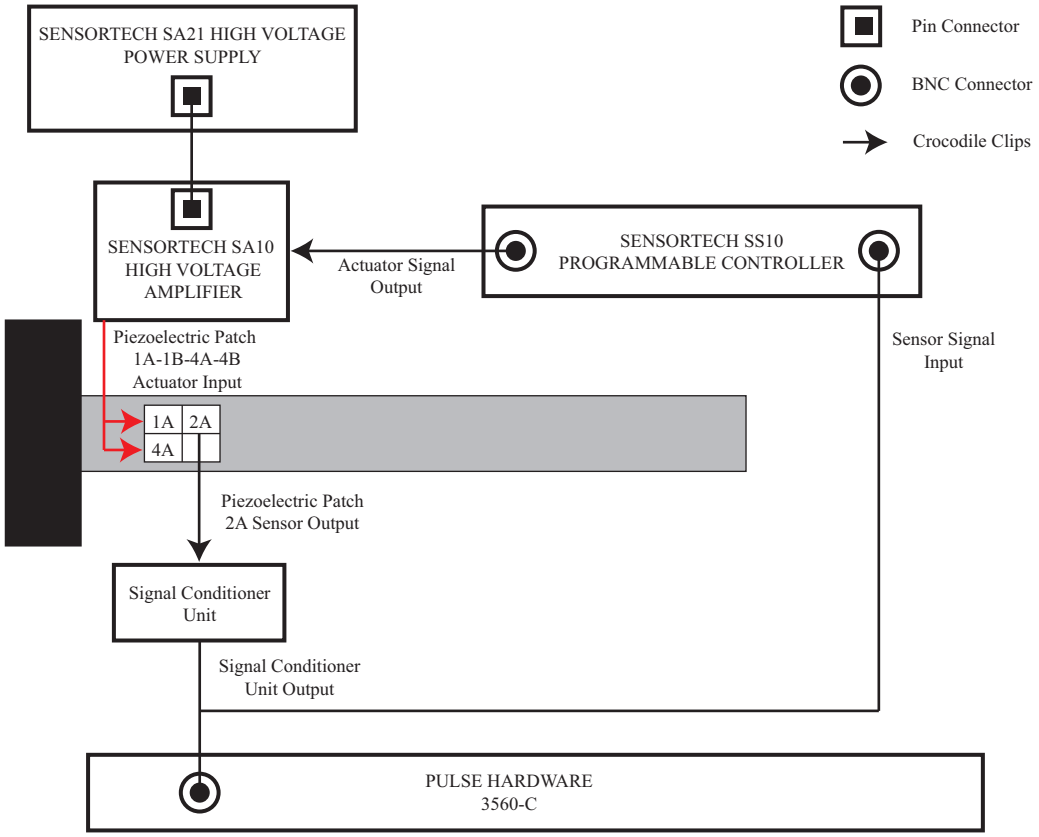

Figure 3.21: Experimental Setup for Controller Applications with Piezoelectric Sensor/Actuator Pair

For the cantilever-beam structures, maximum curvature at the clamped-end corresponds with the maximum tip displacement in the first bending mode. Therefore, monitoring of voltage of piezoelectric patch 2A reflects the tip displacement of smart beam for the free and the first resonance frequency response. The vibration of the smart beam at the first resonance frequency is monitored by piezoelectric patch (2A) while the laser displacement sensor is used to measure tip displacement of the smart beam. Figure 3.22 shows these measurements gathered from laser displacement sensor and piezoelectric patch. Using this measurement, a relation between the output signal of piezoelectric patch 2A and tip displacement of the smart beam is obtained.

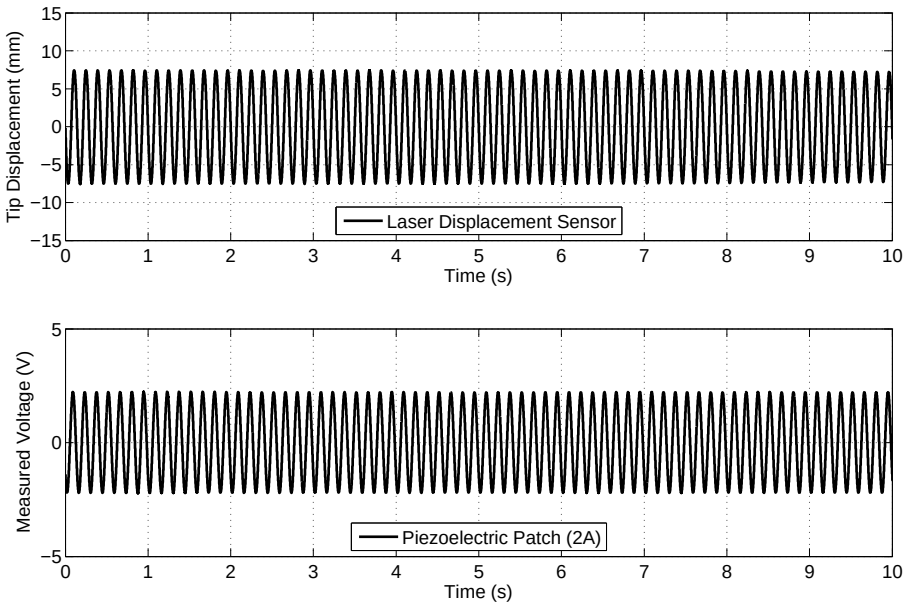

Figure 3.22: Measurements by Laser Displacement Sensor and Piezoelectric Patch (2A)

3.4.2 Suppression of Free Vibration

Analysis of open-loop and closed-loop time responses are performed by applying a 7mm initial tip displacement with zero initial tip velocity which corresponds approximately to 2.2V monitored output voltage of piezoelectric patch 2A. Figure 3.23 shows the open-loop time response for this initial tip displacement. The open-loop time response is obtained when robust controller via piezoelectric sensor/actuator pair is inactive. Whereas, the closed-loop time response shown in Figure 3.24 is acquired when robust controller with piezoelectric sensor/actuator pair is active.

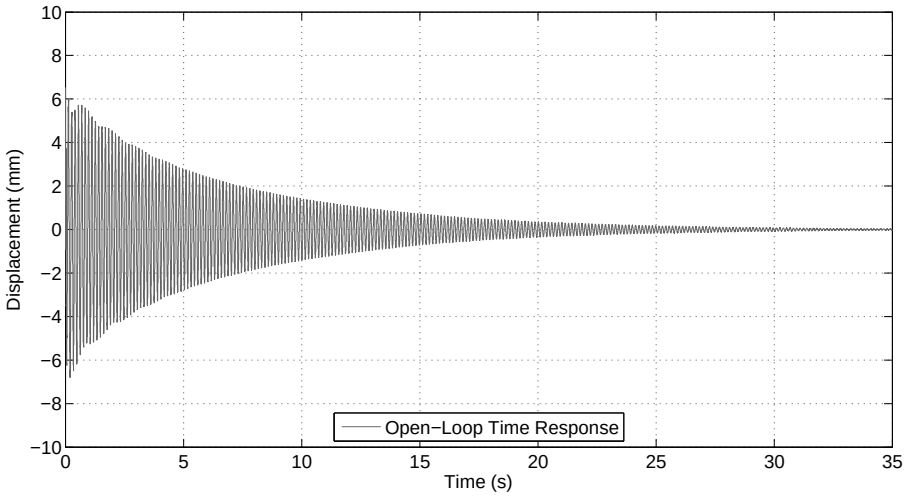

Figure 3.23: Open-Loop Time Response for 7mm Initial Tip Displacement

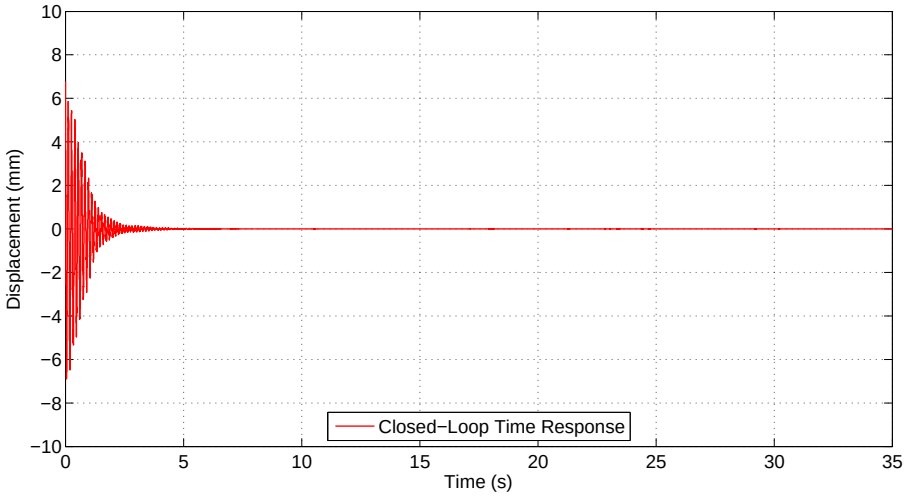

Figure 3.24: Closed-Loop Time Response for 7mm Initial Tip Displacement

3.4.3 Suppression of the First Resonance Forced Vibration

At this part of active vibration control, analysis of open-loop and closed-loop time responses are performed by applying a $150V_{pp}$ sinusoidal signal to bimorph configured piezoelectric patches (3A and 3B) at the first resonance frequency ($7Hz$). Similar to the suppression of free vibration results, the open-loop time response corresponds to the case where the robust

controller with piezoelectric sensor/actuator pair is inactive whereas the closed-loop time response corresponds to that where the active robust controller is on. Corresponding forced-vibration time responses are shown in Figure 3.25 and 3.26 for the open-loop and closed-loop cases, respectively.

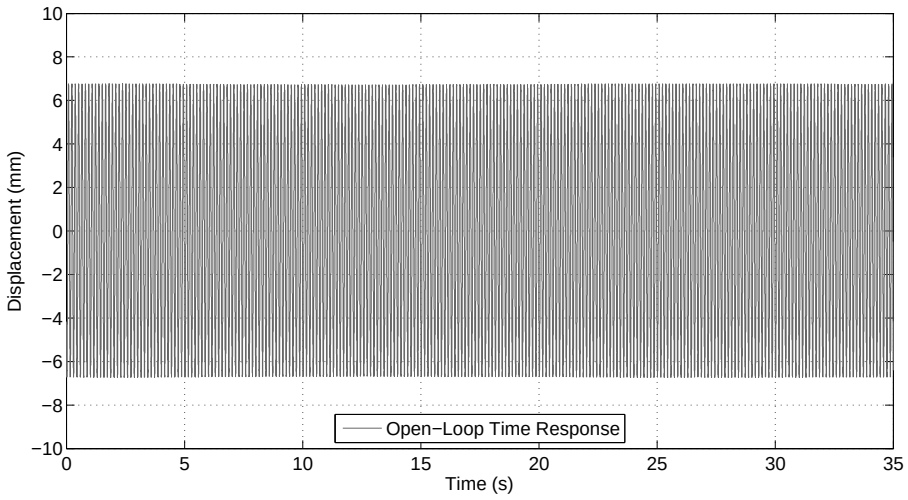

Figure 3.25: Open-Loop Time Response for the First Resonance Forced Vibration

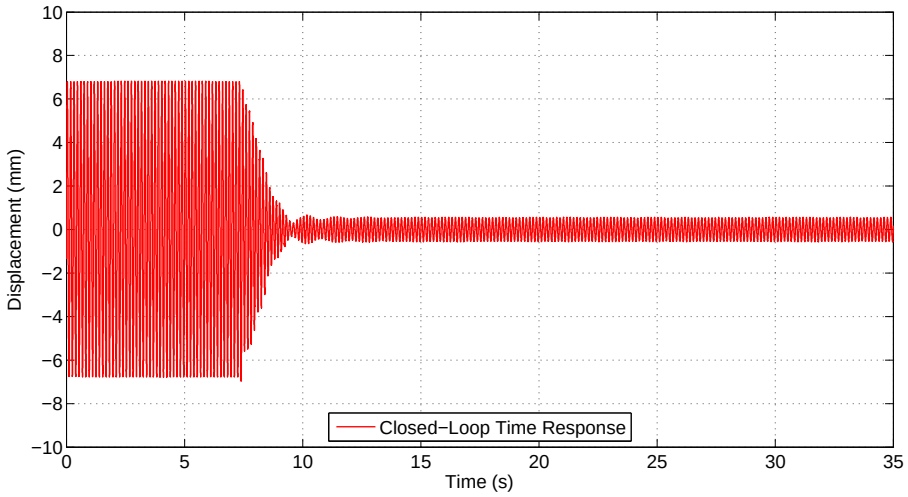

Figure 3.26: Closed-Loop Time Response for the First Resonance Forced Vibration

3.4.4 Vibration Suppression in Frequency Domain

The effectiveness of active vibration suppression via piezoelectric sensor/actuator pair with robust controller is further analyzed by open and closed loop frequency responses. For this purpose, the smart beam is excited with piezoelectric patches (3A-3B) while the response of the smart beam is monitored via piezoelectric patch 2A. At first, the robust controller is set inactive, and the frequency response of the smart beam is obtained between the piezoelectric disturbance patches (3A-3B) and sensor patch 2A. Then, the robust controller via piezoelectric sensor/actuator patch is set active and the measurement of frequency response is repeated. The obtained open and closed loop frequency responses of the smart beam is shown Figure 3.27. As it can be noticed, the vibration attenuation of approximately 15 dB is achieved between the input disturbance signal and output sensor signal.

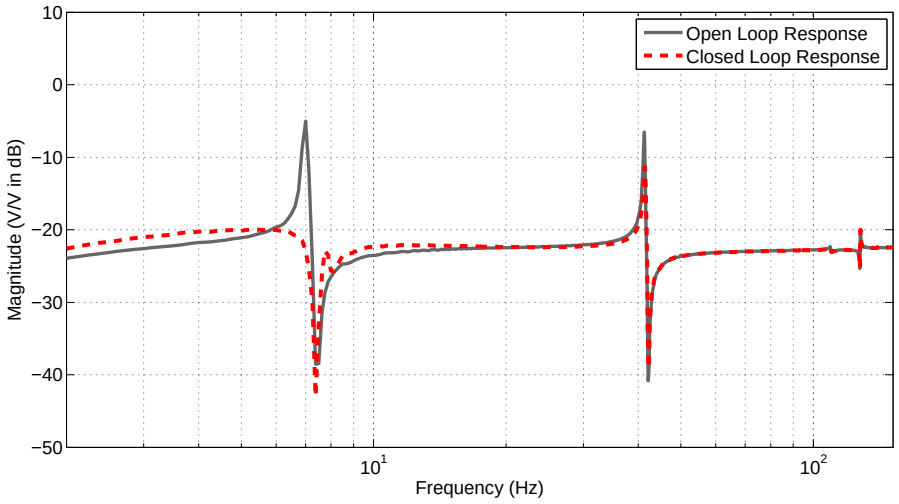

Figure 3.27: Performance Specification in Frequency Domain

3.5 Conclusion

In this chapter, piezoelectric sensor and actuator pair is used for an active vibration suppression of the smart beam with robust controller which is designed for the stable and the effective suppression of free and the first resonance forced vibration.

For the free vibration suppression, reduction of the maximum voltage to the sensor noise level (i.e. full suppression of the vibration) takes more than 30 seconds at the open-loop, however at the closed-loop, suppression of free vibration to the sensor noise level takes only 3 seconds. In the case of forced vibration suppression, the monitored voltage at closed-loop is approximately one-tenth of the monitored voltage at open-loop. This means that the robust controller via piezoelectric sensor and actuator pair can suppress %90 of the amplitude of vibration in the forced vibration case.

As a conclusion of this chapter, active vibration control of the smart beam is achieved by employment of piezoelectric patches as sensors and actuators via designed robust controller. The experimental work performed on the suppression of free and forced vibrations shows the effectiveness of these piezoelectric patches with the robust controller.

CHAPTER 4

ACTIVE VIBRATION CONTROL OF A SMART BEAM VIA SELF-SENSING PIEZOELECTRIC ACTUATOR

4.1 Introduction

This chapter presents self-sensing piezoelectric actuator for the active vibration suppression of the smart beam. In Chapter 3, active control of vibration of the smart beam is considered by using piezoelectric sensor/actuator pair via robust controller. Whereas, in this chapter, the vibration of the smart beam is suppressed by employment of piezoelectric patches as self-sensing actuator. At first, system identification of the smart beam is achieved by using self-sensing piezoelectric actuator. In the self-sensing configuration, piezoelectric patch is used as an actuator and a sensor simultaneously. For this configuration, a special bridge circuit which includes the electrical model of the piezoelectric material is designed and implemented in order to decompose the sensing and actuation signals. After acquiring mathematical model of the smart beam for self-sensing piezoelectric actuator, a robust controller is designed for active vibration suppression of the smart beam via self-sensing piezoelectric actuator by following the same approach used in piezoelectric sensor/actuator pair configuration. Finally, experimental results for suppressions of free and the first resonance forced vibration are presented.

4.2 System Identification of the Smart Beam via Self-Sensing Piezoelectric Actuator

In this section, the main concern is to obtain mathematical model of the smart beam based on experimental frequency response. Piezoelectric patches are used as self-sensing actuators to obtain necessary experimental frequency response for system identification and for this purpose, a special bridge circuit is designed and implemented. Then, piezoelectric patches (1A-1B and 4A-4B) are employed as self-sensing piezoelectric actuators to excite the smart beam and the response of the smart beam is also measured by these piezoelectric patches (1A-1B and 4A-4B). Using the knowledge gained on the vibration characteristics of the smart beam, the smart beam is excited within the bandwidth which covers the first three resonance modes and experimental frequency response of the smart beam with self-seing piezoelectric actuator is acquired. Then, mathematical model of the smart beam is obtained using this experimentally obtained frequency response.

4.2.1 Self-Sensing Piezoelectric Actuator

The aim here is to use four of the piezoelectric patches simultaneously as a sensor and an actuator for the active vibration control. Piezoelectric materials generate electrical signal when they are under mechanical stress. This property of piezoelectric materials enables them to be used as a sensor. On the other hand, piezoelectric materials are mechanically deformed when electric field is applied to them. In consequence of this property, piezoelectric materials can be also used as actuators [12]. Beside these, a piezoelectric material can be simultaneously used as a sensor and an actuator when actuation and sensing signals are decomposed. For this purpose, a special bridge circuit can be used [34, 42].

The bridge circuit used in this study is shown in Figure 4.1. This bridge circuit includes the electrical model of the piezoelectric material with additional circuit elements. The piezoelectric material is modelled as a voltage source $v_P(t)$ with a series capacitor C_p. In essence, when the actuation signal $v_A(t)$ is applied to the piezoelectric patch bonded on the smart beam, the response of the smart beam particular to this excitation can be measured by monitoring the voltage $v_S(t)$ by using this bridge circuit.

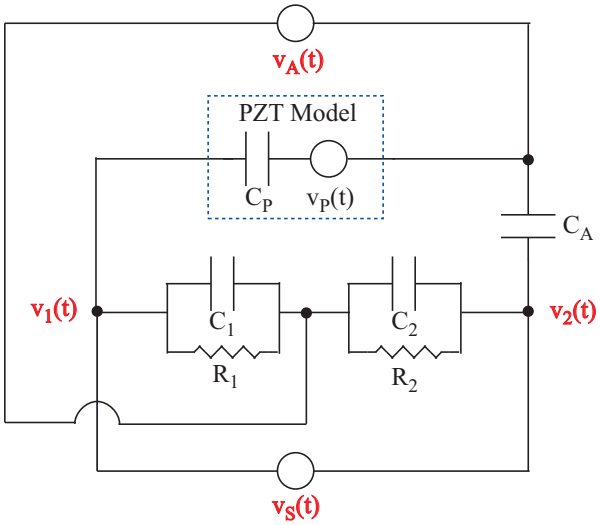

Figure 4.1: Bridge Circuit for Self-Sensing Piezoelectric Actuator

The sensor signal $v_S(t)$ is equivalent to the substraction of the two voltages $v_1(t)$ and $v_2(t)$ at nodes:

$$v_S(t) = v_1(t) - v_2(t) \tag{4.1}$$

By applying Kirchoff's current and voltage laws, the sensor signal in terms of actuation and piezoelectric material voltages can be obtained in time domain. By assuming zero initial conditions and applying Laplace transform, the transfer function for the sensor signal can be found as :

$$V_S(s) = \left(\frac{sC_AR_2}{1+s(C_2R_2+C_AR_2)} - \frac{sC_PR_1}{1+s(C_1R_1+C_PR_1)}\right)V_A(s) + \frac{sC_PR_1}{1+s(C_1R_1+C_PR_1)}V_P(s) \tag{4.2}$$

The details of the application of Kirchoff's laws and obtaining the transfer function for the sensor signal is presented in Appendix B.

In the transfer function shown in Equation 4.2, independency of the sensor voltage from the actuation voltage can be achieved theoretically by selecting the values of capacitors (C_1 and C_2) and resistors (R_1 and R_2) as identical, and setting the amount of capacitance (C_A) to capacitance of piezoelectric material. These conditions for isolating the sensor voltage from the actuation voltage are listed in Equation 4.3:

$$C_A = C_P \qquad C = C_1 = C_2 \qquad \textit{and} \qquad R = R_1 = R_2 \tag{4.3}$$

By assuring the conditions in Equation 4.3, the sensor voltage independent from actuation voltage is acquired as ;

$$V_S(s) = \frac{sC_P R_1}{1 + s(C_1 R_1 + C_P R_1)} V_P(s) \tag{4.4}$$

This sensor voltage in Equation 4.4 is the high-pass filtered form of the piezoelectric material's voltage. In fact, the cut-off frequency of this high pass filter can be determined by selection of resistance and capacitance values in the bridge circuit. In our study, to capture low frequency dynamics of the system, the cut-off frequency of the high pass filter should be kept low. Figure 4.2 shows the frequency response of the high-pass filter defined by Equation 4.4 for $3.3M\Omega$ resistor value and $75nF$ capacitances value.

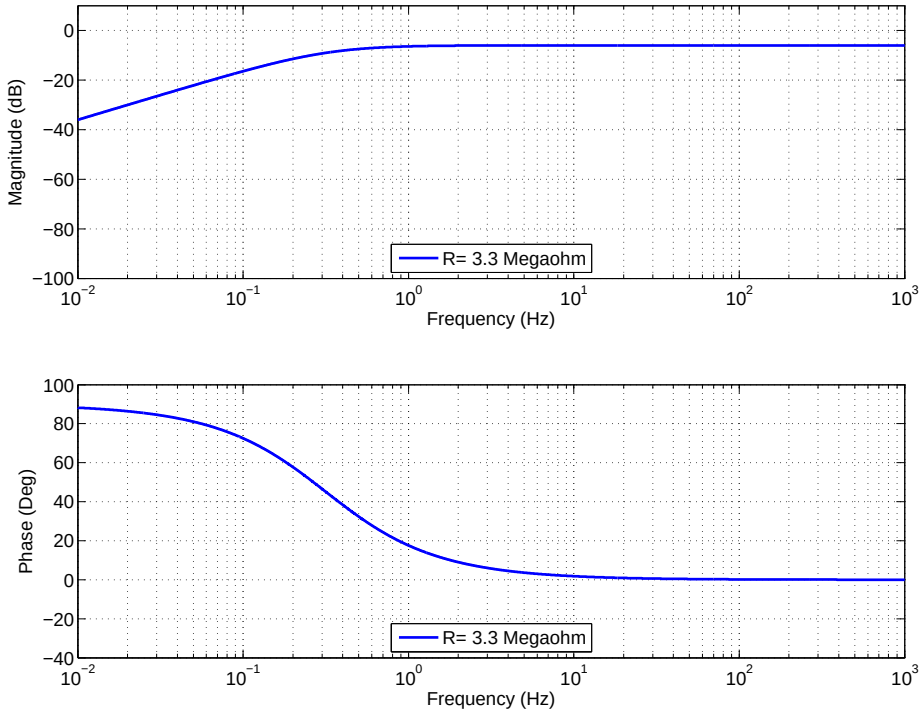

Figure 4.2: High Pass Characteristics of Bridge Circuit

In our study, the total capacitance of the piezoelectric patches (1A-1B and 4A-4B) is measured as 75 nF. The value of the resistances and capacitances are selected as 3.3 MΩ and 72 nF. As aforementioned, the other condition for the independency of the sensor voltage from the actuation voltage is the equivalency the amount of capacitance C_A and piezoelectric material capacitance. So that, the conditions of the independency are provided by adjusting the amount of capacitance C_A.

4.2.2 Experimental Frequency Response

The frequency response of the smart beam is obtained by self-sensing piezoelectric actuator and then the analytical model of the system is gathered for controller applications with self-sensing actuator. Four piezoelectric patches (1A-1B and 4A-4B) are used as self-sensing actuator and using the special bridge circuit explained in Section 4.2.1, the actuation and sensing signals are decomposed.

4.2.2.1 Experimental Setup

The experimental setup for self-sensing piezoelectric actuator configuration is presented in Figure 4.3. Using this configuration, a swept sine signal in the bandwidth 2 Hz to 152 Hz is applied to the bridge circuit while the actuation signal and sensing signal is monitored by PULSE Data Acquisition system.

The analyzer properties of the Brüel and Kjær PULSE 3560C listed in Table 4.1. High resolution in frequency domain is needed to prevent the interlacing of the resonance and anti-resonance modes of the system. By configuring the analyzer, high resolution in frequency domain is achieved by increasing the number of lines.

Table 4.1: Analysis Setup Configuration for System Identification by Self-Sensing Piezoelectric Actuator

Analyzer Property	**Value/Type**
Frequency Span	0 Hz - 200 Hz
Number of Lines	3200 lines
Number of Averages	120 Averages
Duration of Analysis	600 seconds
Averaging Mode	Linear
Analysis Mode	Baseband
Overlap Ratio	%66.67

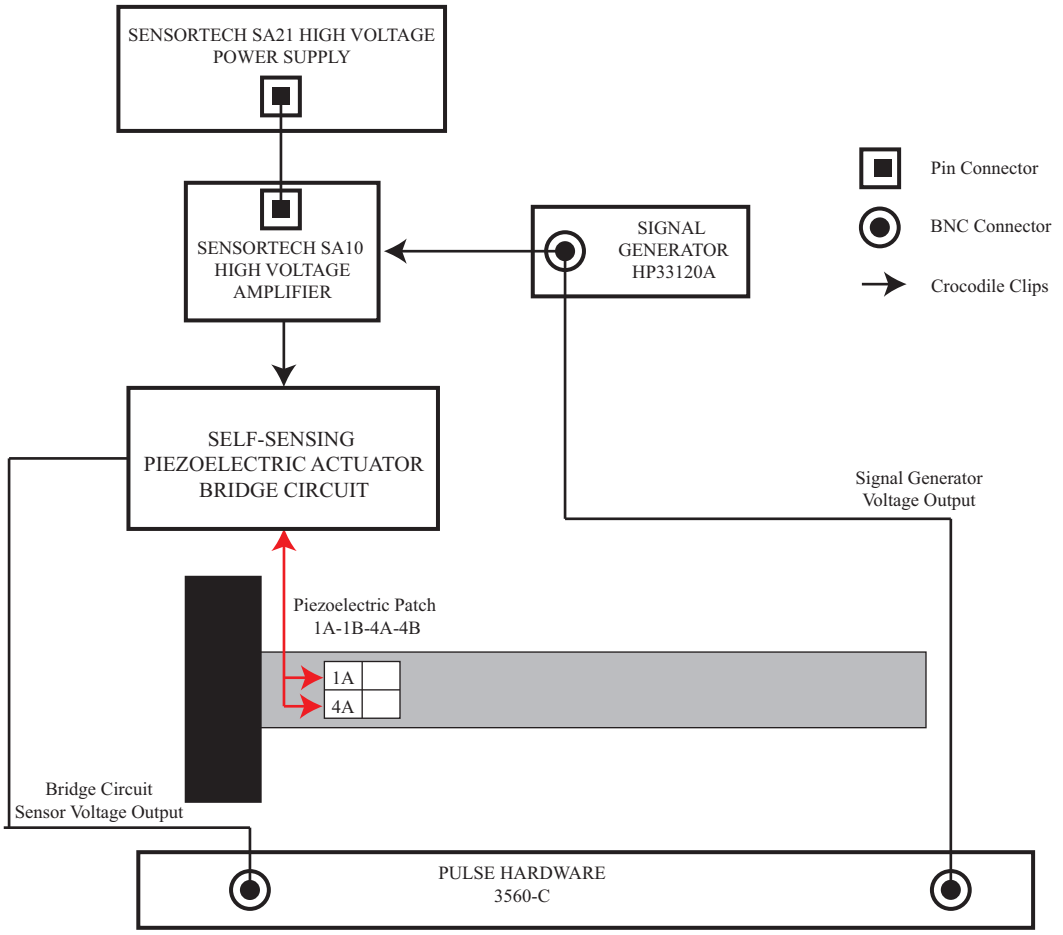

Figure 4.3: Experimental Setup for Modelling

4.2.2.2 Frequency Response

Using the self-sensing piezoelectric actuator, the frequency response in Figure 4.4 is acquired. The measured frequency response of the smart beam with self-sensing piezoelectric actuator has mass-dominated characteristic at the low frequencies. Regarding resonance/anti-resonances, the behavior is similar with the frequency response obtained via piezoelectric sensor/actuator pair. In spite of this fact, the resonance peak amplitudes appear to be very low compared with that of measured via piezoelectric sensor/actuator pair case.

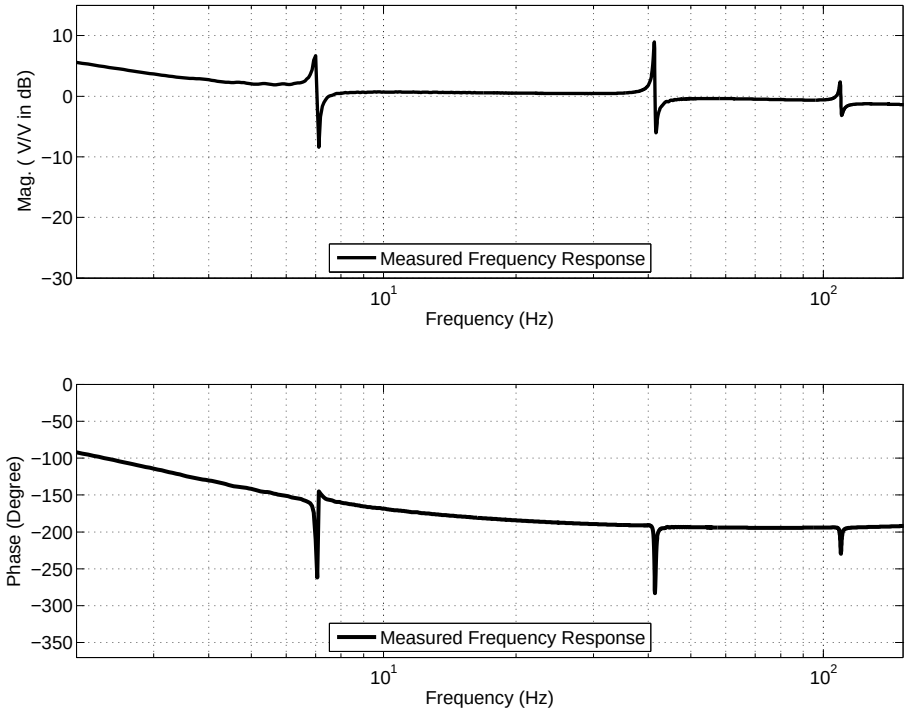

Figure 4.4: Measured Frequency Response for Self-Sensing Piezoelectric Actuator

4.2.3 Analytical Model of the Smart Beam

The mathematical model of the smart beam is derived based on the measured frequency response of the smart beam via self-sensing piezoelectric actuator. As in Chapter 3, MATLAB's "fitsys" command is also used and state-space model of the system is built for 4^{th} , 8^{th} and 16^{th} orders. The frequency responses of these estimated transfer functions are given in Figure 4.5. These transfer functions represent the relation between the excitation signal applied to self-sensing piezoelectric actuators and the sensing voltage acquired from the self-sensing bridge circuit. The 8^{th} order transfer function presented in Equation 4.5 is accurate enough to be used in the controller applications.

$$G(s) = \frac{-0.663s^8 - 499.8s^7 - 3.583\times10^5 s^6 - 2.706\times10^8 s^5 - 1.918\times10^{10}s^4 - \ldots}{s^8 + 449.9\times s^7 + 5.482\times10^5 s^6 + 2.416\times10^8 s^5 + 3.527\times10^{10}s^4 + \ldots} \quad (4.5)$$
$$\frac{1.657\times10^{13}s^3 + 1.764\times10^{14}s^2 - 3.17\times10^{16}s + 4.36\times10^{17}}{1.459\times10^{13}s^3 + 1.794\times10^{14}s^2 + 2.746\times10^{16}s + 2.038\times10^{17}}$$

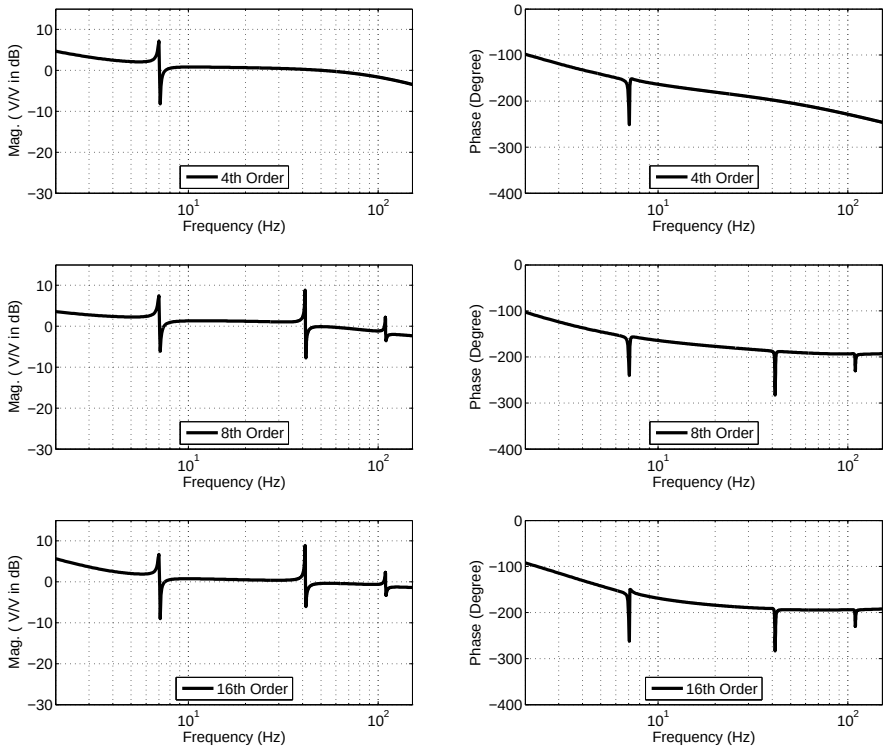

Figure 4.5: Frequency Responses of Estimated Transfer Functions of Smart Beam via Self-Sensing Piezoelectric Actuator

4.3 Robust Controller Design

The suppression of free and the first resonance frequency forced vibration via self-sensing piezoelectric actuator is achieved by designed robust controller. The design process for self-sensing piezoelectric actuator is kept almost similar with piezoelectric sensor/actuator pair case as explained in details in Chapter 3.

In this section, on the other hand, the differences in design and analysis process of the robust controller including H_∞ synthesis and μ analysis are explained. At first, system uncertainties and performance specifications are pointed out. Then, the H_∞ synthesis and μ analysis is conducted for design of robust control. Finally, the performance specifications of robust controller is presented via simulation results.

4.3.1 System Uncertainties and Performance Specifications

As emphasized in Chapter 3, an important phase of robust controller design is the development of system uncertainties and desired performance criterions. In essence, the block diagram used for robust controller design via self-sensing piezoelectric actuator is provided in Figure 4.6. The difference in the block diagram compared to that in piezoelectric sensor/actuator pair case, the additive uncertainty block (W_{add}) is placed instead of multiplicative uncertainty block (W_m). Uncertainties in the mathematical model of the plant can be identified as a normalized transfer function by multiplicative uncertainty and absolute transfer function by additive uncertainty [72]. The additive and multiplicative uncertainties are mathematically convertible [73]. The other blocks which are used to present performance specifications are kept in the same positions, but the transfer function of each block is adopted for self-sensing piezoelectric case. In the following, the development of system uncertainties and performance specifications is revealed.

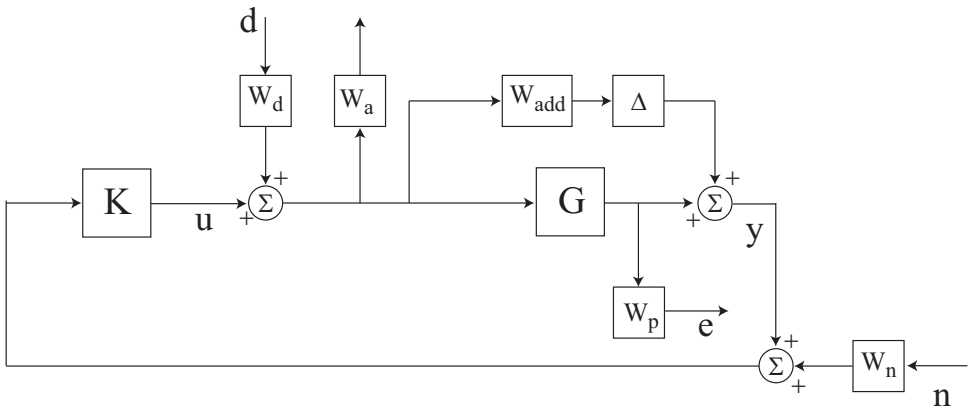

Figure 4.6: Block Diagram for Robust Controller Design via Self-Sensing Piezoelectric Actuator

4.3.1.1 Desired Performance Weight (W_p)

The aim of the robust controller via self-sensing piezoelectric actuator is identical with the prementioned robust controller via piezoelectric sensor/actuator pair. In brief, the desired performance block (W_p) is selected as a low pass filter in the form of second order transfer function and is adopted for self-sensing piezoelectric actuator as shown in Equation 4.6.

$$W_p = \frac{4900}{s^2 + 700s + 122500} \tag{4.6}$$

The frequency response of the transfer function of desired performance W_p is shown in Figure 4.7. The characteristics of desired performance at low frequencies is constant smooth-line up to the first resonance frequency (7 Hz) whereas the magnitude of desired performance slowly decreases after the first resonance frequency of the smart beam since high frequency attenuation is beyond the scope of this study.

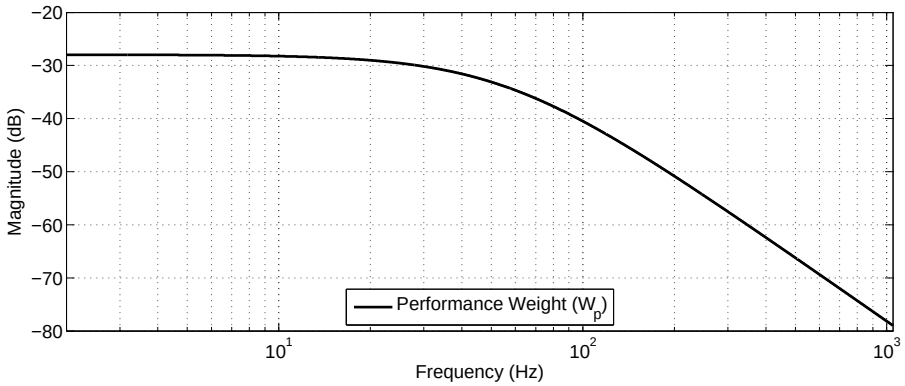

Figure 4.7: Frequency Response of Desired Performance Weight (W_p)

4.3.1.2 Disturbance Weight (W_d)

The disturbance weight is a significant parameter accounting for generation of undesirable behavior of the smart beam during the design process of robust controller. The undesirable behavior of the smart beam is the vibration due to external disturbances at low frequencies. Therefore, the disturbance weight is utilized as in the form of low pass filter and the gain of the filter is adopted for better and stable robust controller via self-sensing piezoelectric actuator. The transfer function of the disturbance is shown in Equation 4.7 and the corresponding frequency response is presented in Figure 4.8.

$$W_d = 1.401 \times \frac{300}{s + 300} \tag{4.7}$$

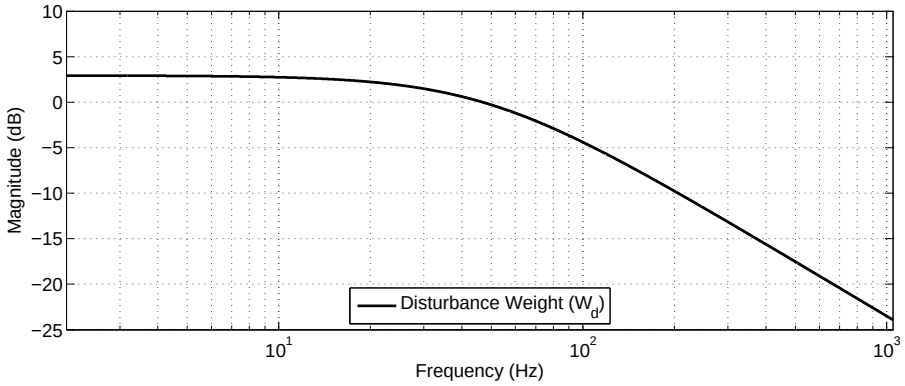

Figure 4.8: Frequency Response of Disturbance Input Weight (W_d)

4.3.1.3 Noise Weight (W_n)

The aim in considering the noise weight during the design phase of robust controller is to quantify the noise in vibration measurement of the smart beam via self-sensing piezoelectric actuator. For this purpose, noise measurement is conducted via programmable controller and presented in Figure 4.9. Figure 4.10 shows the power spectral density of this noise measurement. From this power spectral density of the noise, it is concluded that the signal-to-noise ratio is constant over the frequency range of interest. However, in the self-sensing piezoelectric configuration, the amplitude of the average noise is twice the amplitude measured for piezoelectric sensor/actuator pair case. So that, the noise weight is selected as unity with an amplitude 0.02.

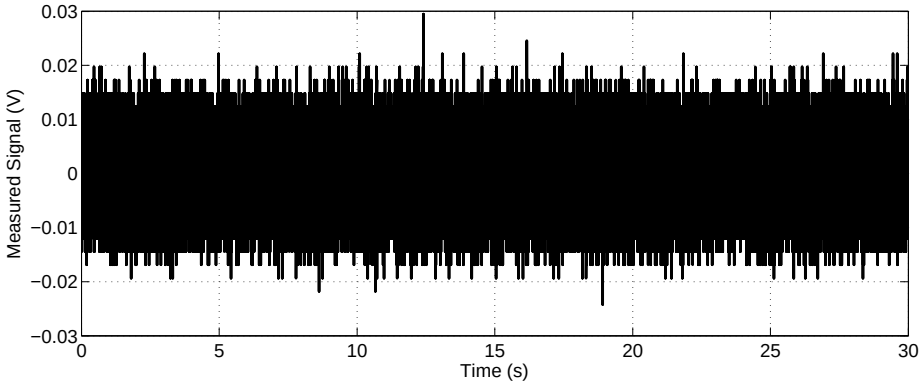

Figure 4.9: Recorded Noise for Self-Sensing Piezoelectric Actuator

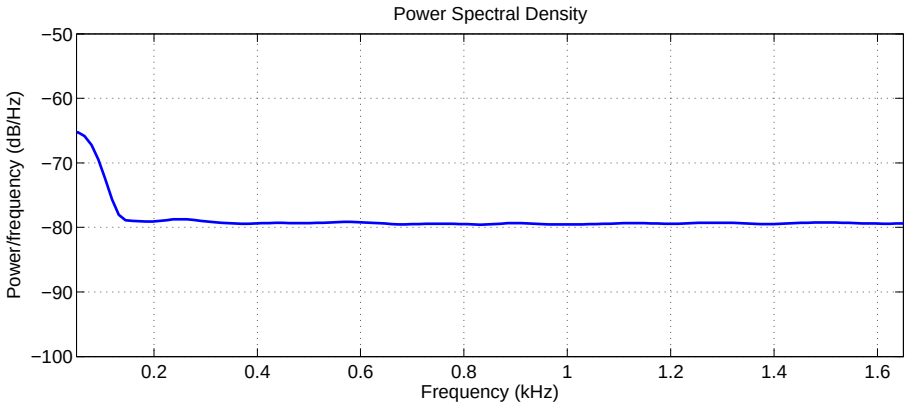

Figure 4.10: Power Spectral Density of the Noise for Self-Sensing Piezoelectric Actuator

4.3.1.4 Actuator Limitation Weight (W_a)

Determining and using the actuator limitation in design process is needed to prevent the piezoelectric patches from high voltage by keeping the output voltage of the programmable controller in limits. The actuator limitation weight (W_a) is again assumed to be constant over the frequency range and its magnitude is calculated as 0.2 by normalizing the unity voltage by the output limit of the controller which is 5V.

4.3.1.5 Additive Uncertainty (W_{add} and Δ)

As described earlier, the decomposition of sensor and actuator signals in self-sensing piezoelectric actuator configuration is utilized by using special bridge circuit. This bridge circuit includes capacitor which has the capacitance value equal to capacitance of self-sensing piezoelectric actuator patch. However, the capacitance of piezoelectric material changes due to the environmental effects such as, room temperature, humidity etc. and this results in a dependency of the sensor signal on actuator signal. The additive uncertainty is included to eliminate this undesirable effect on the sensor voltage in robust controller design. The block diagram for additive uncertainty is shown in Figure 4.11. This diagram includes nominal plant G and additive uncertainty weight W_{add} with structured uncertainty Δ. In addition to these, the perturbed plant G_p is shown with dashed line.

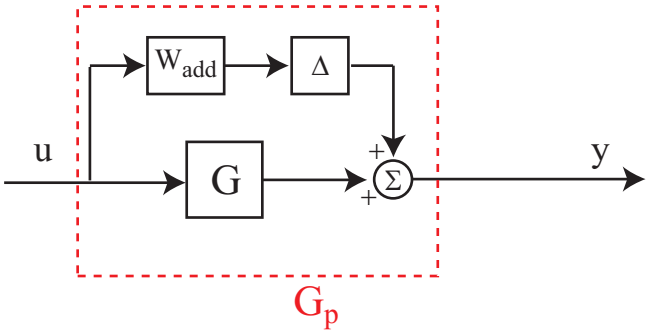

Figure 4.11: Block Diagram for Additive Input Uncertainty

From the relationships between the output signal y and the input signal u, the relation for the perturbed plant can be found as:

$$G_p = G + \Delta W_{add}. \tag{4.8}$$

When the structured uncertainty block is eliminated, the additive uncertainty can be expressed as follows,

$$W_{add} = G_p - G. \tag{4.9}$$

This additive uncertainty weight W_{add} can be obtained experimentally by acquiring the frequency responses of the nominal and perturbed plants. Herein, the nominal plant stands for the analytical model of the smart beam based on measured frequency response via self-sensing piezoelectric actuator. For this frequency response measurement, peak-to-peak $150V$ is applied to the piezoelectric patches and the sensing signal is measured from the special bridge circuit. In order to reveal the perturbed plant because of sensing and actuation signals coupling, three different frequency responses via self-sensing piezoelectric actuator configuration are obtained with different actuation signals. For these measurements, the actuation voltage is selected as a swept sine in the frequency range of $2Hz$ to $152Hz$ with a peak-to-peak $30V$, $90V$ and $120V$. The response of the smart beam particular to each actuation voltage is monitored by the sensor signal through the bridge circuit. These frequency responses are considered as perturbed plants' frequency responses shown in Figure 4.12.

The frequency responses of perturbed plants are averaged and the nominal frequency response is subtracted from this average frequency response. Experimental frequency response of additive uncertainty is obtained with the result of this substraction. In order to consider this experimentally found frequency response of additive uncertainty in controller design, this

substraction is covered by an estimated transfer function shown in Equation 4.10. The frequency responses of measured and estimated additive uncertainties are shown in Figure 4.13. The magnitude of the estimated additive uncertainty is kept constant at high frequencies to also include high frequency dynamics of the smart beam.

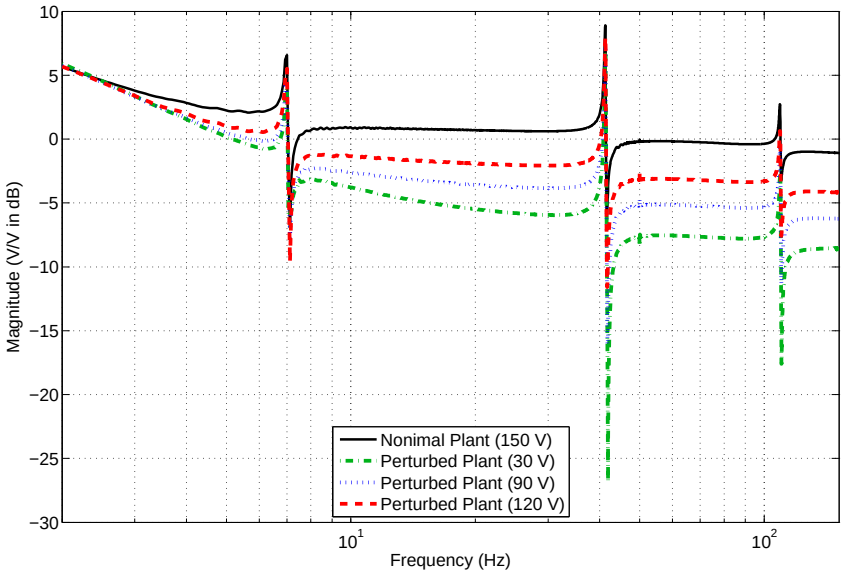

Figure 4.12: Experimental Frequency Responses for Different Actuation Voltages

$$W_{add} = \frac{1.787s^4 + 4447s^3 + 8.089 \times 10^5 s^2 + 2.202 \times 10^6 s + 5.285 \times 10^5}{s^4 + 2388s^3 + 3.906 \times 10^5 s^2 + 3.038 \times 10^6 s + 4.740 \times 10^6} \tag{4.10}$$

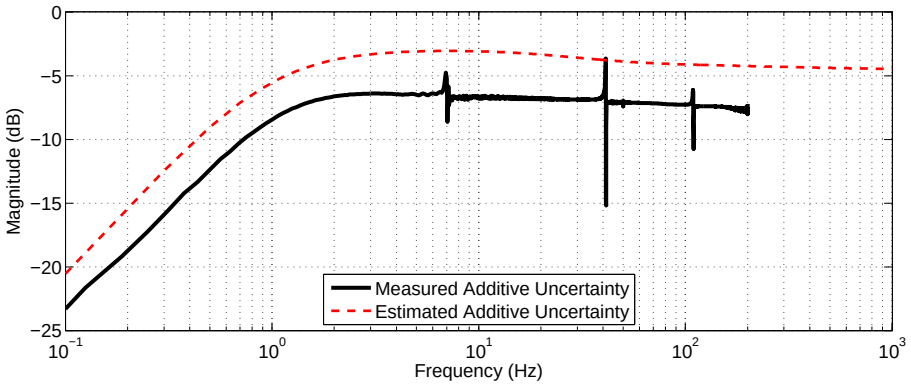

Figure 4.13: Frequency Response of Additive Uncertainty (W_{add})

4.3.2 Synthesis of System Inputs and Outputs

Previously in Chapter 3, the solution of H_∞ controller problem is explained for a plant and a controller in linear fractional transformation form. The main concern in this section is to obtain a lower fractional transformation form of the plant and the controller by considering system uncertainties and performance specifications. For this purpose, each output signal is defined in terms of input signals. Figure 4.14 shows the input and output signals considered in the synthesis of system inputs and outputs.

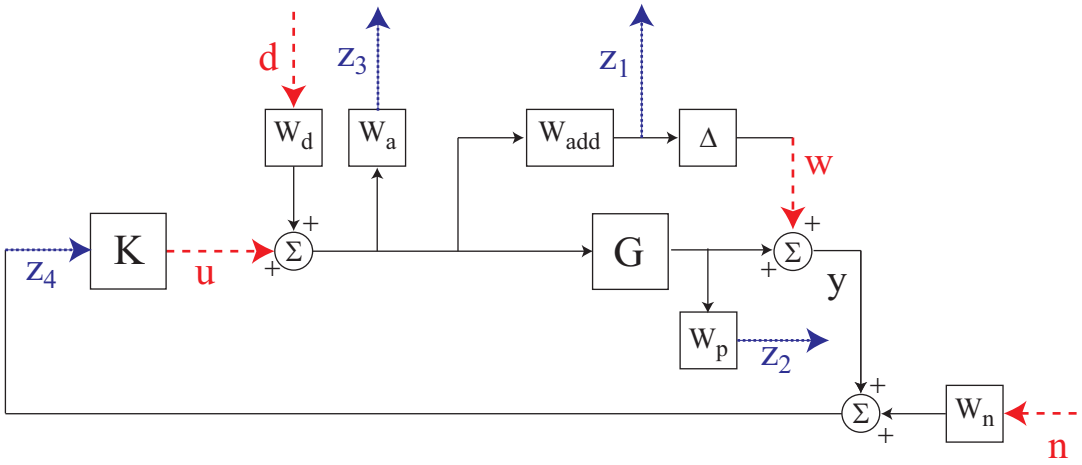

Figure 4.14: Block Diagram for Robust Controller Design

The output signal z_1 is the output signal of additive output uncertainty, z_2 is the output signal of the desired performance weight, z_3 is the output signal of actuator limitation weight, and z_4 is the addition of system output signal and noise weight signal. The input signals are the output signal of uncertainty w, noise signal n, disturbance d and controller u. Equations 4.11 - 4.14 show the relations between the system inputs and outputs.

$$z_1 = W_{add}(W_d d + u) \tag{4.11}$$

$$z_2 = W_p G(W_d d + u) \tag{4.12}$$

$$z_3 = W_a(W_d d + u) \tag{4.13}$$

$$z_4 = w + G(W_d d + u) + W_n n \tag{4.14}$$

The system inputs and outputs are shown in the matrix form in Equation 4.15 as.

$$\begin{bmatrix} z_1 \\ z_2 \\ z_3 \\ z_4 \end{bmatrix} = \underbrace{\begin{bmatrix} 0 & 0 & W_{add}W_d & W_{add} \\ 0 & 0 & W_pW_dG & W_pG \\ 0 & 0 & W_aW_d & W_a \\ 1 & W_n & GW_d & G \end{bmatrix}}_{\mathrm{P}} \times \begin{bmatrix} w \\ n \\ d \\ u \end{bmatrix} \tag{4.15}$$

Figure 4.15 shows corresponding generalized plant P, uncertainty block Δ and controller K with system inputs and outputs.

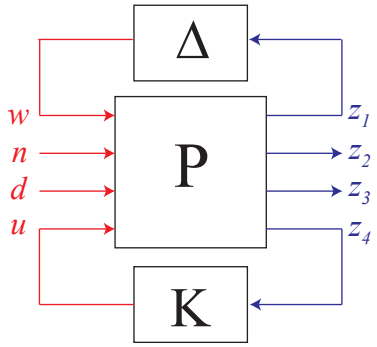

Figure 4.15: Generalized Plant with Inputs and Outputs

In order to acquire lower linear fractional transformation, the input and output signals are grouped as follows in Equation 4.16 and the matrix form of generalized plant is given in Equation 4.17.

$$r = \begin{bmatrix} w \\ n \\ d \end{bmatrix} \qquad z = \begin{bmatrix} z_1 \\ z_2 \\ z_3 \end{bmatrix} \qquad v = z_4 \tag{4.16}$$

$$\begin{bmatrix} z \\ v \end{bmatrix} = \begin{bmatrix} P_{11} & P_{12} \\ P_{21} & P_{22} \end{bmatrix} \times \begin{bmatrix} r \\ u \end{bmatrix} \tag{4.17}$$

The output of controller signal u (Eqn. 4.18 can be expressed with the signal addition of system output and noise signal (formerly z_4, now it is named as v).

$$u = Kv \tag{4.18}$$

Then the equation for each output signal group can be written as follows,

$$z = P_{11}r + P_{12}Kv, \tag{4.19}$$

$$v = P_{21}r + P_{22}Kv, \tag{4.20}$$

where the partitions of the generalized plant P are

$$P_{11} = \begin{bmatrix} 0 & 0 & W_{add} \\ 0 & 0 & W_pW_dG \\ 0 & 0 & W_aW_d \end{bmatrix} \qquad P_{12} = \begin{bmatrix} W_{add} \\ W_pG \\ W_a \end{bmatrix}, \tag{4.21}$$

$$P_{21} = \begin{bmatrix} 1 & W_n & W_dG \end{bmatrix} \qquad P_{22} = \begin{bmatrix} G \end{bmatrix}. \tag{4.22}$$

By solving Equation 4.20 for v, one can obtain,

$$v = (I - P_{22}K)^{-1}P_{21}r, \tag{4.23}$$

and by substituting v in Equation 4.19, we obtain a relation between output signal z and input signal r, which is shown in Equation 4.24, can be obtained.

$$\begin{aligned} z &= \left[P_{11} + (I - P_{22}K)^{-1}P_{21}\right]r, \\ &= F(P,K)r. \end{aligned} \tag{4.24}$$

In Equation 4.24, the weighted output signals are expressed as a function of disturbance and noise. As explained previously in Section 3.3.1, the objective of H_∞ controller is to minimize the $\|F(P,K)\|_\infty$ by finding a stabilizing controller K.

4.3.3 H_∞ Controller Design and Performance Specifications

By considering the system uncertainties and performance criterions, H_∞ controller is designed for self-sensing actuator configuration. The frequency responses of open and closed loops are shown in Figure 4.16. Applying H_∞ controller, a considerable reduction (5 dB) in the first mode is achieved for the self-sensing piezoelectric actuator.

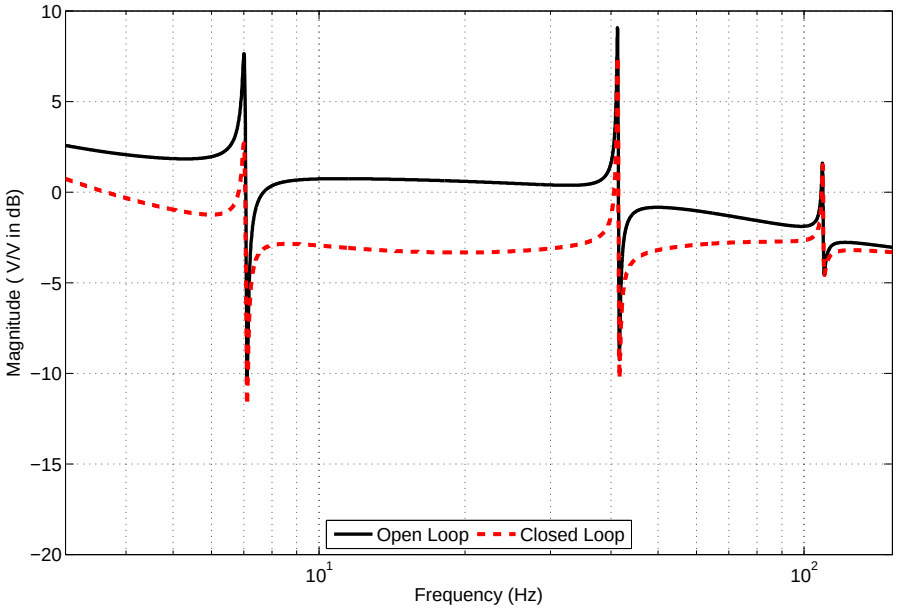

Figure 4.16: Open Loop and Closed Loop Frequency Responses for Self-Sensing Piezoelectric Actuator Configuration

4.3.4 μ Analysis for Designed H_∞ Controller

The designed H_∞ controller is further examined by μ analysis. The output and input signals of the robust controller via self-sensing piezoelectric actuator are kept identical with the piezoelectric sensor/actuator case. So that, μ analysis is conducted in a similar way as explained in Section 3.3.7.

Figure 4.17 shows the singular values of the closed-loop system over the frequency range. From this figure, it can be seen that the maximum singular value is 0.99 at the 2^{nd} bending mode. Since the maximum singular value is smaller than 1, robust performance is guaranteed for the designed H_∞ controller.

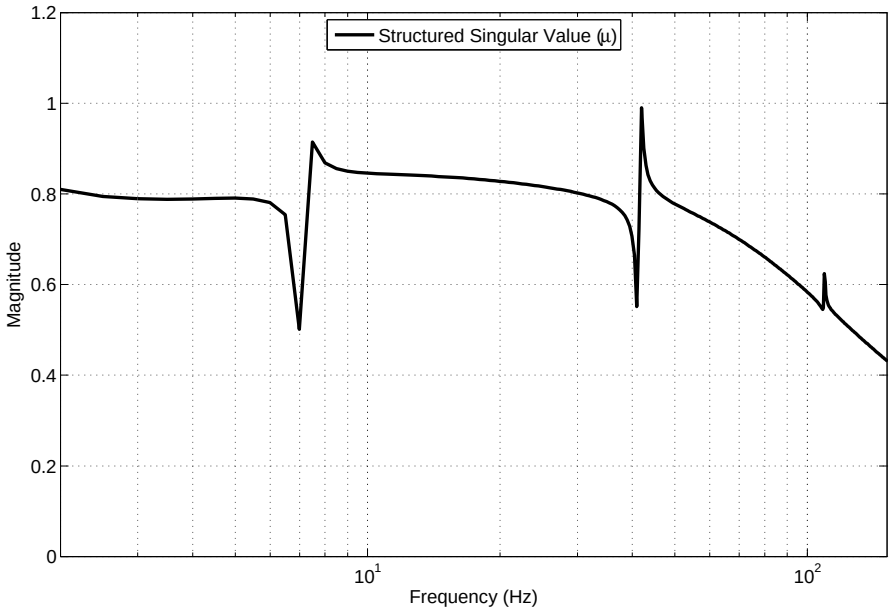

Figure 4.17: Singular Values of the Closed-Loop System with Self-Sensing Piezoelectric Actuator

4.4 Active Vibration Control Experiments

The piezoelectric patches bonded on the surface of cantilever-beam like structure are used as self-sensing actuators to suppress free and forced vibrations. Active vibration control is achieved by using four piezoelectric patches as self-sensing actuators. During the experiments, another piezoelectric patch, 2A, is also used to monitor the vibration of the smart beam. For cantilever-beam structures, maximum curvature at the clamped-end corresponds with the maximum tip displacement in the first bending mode. Therefore, monitoring of voltage of piezoelectric patch 2A reflects the tip displacement of smart beam for the free and the first resonance forced vibrations. Monitoring the vibration of the smart beam by piezoelectric patch 2A provides opportunity to compare the performance of the self-sensing piezoelectric actuator configuration with piezoelectric sensor/actuator pair case.

4.4.1 Experimental Setup

The suppression of vibrations of the smart beam is shown by experiments. The experimental setup of the self-sensing piezoelectric actuator case includes the special bridge circuit explained in Section 4.2.1. The input of the special bridge circuit is the amplified output signal of the programmable controller and the output of the special bridge circuit is directly transferred to the programmable controller as the input signal. Four piezoelectric patches (1A-1B and 4A-4B) are used as self-sensing actuator. In order to compare the performance of self-sensing piezoelectric actuator with results presented in Chapter 3, the output voltage of piezoelectric patch (2A) is also monitored during the experiments.

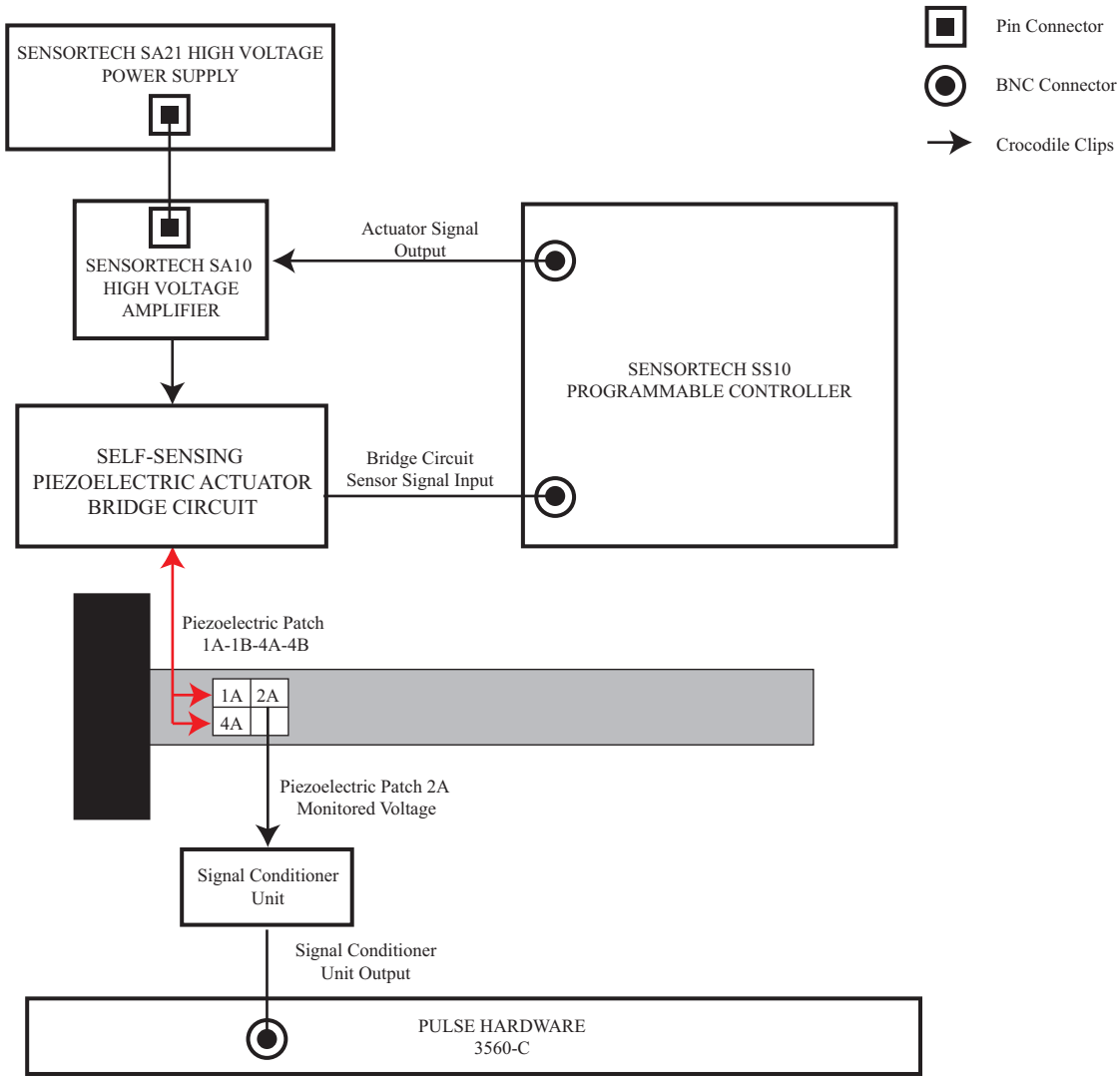

Figure 4.18: Experimental Setup for Controller Applications with Self-Sensing Piezoelectric Actuator

4.4.2 Suppression of Free Vibration

At the first part of active vibration control, analysis of open-loop and closed-loop time responses are performed by applying a 7mm initial tip displacement with zero initial tip velocity. Corresponding time responses are given in Figure 4.19 and 4.20 respectively.

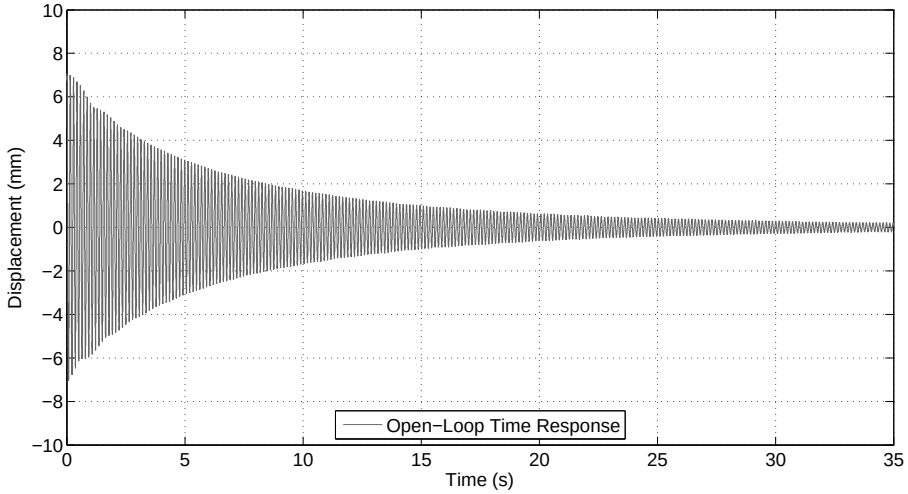

Figure 4.19: Open-Loop Time Response for 7mm Initial Tip Displacement

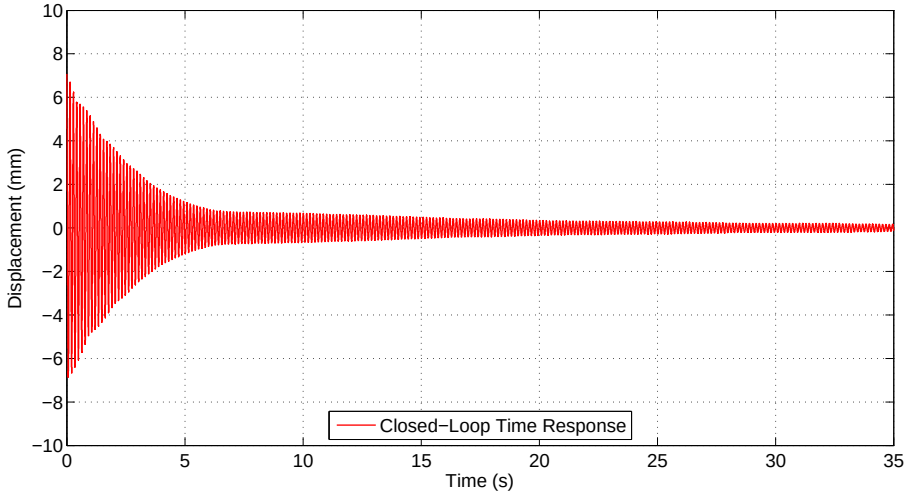

Figure 4.20: Closed-Loop Time Response for 7mm Initial Tip Displacement

4.4.3 Suppression of the First Resonance Forced Vibration

At the second part of active vibration control via self-sensing piezoelectric actuator, analysis of open-loop and closed-loop time responses are performed by applying a 150 V(p-p) sinusoidal signal to bimorph configured piezoelectric patches (3A and 3B) at the first resonance

frequency (7 Hz). Similar to the suppression of free vibration results, the open-loop time response corresponds to the case where the robust controller via self-sensing actuator is inactive whereas the closed-loop time response corresponds to the one when active robust control is achieved via self-sensing actuator. Corresponding forced-vibration time responses are given in Figure 4.21 and 4.22 respectively for the open and closed loop cases.

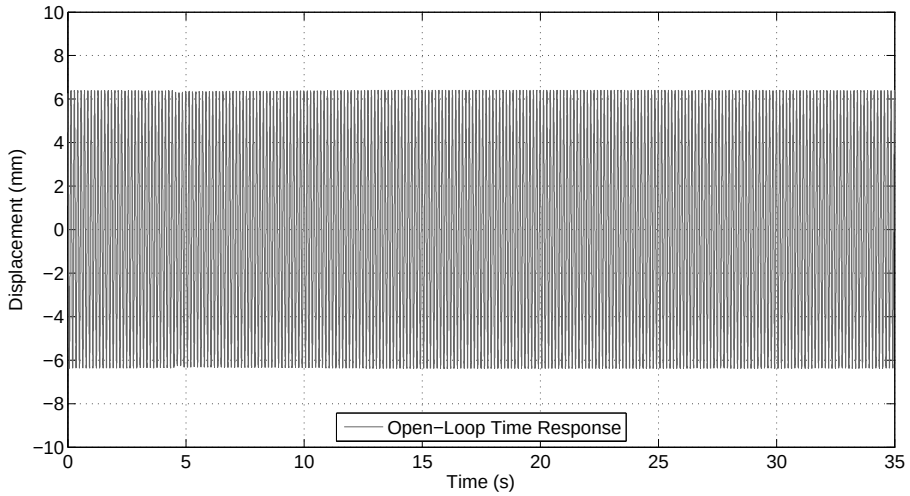

Figure 4.21: Open-Loop Time Response for the First Resonance Forced Vibration

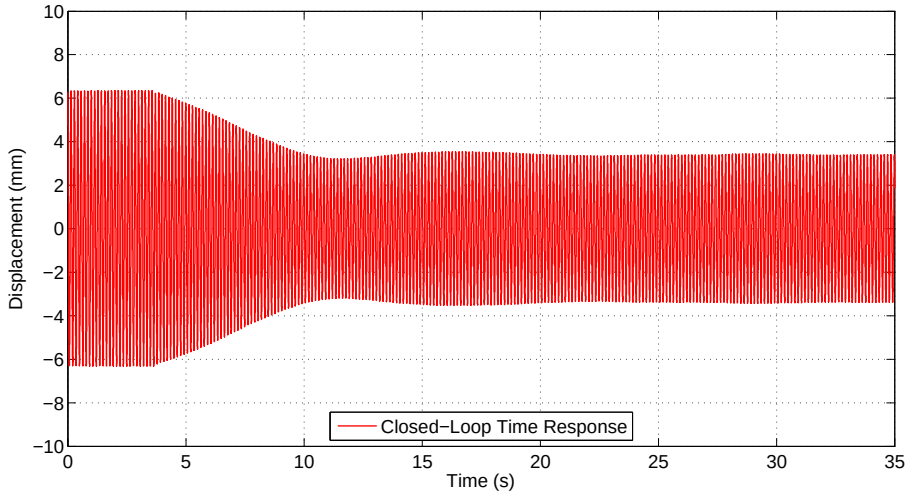

Figure 4.22: Closed-Loop Time Response for the First Resonance Forced Vibration

4.4.4 Vibration Suppression in Frequency Domain

The performance of active vibration suppression via self-sensing piezoelectric actuator with robust controller is further investigated by open and closed loop frequency responses. For this purpose, the smart beam is excited with piezoelectric patches (3A-3B) while the response of

the smart beam is monitored with piezoelectric patch 2A as in the piezoelectric sensor/actuator pair case. The measurement is conducted for inactive (open - loop) and active controller (closed loop) cases. The obtained open and closed loop frequency responses of the smart beam is shown in Figure 4.23. It can be seen from the figure that the vibration attenuation around 5 dB is achieved in between the input disturbance signal and output sensor signal.

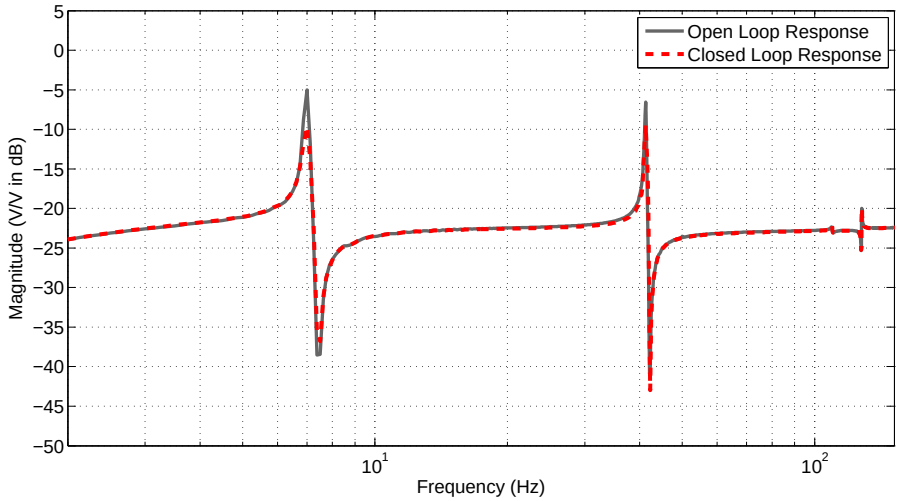

Figure 4.23: Performance Specification in Frequency Domain

4.5 Conclusion

In this section, self-sensing piezoelectric actuator is used for an active vibration suppression of the smart beam with robust controller which is designed for the stable and the effective suppression of free and the first resonance forced vibration.

For the free vibration suppression, reduction of one-quarter of the maximum voltage takes more than 13 seconds at the open-loop, however at the closed-loop, suppression of free vibration to the one-quarter of the maximum voltage takes only 7 seconds. In the case of forced vibration suppression, the monitored voltage at closed-loop is almost the half of the monitored voltage at open-loop. This means that the robust controller via self-sensing actuator can only suppress half of the amplitude of vibration in the forced vibration.

The experimental results show that active vibration suppression of the smart beam via self-sensing piezoelectric actuator configuration is less effective than the vibration suppression achieved by piezoelectric sensor/actuator pair. In self-sensing configuration, the variations of the capacitance of the piezoelectric material severely affect the dynamic characteristics of the bridge circuit which is used for the decomposition of sensing and actuation signals. This unbalanced circuit results in a performance reduction of the robust controller via self-sensing piezoelectric actuator for vibration suppression. This issue of the self-sensing piezoelectric actuator is also reported and studied by researchers [35, 74].

As a conclusion, active vibration control of a smart beam is achieved with employment of piezoelectric patches as self-sensing actuators via designed robust controller. The experimental work performed on the suppression of free and forced vibrations shows the effectiveness of these self-sensing actuators with the robust controller.

CHAPTER 5

DISCUSSION

5.1 Achievements

In this thesis, piezoelectric materials are used as sensors, actuators and self-sensing actuators for the investigation of vibration characteristics and the performances of each piezoelectric sensor/actuator configuration is evaluated for the active vibration suppression of the smart beam.

The investigation of the vibration characteristics of smart beam by employment of piezoelectric patches as sensors and actuators are presented and additionally the effect of location of piezoelectric patch for actuation and sensing and the effect of bimorph configuration of piezoelectric patches are studied. The excitation of smart beam is performed by an impact hammer and the response of smart beam to this excitation is measured by using two piezoelectric patches, a single axis accelerometer and a laser displacement sensor. In further experimental studies in the Chapter 2, the piezoelectric patch is employed as an actuator to excite the smart beam. Similar to the previous configuration, the response of smart beam is again measured both by two piezoelectric patches located at different positions and by commercially available sensing devices. Following this, the vibration characteristics of the smart beam is obtained. For each measurement, sample time records and frequency response functions are presented. By comparing the first three out of plane bending modes of smart beam, it can be concluded that vibration characteristics of smart beam is satisfactorily investigated via piezoelectric sensor with piezoelectric actuator. Additionally, it is observed that the bimorph configuration doubles the actuation authority of piezoelectric patches by also providing better signal to noise ratio.

During this study, piezoelectric sensor and actuator pair is used for an active vibration suppression of the smart beam with robust controller which is designed for the stable and the effective suppression of free and the first resonance forced vibration (Chapter 3). At first, frequency response of the system is obtained by using piezoelectric sensor and actuator patches. Then, analytical system model is acquired from the measured frequency response. Following this, robust controller is designed for the active vibration control of the smart beam. System uncertainties and noise in measurement are experimentally obtained. In order to qualify the effectiveness of the designed robust controller, μ analysis is conducted. Finally, the robust controller is applied by using a programmable controller. The time responses of free and forced vibration at the first resonance frequency of the smart beam are acquired for open-loop and closed-loop cases. For the free vibration suppression, reduction of the maximum voltage to the sensor noise level takes more than 30 seconds at the open-loop, however at the closed-loop, suppression of free vibration to the sensor noise level takes only 3 seconds. In the case of forced vibration suppression, the monitored voltage at closed-loop is approximately one-tenth of the monitored voltage at open-loop case. This means that the robust controller via piezoelectric sensor and actuator pair can suppress approximately %90 of the amplitude of vibration in the forced vibration. In addition to time domain, the effectiveness of the controller is also presented by open-loop and closed-loop frequency responses. As a conclusion of Chapter 3, active vibration control of the smart beam is achieved by employment of piezoelectric patches as sensors and actuators via designed robust controller. The experimental work performed on the suppression of free and forced vibrations shows the effectiveness of these piezoelectric patches with the robust controller.

Self-sensing piezoelectric actuator (Chapter 4) is also used for an active vibration suppression of the smart beam with robust controller which is designed by following the same procedure and for the same purpose as in the piezoelectric sensor/actuator pair case. For self-sensing piezoelectric actuator configuration, time responses of free and forced vibration at the first resonance frequency of the smart beam are also acquired for open-loop and closed-loop cases. For the free vibration suppression, reduction of approximately one-quarter of the maximum voltage takes more than 13 seconds at the open-loop, however at the closed-loop, it takes only 7 seconds. In the case of forced vibration suppression, the monitored voltage at closed-loop is almost the half of the monitored voltage at open-loop. This means that the robust controller via self-sensing actuator can suppress roughly half of the amplitude of vibration in

the forced vibration. As a conclusion, active vibration control of a smart beam is achieved with employment of piezoelectric patches as self-sensing actuators via designed robust controller. The experimental work performed on the suppression of free and forced vibrations shows the effectiveness of these self-sensing actuators with the robust controller.

This study also presented that the performance of piezoelectric sensor/actuator pair is superior than the performance of self-sensing piezoelectric actuator in vibration suppression. One of the objectives in this study, on the other hand, is to show that in case of a failure of any piezoelectric sensor patch, the piezoelectric actuator patch can also be used as a sensor when self-sensing actuator configuration is adapted. The action taken here could be considered as a backup configuration which is extremely crucial from the durability of active vibration control system for flexible structures.

In order to demonstrate the effectiveness of the self-sensing actuator in case of sensor failure; a failure and a back-up configuration scenario is presented in Figure 5.1. In this demonstration, the active vibration suppression of the first resonance forced vibration of the smart beam is aimed. The piezoelectric patch (2A) is selected as vibration sensor, and piezoelectric patches (1A-1B-4A-4B) are selected as actuator and also configured as self-sensing actuator. Throughout the scenario, the smart beam is vibrated in its first resonance frequency by the disturbance of piezoelectric patches (3A-3B). During the first four seconds, active vibration controller is inactive. At the fourth second, the active vibration controller via piezoelectric sensor/actuator pair is started to operate. At the fourteenth second, the failure of piezoelectric sensor is simulated as if the controller via piezoelectric sensor/actuator pair became inactive (fatigue failure of piezoelectric sensor, disconnection of piezoelectric sensor). Due to this sensor failure, the smart beam vibrates freely. However, if the piezoelectric actuator in the piezoelectric sensor/actuator pair is also configured as a self-sensing actuator; by a sensor failure detection mechanism, the self-sensing actuator configuration can be used as a back-up system. In the demonstration, back-up operation of this self-sensing piezoelectric actuator is presented at the nineteenth seconds of the test. As mentioned in Chapter 4, the self-sensing piezoelectric actuator can suppress the half of the vibration at the first resonance forced vibration. Therefore, the self-sensing piezoelectric actuator configuration can be used as a back-up system in case of sensor failures.

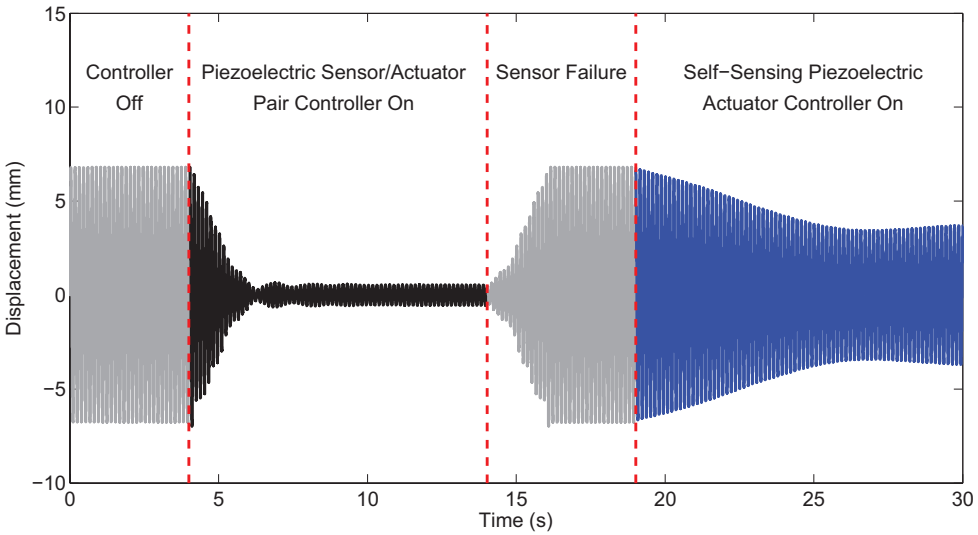

Figure 5.1: Vibration Suppression by Self-Sensing Piezoelectric Actuator Configuration After Sensor Failure of Piezoelectric Sensor/Actuator Pair

5.2 Future Work

In this thesis, piezoelectric materials are used as sensors and actuators and it is concluded that piezoelectric materials can be effectively used in the active vibration control. However, the reliability of the piezoelectric materials should be studied before implementing the real structures. For safer flights, civil aviation authorities require back-up systems for air-vehicles. This thesis presents that in case of the sensor failure of the piezoelectric sensor/actuator pair, self-sensing piezoelectric actuator configuration can be employed as a back-up system. In order to automatically switch sensor and actuator configurations, an online sensor failure detection can be studied and verified experimentally.

As a future topic, the performance of the self-sensing piezoelectric actuator in active vibration suppression of the smart beam can be increased by using adaptive mechanisms for the capacitance variation [35] of the piezoelectric material.

CHAPTER 6

CONCLUSION

The main objective of this thesis is to employ piezoelectric patches bonded on a smart beam as a sensor, actuator and self-sensing actuator in the investigation of vibration characteristics and active vibration control. In order to achieve this aim, the actuation and sensing capabilities of the piezoelectric material are analyzed by obtaining frequency responses of the smart beam and comparing the results gathered via commercially off-the shell sensing and excitation devices. During the study, the piezoelectric sensor with piezoelectric actuator can be satisfactorily used in the investigation of vibration characteristics and the further investigations in active vibration control are conducted.

With the purpose of active vibration suppression of the smart beam, piezoelectric sensor and actuator pair are used to sense the disturbance of the smart beam and counteract to suppress the disturbance with the designed robust controller. Performance expectations are met by simulating open and closed loop frequency responses and in order to demonstrate and validate the effectiveness of the designed controller, active vibration control experiments were performed for the free and the first resonance forced vibrations of the smart beam. The results of the active vibration control experiments proved that piezoelectric sensor/actuator pair is an effective sensor and actuator configuration for active vibration control.

Having demonstrated the performance of piezoelectric sensor/actuator pair on active vibration control, piezoelectric material is intended to be use as a self-sensing actuator. In this configuration, the aim is to employ a piezoelectric material as a sensor and an actuator simultaneously. The system identification of the smart beam is conducted via self-sensing piezoelectric actuator and designing a robust controller in a similar way followed in piezoelectric sensor/actuator pair case, the performance of the self-sensing piezoelectric actuator for active vibration control is presented with experiments.

It can be concluded that piezoelectric materials can satisfactorily suppress the vibration of the smart beam when they are used as sensor, actuator and self-sensing actuator. This study also showed that the performance of piezoelectric sensor/actuator pair on active vibration suppression is superior than that of self-sensing piezoelectric actuator. Moreover, it is proposed that self-sensing actuator mechanism can be used as a back-up configuration in case of sensor failure.

REFERENCES

[1] B. H. K. Lee. Vertical tail buffeting of fighter aircraft. *Progress in Aerospace Sciences*, 36(3-4):193 – 279, 2000.

[2] R. A. Canfield, S. D. Morgenstern, and D. L. Kunz. Alleviation of buffet-induced vibration using piezoelectric actuators. *Computers & Structures*, 86(3-5):281 – 291, 2008.

[3] I. J. Tiemessen, C. T. J. Hulshof, and Frings-Dresen M. H. W. An overview of strategies to reduce whole-body vibration exposure on drivers: A systematic review. *International Journal of Industrial Ergonomics*, 37(3):245 – 256, 2007.

[4] O.O. Okunribido, M. Magnusson, and M.H. Pope. Low back pain in drivers: The relative role of whole-body vibration, posture and manual materials handling. *Journal of Sound and Vibration*, 298(3):540 – 555, 2006.

[5] Y. Chen, V. Wickramasinghe, and D. Zimcik. Development of adaptive seat mounts for helicopter aircrew body vibration reduction. *Journal of Vibration and Control*, 15(12):1809–1825, 2009.

[6] G.F. Abdelal, N. Abuelfoutouh, and A. Hamdy. Mechanical fatigue and spectrum analysis of small-satellite structure. *International Journal of Mechanics and Materials in Design*, Volume 4, Number 3:265–278, 2008.

[7] H. Baier, L. Datashvili, and S. Rapp. Enhancing space satellite performance by integrating smart sensors and actuators for sensing and shape morphing. volume 7493, page 74931U. SPIE, 2009.

[8] T. Maillard, F. Claeyssen, R. LeLetty, O. Sosnicki, A. Pages, and A. Vazquez Carazo. Piezomechatronic-based systems in aircraft, space, and defense applications. volume 7331, page 73310K. SPIE, 2009.

[9] C. Lambert and I. Gursul. Characteristics of fin buffeting over delta wings. *Journal of Fluids and Structures*, 19(3):307 – 319, 2004.

[10] J.J. Wang and Y. Liu. Experimental study on lift characteristics for flow over flexible cropped delta wings. *Journal of Aircraft*, 45(6):2158–2161, 2008.

[11] M. Ciminello, A. Calabr, S. Ameduri, and A. Concilio. Synchronized switched shunt control technique applied on a cantilevered beam: Numerical and experimental investigations. *Journal of Intelligent Material Systems and Structures*, 19(9):1089–1100, 2008.

[12] J. Yang. *An Introduction to the Theory of Piezoelectricity*, volume 9. Springer, New York, 2005.

[13] S. Heinze and M. Karpef. Analysis and wind tunnel testing of a piezoelectric tab for aeroelastic control applications. *Journal of Aircraft*, 43(6):1799–1804, 2006.

[14] H. Ko, H. Jeong, and B. Koc. Piezoelectric actuator for mobile auto focus camera applications. *Journal of Electroceramics*, 23(2-4):530–535, 2009.

[15] C. Spelta, F. Previdi, D. Belloli, M. Madaschi, E. Silani, F. D'Adamo, F. Faginoli, and S.M. Savaresi. Active vibration control of a kitchen hood via piezoelectric patch. In *Control Applications, (CCA) Intelligent Control, (ISIC), 2009 IEEE*, pages 812 –817, 8-10 2009.

[16] S. Devasia, E. Eleftheriou, and S.O.R. Moheimani. A survey of control issues in nanopositioning. *Control Systems Technology, IEEE Transactions on*, 15(5):802 –823, September 2007.

[17] U. Aridogan, Y. Shan, and K. K. Leang. Design and analysis of discrete-time repetitive control for scanning probe microscopes. *Journal of Dynamic Systems, Measurement, and Control*, 131(6):061103, 2009.

[18] M. Sahin, F. M. Karadal, Y. Yaman, O. F. Kircali, V. Nalbantoglu, F. D. Ulker, and T. Caliskan. Smart structures and their applications on active vibration control: Studies in the Department of Aerospace Engineering, METU. *Journal of Electroceramics*, 20(3-4):167–174, 2008.

[19] I. Chopra. Review of state of art of smart structures and integrated systems. *AIAA Journal*, 40(11):2145–2187, 2002.

[20] T. Caliskan. *Piezoelectric Ceramics And Their Applications In Smart Aerospace Structures*. PhD thesis, Middle East Technical University, 2002.

[21] W.P. Mason. Piezoelectricity, its history and applications. *The Journal of the Acoustical Society of America*, 70(6):1561–1566, 1981.

[22] A. Ballato. Piezoelectricity: History and new thrusts. In *Proceedings of the IEEE Ultrasonics Symposium*, volume 1, pages 575–583, 1996.

[23] R. Ly, C. Giraud-Audine, R. Bigot, and G. Abba. Longitudinal vibrations modeling of a piezoelectric actuator used in forming process. In *Proceedings of the 2009 IEEE International Conference on Mechatronics*, pages 1 –6, April 2009.

[24] R. Safaric, J. Cas, G. Skorc, and S.I. Protsenko. Micro and nano robotics. In *Information, Communication and Automation Technologies, 2009. ICAT 2009. XXII International Symposium on*, pages 1 –6, oct. 2009.

[25] R. Barboni, A. Mannini, E. Fantini, and P. Gaudenzi. Optimal placement of pzt actuators for the control of beam dynamics. *Smart Materials and Structures*, 9:110–120, 2000.

[26] D. Halim and S.O.R. Moheimani. An optimization approach to optimal placement of collocated piezoelectric actuators and sensors on a thin plate. *Mechatronics*, 13:27–47, 2003.

[27] J. A. Main, E. Garcia, and D. Howard. Optimal placement and sizing of paired piezoactuators in beams and plates. *Smart Materials and Structures*, 3:373–381, 1994.

[28] L. Bruant, G. Coffignal, and F. Lene. A methodology for determination of piezoelectric actuator and sensor location on beam structures. *Journal of Sound and Vibration*, 243(5):861–882, 2001.

[29] A. R. Mehrabian and A. Yousefi-Koma. A novel technique for optimal placement of piezoelectric actuators on smart structures. *Journal of the Franklin Institute*, In Press, Corrected Proof:–, 2009.

[30] V. Giurgiutiu, A. Zagrai, and J. Bao. Damage identification in aging aircraft structures with piezoelectric wafer active sensors. *Journal of Intelligent Material Systems and Structures*, 15(9-10):673–687, 2004.

[31] S. Liberatore, J. L. Speyer, and A. C. Hsu. Application of a fault detection filter to structural health monitoring. *Automatica*, 42:1199–1209, 2006.

[32] S. D. Glaser, H. Li, M. L. Wang, J. Ou, and J. Lynch. Sensor technology innovation for the advancement of structural health monitoring: a strategic program of us-china research for the next decade. *Smart Structures and Systems*, 3(2):221–244, 2007.

[33] M. J. Guan and W. H. Liao. On the equivalent circuit models of piezoelectric ceramics. *Ferroelectrics*, 386(1):77 – 87, 2009.

[34] A.S. Putra, S. Huang, K. K. Tan, S. K. Panda, and H. T. Lee. Self-sensing actuation with adaptive control in applications with switching trajectory. *IEEE/ASME Transactions on Mechatronics*, 13(1):104–111, 2008.

[35] G. E. Simmers Jr., J. R. Hodgkins, D. D. Mascarenas, G. Park, and H. Sohn. Improved piezoelectric self-sensing actuation. *Journal of Intelligent Material Systems and Structures*, 15(12):941–953, 2004.

[36] E.F. Crawley and J. Luis. Use of piezoelectric actuators as elements of intelligent structures. *AIAA*, 25(10):1373–1385, 1987.

[37] R. Alkhatib and M. F. Golnaraghi. Active structural vibration control: A review. *Shock and Vibration Digest*, 35(5):367–383, 2003.

[38] J. Bontsema and R.F. Curtain. A note on spillover and robustness for flexible systems. *Automatic Control, IEEE Transactions on*, 33(6):567 –569, June 1988.

[39] S.O.R. Moheimani, B.J.G. Vautier, and B. Bhikkaji. Experimental implementation of extended multivariable ppf control on an active structure. *Control Systems Technology, IEEE Transactions on*, 14(3):443 – 455, May 2006.

[40] L. Wang. Positive position feedback based vibration attenuation for a flexible aerospace structure using multiple piezoelectric actuators. In *Proceedings of the 22nd Digital Avionics Systems Conference*, IN, USA, 2003.

[41] S.S. Aphale, A.J. Fleming, and S.O.R. Moheimani. Integral resonant control of collocated smart structures. *Smart Materials and Structures*, 16(2):439–446, 2007.

[42] W. Zhang, J. Qiu, and J. Tani. Robust vibration control of a plate using self-sensing actuators of piezoelectric patches. *Journal of Intelligent Material Systems and Structures*, 15:923–931, 2004.

[43] K. Zhou and J. C. Doyle. *Essentials of Robust Control*. Prentice-Hall, Inc., Uper Saddle River, NJ, 1998.

[44] G. Zames. Feedback and optimal sensitivity : Model reference transformations, multiplicative seminorms, and approximate inverses. *IEEE Transactions on Automatic Control*, 26(2):301– 320, 1981.

[45] B.A. Francis and J.C. Doyle. Linear control theory with an H_∞ optimality criterion. *SIAM Journal of Control and Optimization*, 25(4):815–844, 1987.

[46] K. Glover and J. C. Doyle. State-space formulae for all stabilizing controllers that satisfy an H_∞ norm bound and relations to risk sensitivity. *1988*, 11(3):167–172, 1988.

[47] J.C. Doyle, K. Glover, P.P. Khargonekar, and B.A. Francis. State-space solutions to standard H_2 and H_∞ control problems. *IEEE Transactions on Automatic Control*, 34(8):831 – 847, 1989.

[48] X. Zhang, C. Shao, S. Li, D. Xu, and A. G. Erdman. Robust H_∞ vibration control for flexible linkage mechanism systems with piezoelectric sensors and actuators. *Journal of Sound and Vibration*, 243(1):145 – 155, 2001.

[49] K. Seto and I.N. Kar. A comparative study on H_∞ based vibration controller of a flexible structure system. In *American Control Conference, 2000. Proceedings of the 2000*, volume 1, pages 513 –518 vol.1, sep 2000.

[50] O.F. Kircali, Y. Yaman, V. Nalbantoglu, M. Sahin, F.M. Karadal, and F.D. Ulker. Spatial control of a smart beam. *Journal of Electroceramics*, 20(3-4):175–185, 2008.

[51] Y. Yaman, Caliskan T, V. Nalbantoglu, F. D. Ulker, E. Prasad, D. Waechter, and B. Yan. Active vibration control of smart plates by using piezoelectric actuators. In *ESDA2002, 6th Biennial Conference on Engineering Systems Design and Analysis*, number APM-018, Istanbul, Turkey, 2002.

[52] D. F. Ulker. Active Vibration Control of Smart Structures. Master's thesis, Middle East Technical University, 2003.

[53] O. F. Kircali. Active Vibration Control of a Smart Beam: A Spatial Approach. Master's thesis, Middle East Technical University, 2006.

[54] F. M. Karadal. Active Flutter Suppression of a Smart Fin. Master's thesis, Middle East Technical University, 2008.

[55] U. Aridogan, M. Sahin, V. Nalbantoglu, and Y. Yaman. Piezoelektrik yamalarin akilli bir kirisin titresim ozelliklerinin bulunmasinda algilayici olarak kullanilmasi. In *XVI. Ulusal Mekanik Kongresi, Erciyes Universitesi*, Kayseri, Turkey, 2009 (In Turkish).

[56] U. Aridogan, M. Sahin, V. Nalbantoglu, and Y. Yaman. Piezoelektrik yamalarin akilli bir kirisin titresim kontrolunde algilayici ve uyarici olarak kullanilmasi. In *UMTS2009, 14. Ulusal Makina Teorisi Sempozyumu, ODTU Kuzey Kibris Kampusu Bildiriler Kitabi*, pages 275–281, Guzelyurt, Northern Cyprus, 2009 (In Turkish).

[57] U. Aridogan, M. Sahin, Y Yaman, and V. Nalbantoglu. Active vibration suppression of a smart beam via self-sensing piezoelectric actuator. In *AIAC2009, 5. Ankara International Aerospace Conference, METU, AIAC-2009-034*, Ankara, Turkey, 2009.

[58] Sensor Technologies Limited. *BM-500 Lead Zirconate Titanate Product Data Sheet*, 2002.

[59] Brüel and Kjær. *Product Data of Pulse Analyzer Platform Type Portable Pulse - 3560C System*, November 2008.

[60] Brüel and Kjær. *Product Data of Impact Hammer Type 8206*, 2005.

[61] Brüel and Kjær. *PULSE 13.5 - Modal Test Consultant*, 2009.

[62] D. J. Ewins. *Modal Testing : Theory and Practice*. John Wiley and Wiley Inc,, 1995.

[63] Brüel and Kjær. *Product Data of Miniature DeltaTron TEDS Accelerometer Type 4508 B*, April 2006.

[64] Keyence. *Instruction Manual For Laser Displacement Sensor LB-1000(W) Series*, 1992.

[65] Hewlett-Packard Company. *HP 33120A Function Generator/Arbitrary Waveform Generator User's Guide*, August 1997.

[66] Sensor Technologies Limited. *SA10 - Two-channel High Voltage Amplifier Product Data Sheet*, December 2005.

[67] M. A. Demetriou, K. M. Grigoriadis, and R. J. Sweeney. Collocated H_∞ control of a cantilevered beam using an analytical upper-bound approach. *Journal of Intelligent Material Systems and Structures*, 20(7):865–873, 2009.

[68] G. J. Balas, J. C. Doyle, K. Glover, A. Packard, and R. Smith. *μ Analysis and Synthesis Toolbox For Use with MATLAB*, June 2001.

[69] K. Zhou, J. Doyle, and K. Glover. *Robust and Optimal Control*. Prentice-Hall, Inc., 1995.

[70] D. D. Bueno, C. R. Marqui, R. B. Santos, C. M. Neto, and V. Lopes Jr. Experimental active vibration control in truss structures considering uncertainties in system parameters. *Mathematical Problems in Engineering*, 2008, 2008.

[71] J. B. Burl. *Linear optimal control : H_2 and H_∞ methods*. Addison Wesley Longman, Inc., Menlo Park, CA, 1999.

[72] M.J. Grimble and M.A. Johnson. H_∞ robust control design-a tutorial review. *Computing Control Engineering Journal*, 2(6):275 –282, nov 1991.

[73] C.M. Kwan, H. Xu, C. Lin, L. Haynes, J. Dohner, M. Regelbrugge, and N. Shankar. H_∞ control of chatter in octahedral hexapod machine. In *American Control Conference, 1997. Proceedings of the 1997*, volume 2, pages 1015 –1016 vol.2, 4-6 1997.

[74] H. Hongsheng, Q. Suxiang, and Q. Linfang. Self-sensing piezoelectric actuator for active vibration control based on adaptive filter. In *Mechatronics and Automation, 2007. ICMA 2007. International Conference on*, pages 2564 –2569, 5-8 2007.

APPENDIX A

INVERTING VOLTAGE AMPLIFIER CIRCUIT

Inverting voltage amplifier circuit shown in Figure A.1 includes two resistors and an operational amplifier. The main function of voltage amplifier circuit is to capture low frequency piezoelectric material voltage output and to convert it to low impedance signal. The secondary function of voltage amplifier circuit is to amplify the input signal by the ratio of resistor values of Resistance 2 and Resistance 1 by inverting the sign of the signal.

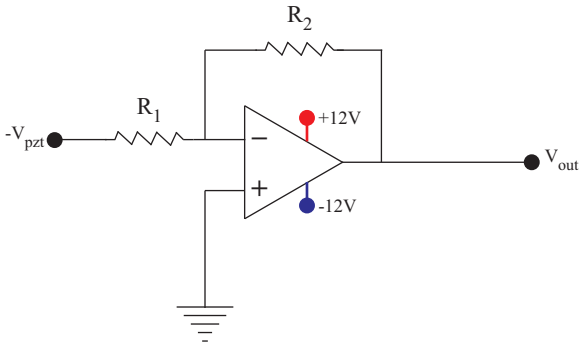

Figure A.1: Inverting Voltage Amplifier Circuit

In Figure A.1, the piezoelectric material's voltage is presented with v_{pzt} and the sensor signal, which is the output of the operational amplifier, is denoted by v_{out}. The resistance value of Resistor 1 (R_1) and Resistor 2 (R_2) are $4.7M\Omega$ and $1M\Omega$, respectively. The operational amplifier used in this study is supplied with $+12V$ and $-12V$.

APPENDIX B

SELF-SENSING BRIDGE CIRCUIT ANALYSIS

As mentioned in Section 4.2.1, the relationship for the sensing signal of the self-sensing bridge circuit can be obtained by using Kirchoff's laws. Figure B.1 shows voltage loop analyses of the self-sensing bride circuit for the application of Kirchoff's voltage and current laws.

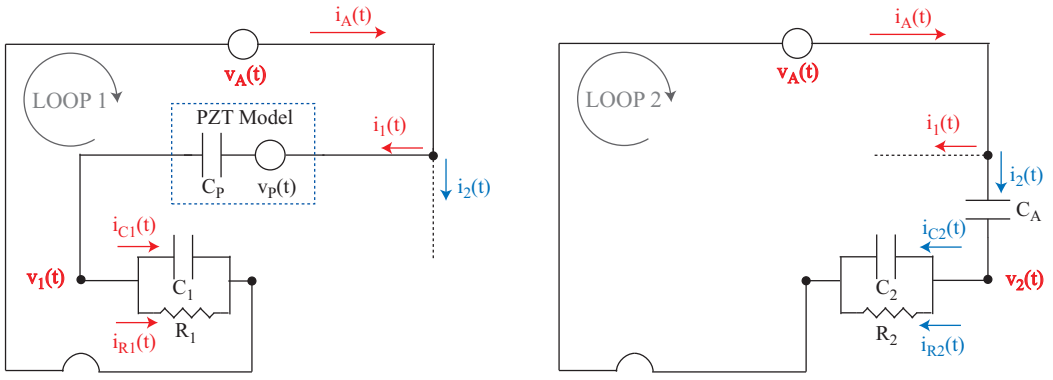

(a) Loop-1 Analysis (b) Loop-2 Analysis

Figure B.1: Application of Kirchoff's Voltage Law **(a)** Loop-1 Analysis **(b)** Loop-2 Analysis

The current flow $i_A(t)$ from the actuator voltage is divided into two components $i_1(t)$ and $i_2(t)$ at the current junction,

$$i_A(t) = i_1(t) + i_2(t) \tag{B.1}$$

For the loop-1 analysis, following equation is written,

$$v_A(t) - v_P(t) - \frac{1}{C_p}\int i_1(t)dt - v_1(t) = 0 \tag{B.2}$$

Here, the current $i_1(t)$ is divided into two parts for the parallel capacitor C_1 and resistor R_1 connection,

$$i_1(t) = i_{R1}(t) + i_{C1}(t) \qquad where \qquad i_{R1} = \frac{v_1(t)}{R_1} \qquad i_{C1} = C_1\frac{dv_1(t)}{dt} \tag{B.3}$$

Then, when $i_1(t)$ is substituted into Equation B.2 , the equation for $v_1(t)$ is obtained as follows:

$$v_1(t) = v_A(t) - v_P(t) - \frac{1}{C_p}\int\left(\frac{v_1(t)}{R_1} + C_1\frac{dv_1(t)}{dt}\right)dt \tag{B.4}$$

For the loop-2 analysis, following equation is written,

$$v_A(t) - \frac{1}{C_A}\int i_2(t)dt - v_2(t) = 0 \tag{B.5}$$

Here, the current $i_2(t)$ is divided into two parts for the leg which includes parallel capacitor C_2 and resistor R_2 connection,

$$i_2(t) = i_{R2}(t) + i_{C2}(t) \qquad where \qquad i_{R2} = \frac{v_2(t)}{R_2} \qquad i_{C2} = C_2\frac{dv_2(t)}{dt} \tag{B.6}$$

Then, when $i_2(t)$ is substituted into Equation B.5, the equation for $v_2(t)$ is obtained as follows:

$$v_2(t) = v_A(t) - \frac{1}{C_A}\int\left(\frac{v_2(t)}{R_2} + C_2\frac{dv_2(t)}{dt}\right)dt \tag{B.7}$$

A transfer function model of the sensor signal $(v_2(t)-v_1(t))$ can be obtained as follows: Taking the Laplace transforms of Equations B.4 and B.7, assuming zero initial conditions, following equations obtained,

$$V_1(s) = V_A(s) - V_P(s) - \frac{1}{sC_p}\left(\frac{V_1(s)}{R_1} + sC_1V_{C1}(s)\right) \tag{B.8}$$

$$V_2(s) = V_A(s) - \frac{1}{sC_A}\left(\frac{v_2(t)}{R_2} + sC_2V_2(s)\right). \tag{B.9}$$

Then, the transfer function for $V_1(s)$ and $V_2(s)$ dependent on actuator voltage $V_A(s)$ and piezoelectric material voltage V_P is found to be:

$$V_1(s) = \frac{sC_PR_1}{1 + s(C_1R_1 + C_PR_1)}(V_A(s) - V_P(s)) \quad V_2(s) = \frac{sC_AR_2}{1 + s(C_2R_2 + C_AR_2)}V_A(s) \tag{B.10}$$

Then, the transfer function for the sensor signal (V_S) can be acquired as:

$$V_S(s) = \left(\frac{sC_AR_2}{1 + s(C_2R_2 + C_AR_2)} - \frac{sC_PR_1}{1 + s(C_1R_1 + C_PR_1)}\right)V_A(s) + \frac{sC_PR_1}{1 + s(C_1R_1 + C_PR_1)}V_P(s) \tag{B.11}$$

Equation B.11 is the equivalent to Equation 4.2.